The Frequency Agile HF Antenna

David.

D. Hellicar

May 1992

graduated 1993

Statement

This thesis contains no material which has been accepted for the award of any other higher degree or graduate diploma in any tertiary institution and, to the best of my knowledge and belief, this theses contains no material previously published or written by another person, except where due reference is made in the text of the thesis.

David Hellicar

Contents

List of Figures

List of Tables

ACKNOWLEDGEMENTS

I wish to thank Professor P.A.Hamilton, of the Physics Department, Faculty of Science, University of Tasmania, for his guidance and assistance with this project.

I also wish to thank the Management and Staff of Moonraker Australia, in particular Mr. L.W.Edwards without whom this project would not have eventuated.

Finally my thanks go to my family for their moral support over the past few years.

ABSTRACT

This thesis examines the theory and practice of the 'AT' series antenna manufactured by MOONRAKER AUSTRALIA. A model has been developed based on the superposition of symmetric and asymmetric dipoles, which has been confirmed by numerical techniques. A test system has been developed which allows the manufacturer to rapidly test production, using unskilled staff, whilst building a data base for future analysis of the antenna and its production.

Chapter 1

INTRODUCTION

The advent of satellite communication systems has not spelt the end of HF radio as a popular means of communication and will probably not displace it in the near future.

One of the prime reasons for this is the cost involved. The initial investment is much lower for an HF system and running costs are minimal as an HF user only pays an annual licence fee as opposed to being charged for useage in much the same manner as the telecommunications user is charged.

For mobile users, both land and marine, an added problem is the fact that there is no commercially viable antenna system available (mainly because such antennas must be highly directive and require an expensive continuous pointing system), eventually this will be overcome in an inexpensive way.

A third factor is that HF systems do not require the high level of technical skills and sophistication of test equipment that is required to maintain and repair satellite equipment, making HF an attractive option for developing and sparsely populated countries.

HF systems are also used by military and diplomatic communication networks as emergency or backup systems because of the difficulty in 'jamming' HF communications.

For the purposes of this thesis HF refers to the common usage in Australia,

i.e. frequencies in the range 2 to 30 MHz although the standard definition is 3 to 30 MHz with 2MHz in the MF band (0.3 to 3 MHz).

HF radio is used for a number of land and marine distress frequencies (i.e. 2182 kHz) and the Royal Flying Doctor Service uses a number of HF channels (i.e. VJD Alice Springs RFDS operates on 2020, 4350, 5410 and 6950 kHz). There are also a number of radphone and School of the Air channels in the 4 to 8 MHz range.

Modern synthesised transceivers achieve rapid switching between channels and can be programmed with a large number of channel frequencies (the CODAN 8528 HF Transceiver allows the user to program up to 600 channels in the latest model). The reason for the large number of channels is that HF links suffer degradation due to atmospheric and ionospheric conditions so that a frequency must be chosen for a particular link. Users can obtain predictions on link behaviour from the Ionospheric Prediction Service in printed form or can use a computer package, Advanced Stand Alone Prediction System (ASAPS), to perform radio link analysis.

A number of transceivers are fitted with a SELCALL facility which will automatically select the best channel for the required link between two preprogrammed units, using a preprogrammed table to select frequencies and then testing the link for suitability.

The capacity for rapid switching between channels over the entire HF range means that users expect an antenna system to achieve the same response at an acceptable cost. There is of necessity a compromise between cost, tuning time and convenience.

For example helically wound tapped whip antennas are available at a relatively low cost but the user has to manually set the tap point by plugging a short circuit into the antenna thus bypassing turns to obtain the required resonant frequency. This is not convenient for mobile communications.

Because of the wavelengths involved (150m down to 10m for the HF range) HF antennas tend to be physically large for fixed installations, mobile installations however have height limitations which make the antennas very short

electrically.

There are several options available to match an electrically short antenna to its source impedance either by providing external matching circuitry or by loading the antenna with an inductive load which has the effect of electrically lengthening the antenna thus increasing its radiation resistance.

This thesis examines the centre loaded frequency agile HF antenna with particular emphasis on the 'AT' series loaded monopole antennas manufactured by MOONRAKER AUSTRALIA. The aim is to develop a computer model which is applicable to the production antennas. This model is to be used to predict changes in antenna performance due to variations in the characteristics of antenna components. This will result in a greatly reduced lead time between design changes and the appearance of the product on the market. The experimental techniques used are targeted at the manufacturing environment rather than the pure research environment. The experimental results aimed at enabling rapid production testing and greater information for both product development and quality control.

This thesis forms part of a project funded by the Department of Industry, Trade and Commerce (DITAC) together with MOONRAKER AUSTRALIA under the Teaching Company Scheme with the participation of the Physics Department of the Faculty of Science, University of Tasmania.

The overall purpose of the project was to investigate the use of the frequency agile antenna on Helicopters and light aircraft. Aircraft specific details have been omitted as any antenna changes are of a purely regulatory nature rather than scientific. Similarly commercial details have also been omitted.

This thesis examines the theoretical aspects of the cylindrical antenna by first discussing the mathematics of electromagnetic theory. The equations are then used to develop Hallén's equation, along the lines presented by Kraus [2], as used on the cylindrical dipole. Image theory is then used to extend into the monopole mode with qualitative examination of ground effects on monopole performance.

The practical aspects of impedance matching are discussed with particular

reference to communications requirements. The effects of antenna loading are introduced with emphasis on the centre loaded antenna.

Computational techniques are discussed and the Method of Moments (MOM) is used to analyse antenna models. Two commercially available MOM packages are compared and used to provide numerical data on various aspects of HF antenna characteristics.

The MOONRAKER 'AT' series antenna is introduced and studied using the methods developed in the earlier chapters.

The final section outlines the experimental methods used and results obtained and provides a link between the theoretical and experimental requirements of the antenna manufacturer.

Chapter 2

LITERATURE REVIEW

There is a considerable body of literature pertaining to the linear antenna which is well summarised in an article by KING [1]. In this article KING covers the development of antenna theory from the experiments of Hertz in 1887 up to the time of his writing in 1967. A comprehensive analysis of the linear antenna is also provided by KING in another work [2] which provides a number of analytical solutions to various cylindrical dipole problems, including combinations of cylindrical dipoles.

Far less comprehensive but far easier to follow is the section on the cylindrical dipole in the book by KRAUSS [3] , in which Halléns equation is developed from basic electromagnetic theory. A similar section in the book by BALANIS [4] also introduces the fields due to a magnetic current source and briefly covers the equivalent nature of the various solutions to the field equations. This concept is covered in far more depth in the article by THIELE in the book edited by MITTRA [5].

Ground plane effects are briefly discussed by BALANIS [4] with an in depth analysis in the book edited by JASIK [6] for monopoles of any height at the centre of a ground plane of diameter of the order of 10λ. The effects of smaller radii (down to zero) on a quarter wavelength monopole are investigated by WIENER [7].

The monopole with inductive loading is covered in some detail in a paper by HARRISON [8] in which the principle of superposition is used to model the

equivalent loaded dipole from a number of sub-antennas.

Over the last twenty years or so Computational Electromagnetics (CEM) has (for obvious reasons) been a rapidly expanding tool of science. MILLER [9] performs a sterling service by summarising the numerous theories and techniques contained in the literature.

The Method of Moments (MOM) (HARRINGTON [10]) is covered in a number of books and papers notably in the article by THIELE (MITTRA [5]) which covers a general application to wire grid bodies with attached antennas and more briefly by KRAUSS [3] and BALANIS [4] in relation to the cylindrical dipole.

Two software packages have been used in this project, MININEC [11] and ELNEC [12], both written for IBM AT computers.

MININEC has an excellent manual which covers all aspects of the theory and techniques used in a manner which is easy to follow and is well referenced for further reading. Unfortunately the version used came with executeable files with a segment limit of 40 which could be overcome by running (or recompiling) the basic programs with a larger segment limit. The user interface is tedious by modern standards.

ELNEC on the other hand has been rewritten to provide an extremely useable package but has little in the way of theoretical background. ELNEC was written by a radio amateur for radio amateurs and the documentation has the irritating 'folksy' style used by that ilk. Apart from this ELNEC is an excellent package for analysis of antenna problems and has a segment limit of 127.

Chapter 3

THE CYLINDRICAL ANTENNA

3.1 INTRODUCTION

The starting point for any solution to an electro-magnetic problem is the set of equations known as Maxwells' Equations, after James Clerk Maxwell (1835-1879). These equations have the general differential form:

$$\begin{aligned} \nabla \times \underline{H} &= \underline{J} + \frac{d\underline{D}}{dt} \\ \nabla \times \underline{E} &= -\frac{d\underline{B}}{dt} \\ \nabla \cdot \underline{D} &= \rho \\ \nabla \cdot \underline{B} &= 0 \end{aligned} \tag{3.1}$$

and together with the equation of continuity of electric charge

$$\nabla \cdot \underline{J} + \frac{d\rho}{dt} = 0$$

or its harmonic form

$$\nabla \cdot \underline{J} + j\omega\rho = 0 \tag{3.2}$$

form the basis for the solution to a number of electromagnetic problems.

In the analysis of the cylindrical dipole it is useful to use the Magnetic Vector Potential ($\underline{A}$) and the Electric Scalar Potential (Φ). These are defined as

$$\begin{aligned} \underline{A}(\underline{r},t) &= \frac{\mu}{4\pi}\int_{V'}\frac{\underline{J}(\underline{r}',t)'}{|\underline{r}-\underline{r}'|}dV' \\ \Phi(\underline{r},t) &= \frac{1}{4\pi\epsilon}\int_{V'}\frac{\rho(\underline{r}',t')}{|\underline{r}-\underline{r}'|}dV' \end{aligned} \tag{3.3}$$

where t' = t - $\frac{|\underline{r}-\underline{r}'|}{c}$ is the retarded time and c is the speed of light in vacuo.

The harmonic form of 3.3 is

$$\begin{aligned} \underline{A}(\underline{r}) &= \frac{\mu}{4\pi}\int_{V'}\frac{\underline{J}(\underline{r}')exp(jk|\underline{r}-\underline{r}'|)}{|\underline{r}-\underline{r}'|}dV' \\ \Phi(\underline{r}) &= \frac{1}{4\pi\epsilon}\int_{V'}\frac{\rho(\underline{r}')exp(jk|\underline{r}-\underline{r}'|)}{|\underline{r}-\underline{r}'|}dV'. \end{aligned} \tag{3.4}$$

The potentials are related by the equation of charge continuity (3.2) from which Φ is obtained in terms of $\underline{A}$ as

$$\Phi = \frac{jc^2}{\omega}\nabla\cdot\underline{A} \tag{3.5}$$

which is the Lorentz condition.

The electric and magnetic fields in terms of the potentials are

$$\begin{aligned} \underline{E} &= -\frac{d\underline{A}}{dt} - \nabla\Phi \\ &= -\frac{d\underline{A}}{dt} - j\frac{c^2}{\omega}\nabla(\nabla\cdot\underline{A}) \\ \underline{H} &= \frac{1}{\mu}\nabla\times\underline{A}. \end{aligned} \tag{3.6}$$

There is also a set of equations analogous to 3.1 to 3.6 involving the Magnetic Current ($\underline{M}$) and the Electric Vector Potential ($\underline{F}$). The equivalent values are shown in table 3.1 The superposition of solutions to these two sets of

$\underline{J} <> 0, \underline{M} = 0$	$\underline{M} <> 0, \underline{J} = 0$
$\underline{E_A}$	$\underline{H_F}$
$\underline{H_A}$	$\underline{E_F}$
$\underline{A}$	$\underline{F}$
ϵ	μ
μ	ϵ
k	k

Table 3.1: Equivalent symbols for electric and magnetic sources

equations allows solutions to complex electomagnetic problems containing dielectric and magnetic volumes. Note that Φ is not used due to the lack of magnetic charge, however some models do use a magnetic charge density (m) to enable complete interchange of equations using Φ (i.e. MITTRA [5]).

The conditions at the boundary of two media characterised by (μ_1,ϵ_1),(μ_2,ϵ_2), where $(\mu_1,\epsilon_1) \neq (\mu_2,\epsilon_2)$, are:

(i) the tangential component of the E field (E_t) and the normal component of the H field (H_n) are continuous and

(ii) the other two components (E_n,H_t) are discontinuous.

In particular at the boundary between free space and a conducting surface the condition for the tangential electric field is

$$\begin{aligned} \hat{n} \times \underline{E} &= 0 \\ \text{where } \underline{E} &= E_s + I_s Z_s. \end{aligned} \tag{3.7}$$

Therefore $E_s = -I_s Z_s$, where E_s is the tangential electric field above the surface and Z_s is the surface impedance due to 'skin effect' with I_s the surface current in the 'skin'.

The skin effect refers to the current distibution within the surface region.

The current distribution is of the form

$$\begin{aligned} |I(z)| &= I_o e^{\frac{-z}{\sigma}} \\ \text{where } \sigma &= \sqrt{\frac{\rho}{\pi \mu f}} \end{aligned} \tag{3.8}$$

is the skin depth. The surface current I_s takes the rms value of the current in the 'skin' or $I_s = \frac{I_o}{\sqrt{2}}$.

The radiation field due to a current element I_z flowing in the positive z direction is obtained in spherical coordinates as (where (r_z, θ_z, ϕ_z) = (z,0,0))

$$\begin{aligned} E_r &= 60k^2 \int_z I(z)(\frac{1}{(kr)^2} - \frac{j}{(kr)^3}) \cos\theta e^{-jkr} dz \\ E_\theta &= j30k^2 \int_z I(z)(\frac{1}{kr} - \frac{j}{(kr)^2} - \frac{1}{(kr)^3}) \sin\theta e^{-jkr} dz \\ H_\phi &= j\frac{k^2}{4\pi} \int_z I(z)(\frac{1}{(kr)} - \frac{j}{(kr)^2}) \sin\theta e^{-jkr} dz \\ E_\phi &= H_r = H_\theta = 0. \end{aligned} \tag{3.9}$$

The far field is determined from the current distribution in a radiating element as

$$\begin{aligned} E_\theta &= j30k \int_z I(z) \sin\theta \frac{e^{-jkr}}{r} dz \\ H_\phi &= \frac{jk}{4\pi} \int_z I(z) \sin\theta \frac{e^{-jkr}}{r} dz \\ H_\phi &= \frac{E_\theta}{120\pi}. \end{aligned} \tag{3.10}$$

The radiated power in the direction (θ, ϕ) is obtained from the Poynting Vector $E_\theta(\theta) \times H_\phi{}^*(\phi)$ in 3.10.

The gain of the antenna in the direction (θ, ϕ) is

$$4\pi \frac{|\int_{\delta\theta}\int_{\delta\phi} E_\theta(\theta) H_\phi{}^*(\phi) d\phi d\theta|}{|\int_{2\pi}\int_{-\frac{\pi}{2}}^{\frac{\pi}{2}} E_\theta(\theta) H_\phi{}^*(\phi) d\phi d\theta|}. \tag{3.11}$$

By substituting 3.10 in 3.11

$$4\pi \frac{|\int_{\delta\theta}\int_{\delta\phi} E_\theta(\theta) E_\theta{}^*(\theta) d\phi d\theta|}{|\int_{2\pi}\int_{-\frac{\pi}{2}}^{\frac{\pi}{2}} E_\theta(\theta) E_\theta{}^*(\theta) d\phi d\theta|}. \tag{3.12}$$

For a radiating body consisting of a number of elements the gain is

$$4\pi \frac{|\sum \int_{\delta\theta}\int_{\delta\phi} E_\theta(\theta) E_\theta{}^*(\theta) d\phi d\theta|}{|\sum \int_{2\pi}\int_{-\frac{\pi}{2}}^{\frac{\pi}{2}} E_\theta(\theta) E_\theta{}^*(\theta) d\phi d\theta|}. \tag{3.13}$$

3.2 THE CYLINDRICAL DIPOLE

The current distribution in a cylindrical dipole antenna in free space is determined by the continuity of the E and H fields at all points on the antenna surface. In the thin cylindrical antenna of figure 3.1 (where a$<<\lambda$) the current is assumed to be zero at the ends of the antenna and so the problem becomes single dimensional with

$$\underline{A} = A_z, \underline{E} = E_z, \underline{J} = J_z. \tag{3.14}$$

$\underline{J}$ is represented by a filament of current I_z flowing along the axis of the conductor where

$$J_z = \frac{I_z}{\pi a}. \tag{3.15}$$

Equation 3.6 then becomes

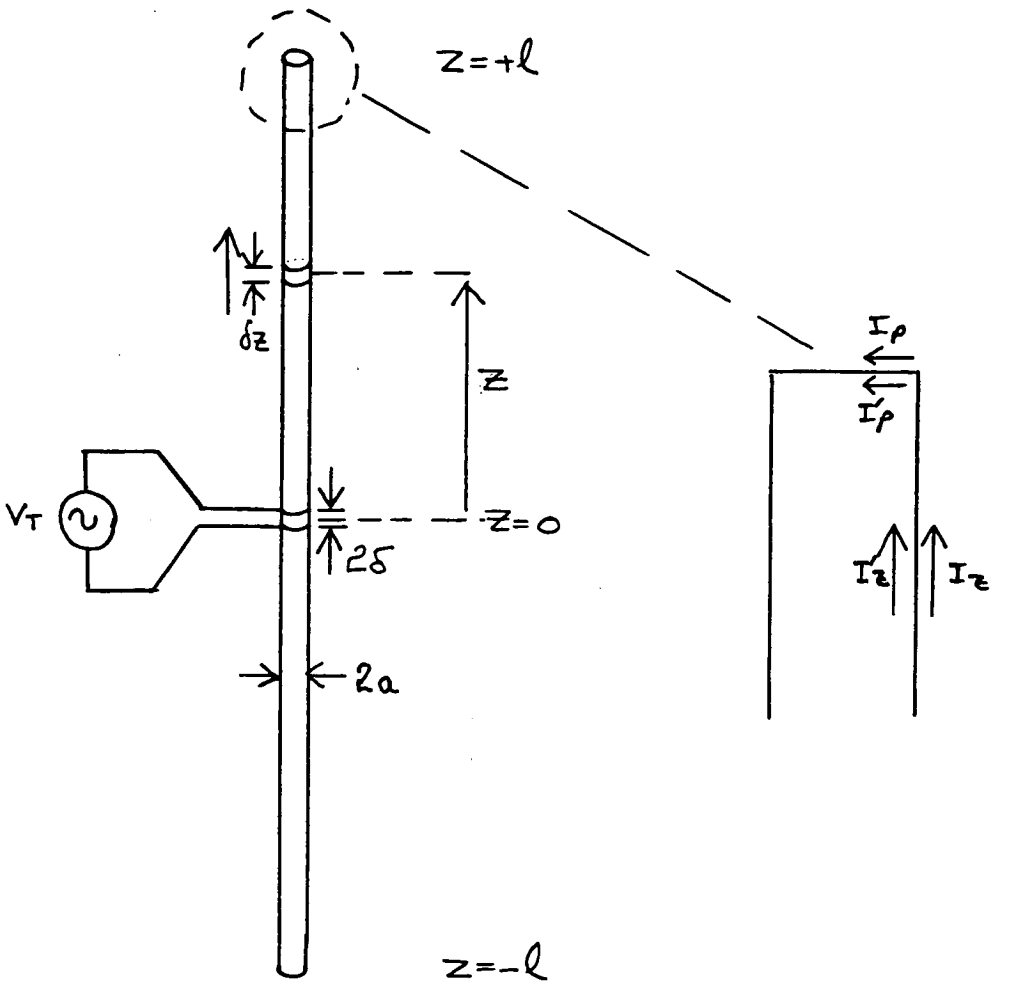

Figure 3.1: The cylindrical dipole

$$E_z{}^s = -j\frac{\omega}{k^2}(\frac{d^2A_z}{dt^2} + k^2A_z), \tag{3.16}$$

and by continuity of the tangential electric field

$$\frac{d^2A_z}{dt^2} + k^2A_z = j\frac{k^2}{\omega}ZI_z. \tag{3.17}$$

The solution to the homogeneous equation is the complementary function

$$A_c = C_1 \cos kz + C_2 \sin kz. \tag{3.18}$$

The solution to the non-homogeneous equation is the particular integral

$$A_r = j\frac{Z}{c}\int_0^z I(s) \sin k(z-s)ds. \tag{3.19}$$

Hence the magnetic vector potential is

$$A_z = -\frac{j}{c}(C_1 \cos kz + C_2 \sin k|z|) + j\frac{Z}{c}\int_0^z I(s) \sin(z-s)ds \tag{3.20}$$

where $|z|$ is used to maintain symmetry about $z = 0$.

The constant C_2 can be evaluated by substituting for A_z in equation 3.5 and determining Φ as $z = \pm\delta$. From symmetry about $z = 0$

$$\begin{aligned} I(z) &= I(-z) \\ \Phi(z) &= -\Phi(-z) \\ \text{and so} & \\ \Phi(\delta) &= C_2 \\ \Phi(\delta) - \Phi(-\delta) &= V_T = 2C_2. \end{aligned} \tag{3.21}$$

Hence C_2 is half the voltage at the antenna terminals.

Equation 3.20 can be substituted into $\underline{A}$ in 3.4 and rewritten to give

$$j\frac{c\mu}{4\pi}\int_{-\ell}^{+\ell}\frac{I_{z'}exp(-jkr)}{r}dz' = C_1\cos kz + \frac{V_T}{2}\sin k|z| - Z\int_0^z I(s)\sin(z-s)ds$$
$$\text{where } r = \sqrt{(a^2+(z'-z)^2)}. \qquad (3.22)$$

Equation 3.22 is known as Halléns' equation (after Erik Hallén who first published the equation in 1938) and it completely determines the current distribution in the cylindrical dipole.

The solution to 3.22 is initially obtained by assuming that the surface impedance is zero, in practice this is acceptable. For example the radiation resistance of a $\lambda/2$ dipole is approximately 75Ω. An aluminium dipole at 30 MHz (length 5m and diameter 32mm) has a total rf loss resistance of approximately 0.12Ω. A sinusoidal current distribution (a reasonable approximation for a $\lambda/2$ dipole), reduces this value to 0.06Ω giving an efficiency of 99.9%. The loss resistance in a dipole at 2MHz with the same length/diameter ratio is 0.23Ω or an efficiency of 99.7%.

Halléns equation becomes

$$j\frac{c\mu}{4\pi}\int_{-\ell}^{+\ell}\frac{I_{z'}exp(-jkr)}{r}dz' = C_1\cos kz + \frac{V_T}{2}\sin k|z|. \qquad (3.23)$$

The integral can be solved by adding and subtracting $\frac{I_z}{r}$ so that

$$\int_{-\ell}^{+\ell}\frac{I_{z'}exp(-jkr)}{r}dz' = I_z\int_{-\ell}^{+\ell}\frac{1}{r}dz' + \int_{-\ell}^{+\ell}\frac{I_{z'}exp(-jkr)-I_z}{r}dz'. \qquad (3.24)$$

The integral in the first term of the right hand side of 3.24 evaluates as

$$2ln\frac{2\ell}{a} + ln(1-(\frac{z}{l})^2)$$

$$+ln\left\{\frac{1}{4}(\sqrt{1+(\frac{a}{z-l})^2}+1)(\sqrt{1+(\frac{a}{z+l})^2}+1)\right\}. \qquad (3.25)$$

note that the second and third terms of 3.25 tend to $ln\Delta z - ln\Delta z$ + const as z = $\ell - \Delta z$, $\Delta z \rightarrow 0$.

The first and third terms of 3.25 are labelled Ω and δ in the literature and these symbols will mean this from here on in this section .

3.22 becomes

$$\begin{aligned} I_z &= -\frac{j}{30\Omega}(C_1 \cos kz + \frac{V_T}{2}\sin k|z|) \\ &- \frac{1}{\Omega}\left\{I_z ln(1-(\frac{z}{l})^2) + I_z\delta + \int_{-\ell}^{+\ell}\frac{I_{z'}exp(-jkr)-I_z}{r}dz'\right\}. \end{aligned} \qquad (3.26)$$

Solving 3.26 at the ends of the dipole where z=ℓ and $I_z = 0$ gives

$$\begin{aligned} 0 &= \frac{-j}{30\Omega}(C_1 \cos k\ell + \frac{V_T}{2}\sin k\ell) \\ &- \frac{1}{\Omega}\int_{-\ell}^{+\ell}\frac{I_{z'}exp(-jkr_1)}{r_1}dz'. \\ \text{where } r_1 &= \sqrt{a^2+(l-z')^2}. \end{aligned} \qquad (3.27)$$

3.27 can then be added to 3.26 to give the solution

$$\begin{aligned} I_z &= \frac{j}{30\Omega}(C_1(\cos k\ell - \cos kz) + \frac{V_T}{2}(\sin k\ell - \sin k|z|)) \\ &- \frac{1}{\Omega}\left\{I_z ln(1-(\frac{z}{l})^2) + I_z\delta\right\} \\ &- \frac{1}{\Omega}\left\{\int_{-\ell}^{+\ell}\frac{I_{z'}exp(-jkr)-I_z}{r}dz' - \int_{-\ell}^{+\ell}\frac{I_{z'}exp(-jkr_1)}{r_1}dz'\right\}. \end{aligned} \qquad (3.28)$$

The terms in braces are taken as zero for the zeroeth order approximation

$$I_{z0} = \frac{-j}{30\Omega}(C_1 F_{0z} + \frac{V_T}{2}G_{0z}) \qquad (3.29)$$

with the functions F_{0z} and G_{0z} defined by

$$\begin{aligned} F_{0z} &= \cos kz - \cos k\ell \\ G_{0z} &= \sin k|z| - \sin k\ell. \end{aligned} \tag{3.30}$$

The first, second and subsequent approximations are obtained by successive substitution of the previously obtained solution.

Successive functions F are given by KING [2] as

$$\begin{aligned} F_{nz} &= F_n(z) - F_n(\ell) \\ F_n(z) &= \frac{j4\pi Z}{\eta_o}\int_0^z F_{n-1,s}\sin k(z-s)ds - F_{n-1,z}ln(1-(\frac{z}{\ell})^2) \\ &+ F_{n-1,z}\delta - \int_{-\ell}^{+\ell}\frac{F_{n-1,z'}exp(-jkr) - F_{n-1,z}}{r}dz' \\ F_n(\ell) &= \frac{j4\pi Z}{\eta_o}\int_0^z F_{n-1,s}\sin k(z-s)ds \\ &- \int_{-\ell}^{\ell}\frac{F_{n-1,z'}exp(-jkr_1)}{r_1}dz' \end{aligned} \tag{3.31}$$

where the effects of surface impedance have been reintroduced. It should be noted that the effects of surface impedance are asymmetric in this form and should use the absolute value of $(z-s)$.

The functions G_n are the same as the functions F_n but with F_{n-1} replaced by G_{n-1}.

The current in the dipole is then obtained by substitution of the functions F and G in the terms in braces in equation 3.28 and rearanging to give

$$I_z = \frac{-j}{30\Omega}\left\{C_1(F_{oz} + \frac{F_{1z}}{\Omega} + \frac{F_{2z}}{\Omega^2} + \cdots) + \frac{V_T}{2}(G_{oz} + \frac{G_{1z}}{\Omega} + \frac{G_{2z}}{\Omega^2} + \cdots)\right\}. \tag{3.32}$$

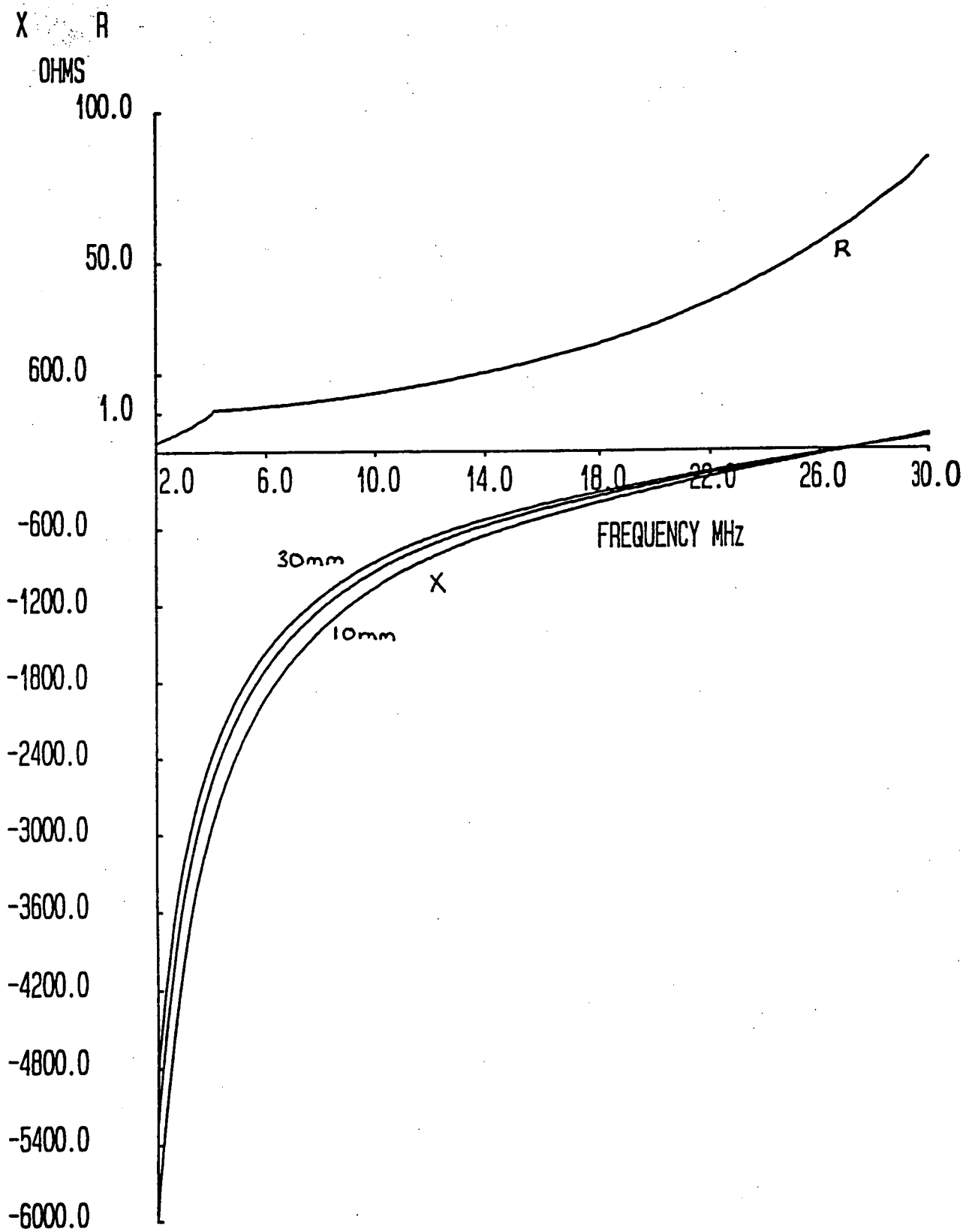

Figure 3.2: Impedance of 2.7m dipole with diameters of 10, 20 and 30 mm calculated using equation 3.36

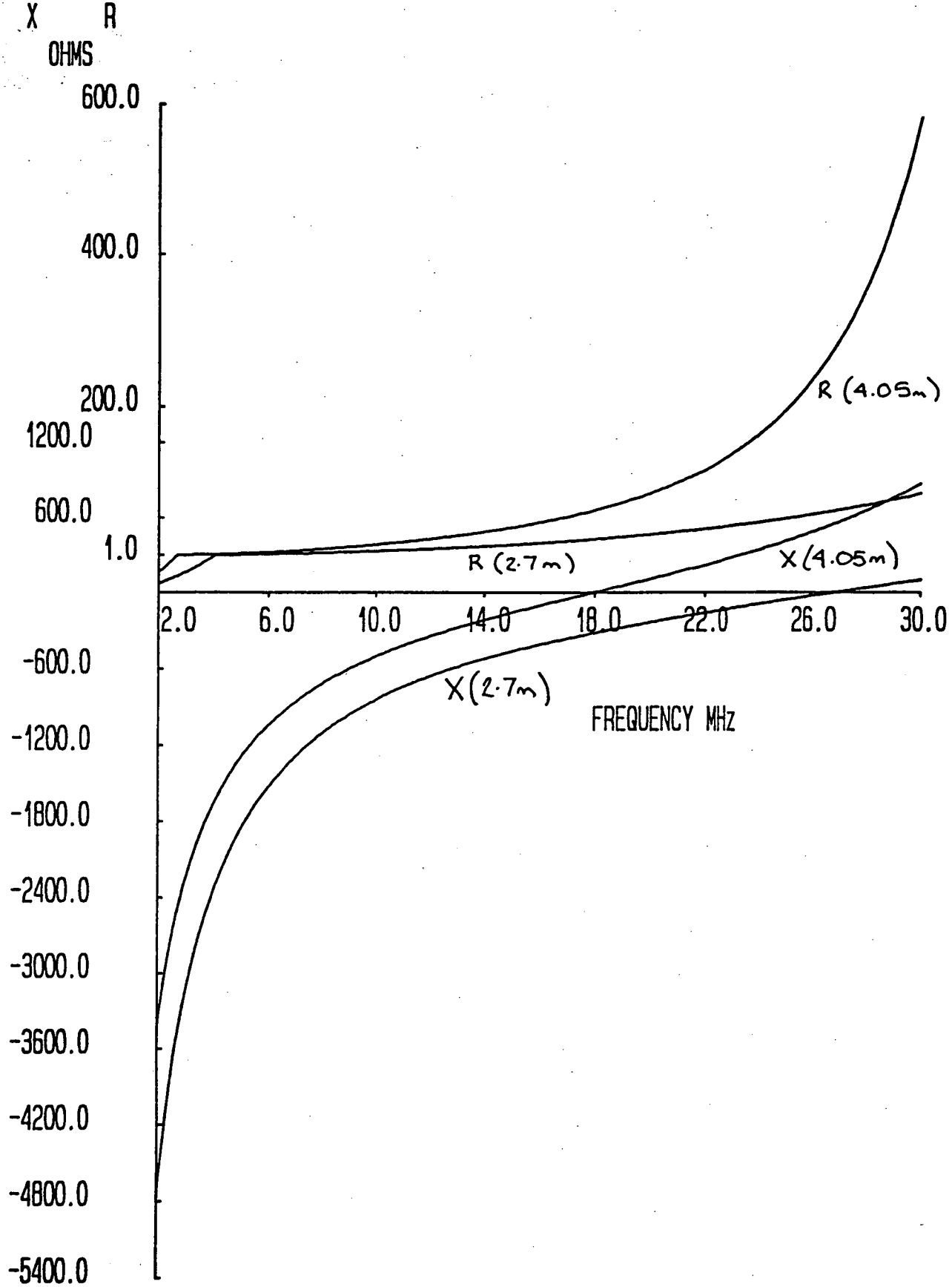

Figure 3.3: Impedance of 2.7m and 4.05m dipole of 32mm diameter calculated using equation 3.36

The constant C_1 is evaluated by taking the current at the end of the antenna as zero and solving

$$C_1 = -\frac{1}{2}V_T \left\{ \frac{G_0(\ell) + (\frac{1}{\Omega})G_1(\ell) + \cdots}{F_0(\ell) + (\frac{1}{\Omega})F_1(\ell) + \cdots} \right\}. \tag{3.33}$$

The current distribution is then finally determined by substituting C_1 into equation 3.28 to give the first order current distribution

$$I_z = \frac{jV_T}{60\Omega} \left\{ \frac{\sin(k\ell - |z|) + \frac{b_1}{\Omega}}{\cos k\ell + \frac{d_1}{\Omega}} \right\}. \tag{3.34}$$

The functions b_1 and d_1 in 3.34 are

$$\begin{aligned} b_1 &= F_1(z)\sin k\ell - F_1(\ell)\sin k|z| + G_1(\ell)\cos kz - G_1(z)\cos k\ell \\ d_1 &= F_1(\ell). \end{aligned} \tag{3.35}$$

The first order terminal impedance is obtained from 3.34 as

$$Z_T = -j60\Omega \left\{ \frac{\cos k\ell + \frac{d_1}{\Omega}}{\sin k\ell + \frac{b_1}{\Omega}} \right\} \tag{3.36}$$

with b_1 evaluated at z=0.

Computed first order impedances are shown in figure 3.2 for a dipole of half length 2.7m with diameters of 10, 20 and 30 mm and in figure 3.3 for dipoles of half length 2.7m and 4.05m with a diameter of 32mm (NOTE THE CHANGE OF SCALE FOR RESISTANCE VALUES OF LESS THAN 1.0 Ω).

The dipole of half length 2.7m has very low values of radiation resistance and high values of reactance at low frequencies. Thus the electrically short antenna is characterised by low r_{rad} and high X_{ant}, consequently the bandwidth is low when matched to a source by a resonant matching circuit. The Reactance decreases with increased diameter which is one method of increasing

bandwidth, while radiation resistance is unaffected by dipole diameter, although as the diameter decreases the surface loss resistance will increase thus reducing efficiency (note that surface loss resistance has not been included in these impedance calculations).

The comparison between the two dipoles of half length 2.7m and 4.05m show that the radiation resistance roughly doubles at low frequencies ($< \lambda/4$) for a 50% increase in length. The reactance of the shorter dipole is approximately 40% more than that of the longer dipole.

In each case there is a resonance (where the impedance is purely resistive) at a frequency somewhat less than the frequency where $\ell = \lambda/4$, when the dipole impedance is approximately 75 Ω.

3.3 THE MONOPOLE ANTENNA

The method of images is used to obtain the characteristics of the monopole above an ideal ground plane. The field at the point P, shown in figure 3.4, due to a vertical current element I_v, is the sum of the direct field and the reflected field. The reflected field can be considered to be the field due to the current element $I_{v'}$ which is the image of I_v at -z. Because of the phase reversal on reflection $I_{v'}$ must be flowing in the same direction as I_v. The horizontal component of current above an ideal ground plane is shown as I_h and $I_{h'}$. In the case where the ground plane is a magnetic media the image currents are reversed. Similarly if the currents I_v and I_h were magnetic currents then the image currents are again reversed (i.e figure 3.4 also represents a magnetic ground plane for magnetic current elements).

Hence the current distibution in the monopole antenna of length ℓ, above an perfectly conducting infinite ground plane, must be the same as that of the equivalent dipole of half length ℓ. It also follows that the terminal impedance of the monopole antenna is half that of the corresponding dipole.

The effects of ground plane radius on the terminal impedance of a monopole

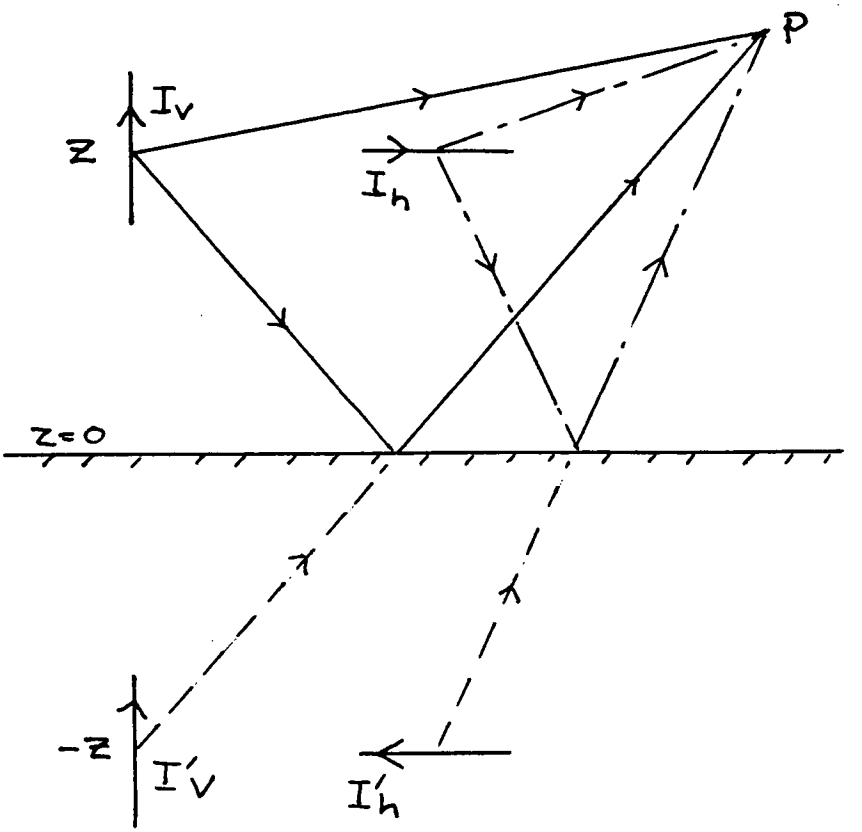

Figure 3.4: An antenna element above an ideal ground plane

antenna, at large radii (r > = 5λ), can be determined from (JASIK [6])

$$\Delta Z = j\frac{60}{kd}e^{-jkd}|k\int_0^h \frac{I(z)}{I(0)}dz|^2 \tag{3.37}$$

where h is the antenna height and d the ground plane diameter.

At smaller radii the radiation resistance approaches half its value at infinite ground plane (WIENER [7]). The effects on reactance are more difficult to determine because of the effects of element radius on monopole reactance.

3.4 IMPEDANCE MATCHING OF ELECTRICALLY SHORT MONOPOLES

The terminal impedance of the electrically short monopole is half that of the corresponding dipole. This can be approximated by (JASIK [6])

$$Z_{mono} = \frac{1}{2}\left\{20(k\ell)^2 - j\frac{120}{k\ell}[ln(\frac{\ell}{a}) - 1]\right\}. \tag{3.38}$$

There are two techniques used to match an antenna to its source impedance (or load in the case of a receive antenna), impedance matching and antenna loading.

In order to match such an impedance to a 50Ω feed the circuit of figure 3.5 is used. Using normalised values of impedance in the circuit

$$\begin{aligned} x_L &= |x_C| \pm \sqrt{r}\sqrt{1-r} \\ x_P &= \mp\frac{\sqrt{1-r}}{\sqrt{r}} \end{aligned} \tag{3.39}$$

for load resistances of less than 50Ω (r < 1).

In practice the inductors used have losses of $r_{loss} = \frac{X_L}{Q_{coil}}$ consequently $r = r_{rad} + r_{loss}$ in 3.39.

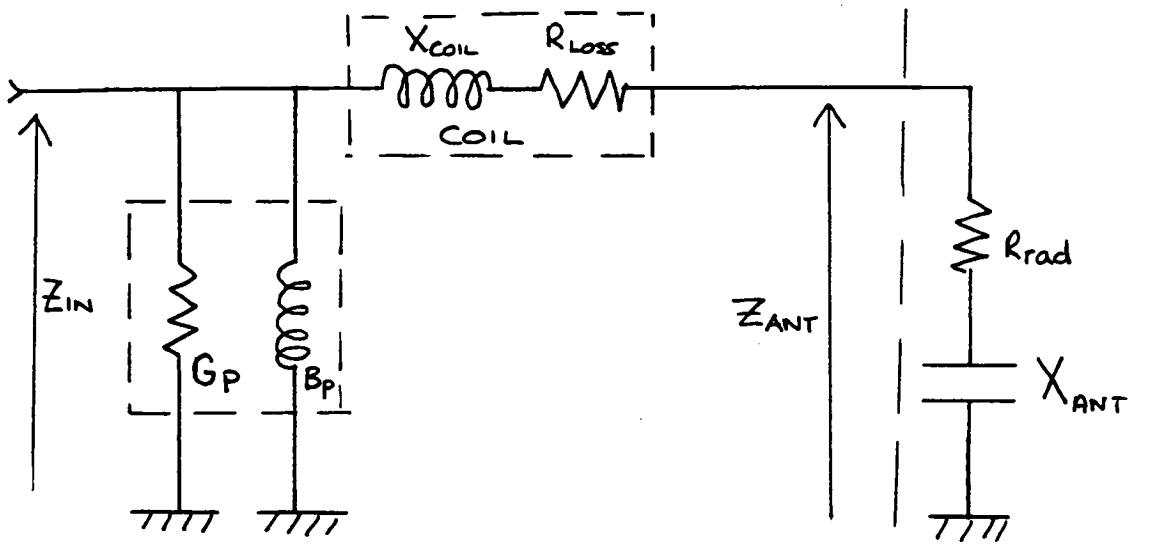

Figure 3.5: Impedance matching of electrically short monopole

Equation 3.39 shows that for a lossless matching system

$$Q = \frac{6}{(k\ell)^3}[ln(\tfrac{\ell}{a}) - 1]$$

and so half power bandwidth is $(\frac{2\pi\ell}{c})^3 f^4 (6[ln(\frac{\ell}{a}) - 1])^{-1}$.

A minimum requirement for voice communications is the CCITT standard for telecommunications, which requires a maximum 3dB variation for the communications link over the frequency range 300Hz to 3.4kHz (or a bandwidth of 6.8kHz for AM or DSB communications). Where two antenna systems of the same type are in use this implies a maximum 1.5dB variation over the frequency range, or a VSWR of $\approx$ 3.0:1.

A practical base matching coil requires extra losses to maintain communications bandwidth. By substituting $r = x_C \frac{BW}{f_0}$ into 3.39 the maximum efficiency can be determined as

$$\frac{r_{rad} f_0}{x_C BW} = \frac{(k\ell)^3}{6[ln(\frac{\ell}{a}) - 1]} \frac{f_0}{BW}. \tag{3.40}$$

Figure 3.6 shows the efficiency and bandwidth of a 2.7m monopole of 32mm radius with coils of Q 100, 200 and 300 over the low HF band, it should be noted that the approximations used for bandwidth break down at the higher frequencies but bandwidth is no longer a problem because the required percentage decreases with increasing carrier frequency.

The block diagram of a commercial Antenna Tuning Unit is shown in figure 3.7. During tuning a pad is placed between the transceiver and tuning circuitry to minimise switching effects on the transceiver. The fixed inductors, which are oriented for minimum mutual inductance, and capacitors are switched in and out of circuit until the detector finds the best match. The detector uses comparators to determine whether the load is capacitive or inductive and whether the magnitude of the loaded impedance is $<$ or $>$ 50Ω. Such systems can rapidly retune an antenna to a new frequency or use preset values for a fixed installation where the antenna impedance is unaffected by local environmental changes.

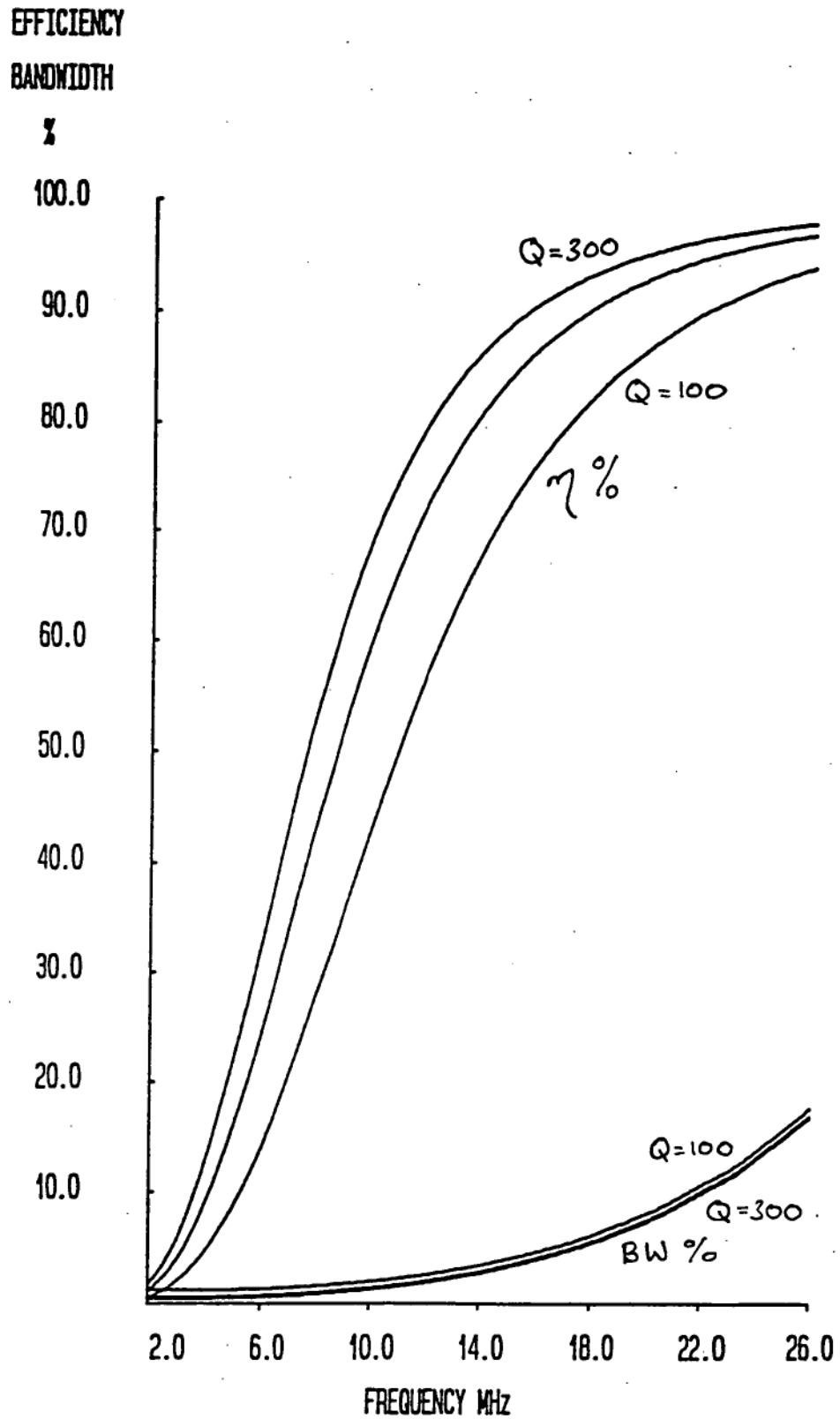

Figure 3.6: The efficiency and bandwidth of a 2.7m whip of radius 16mm based on equation 3.36

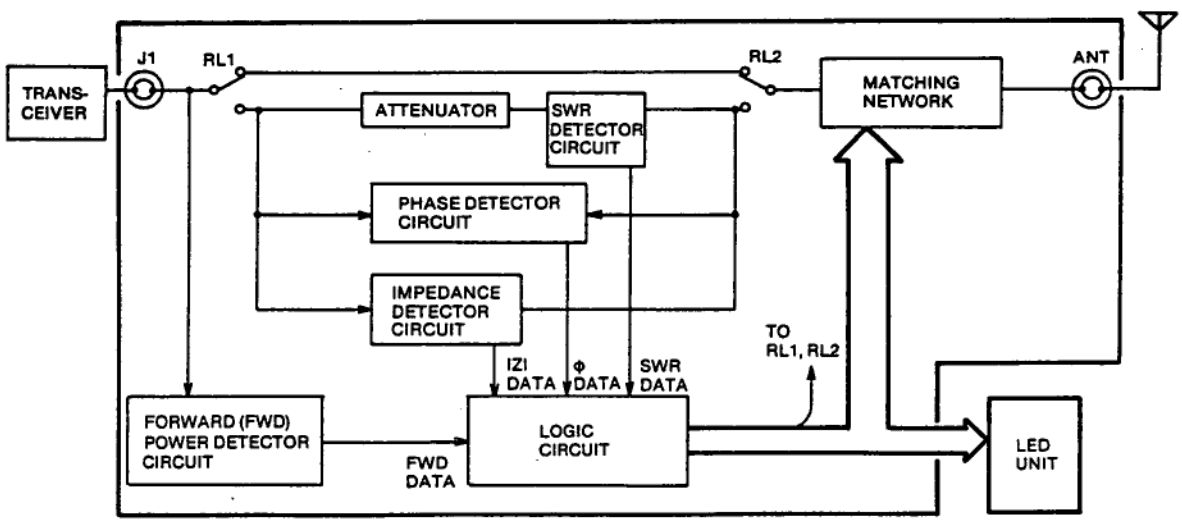

Figure 3.7: Block diagram of a commercial antenna tuning unit

A consequence of the limited number of matching components is that the coil losses need to be high enough to allow tuning over the full frequency range which results in a lower system efficiency.

An important consideration in the use of antenna tuning units is the voltage at the base of the antenna. A lossless antenna and matching system which is transmitting P watts has a base voltage of

$$V_{base} = \frac{19\sqrt{P}[ln(\frac{\ell}{a}) - 1]}{(k\ell)^2}. \tag{3.41}$$

For example a 10m long 90mm diameter monopole, transmitting 1kW at 2MHz, has an rms base voltage of 15kV.

Base mounted antennas of this type are in common use for marine communications and require a base insulator which has structural strength to withstand the bending moment due to wind together with a large dielectric breakdown voltage and minimal loss tangent as

$$P_{loss} = \frac{V_{base}^2}{|X_{C(base)}|} \tan \delta. \tag{3.42}$$

Shorter antennas which have lower power rating still have very high base voltages. For example a 2.5m whip with the same length/diameter ratio as in the previous example has the same base voltage at a power level of 4W. Consequently base matching is unsuitable for mobile HF antennas operating at low frequencies.

These problems are overcome by using the technique known as loading where impedances are placed within the antenna thus modifying the current distribution. Loading can be combined with base matching to improve overall system performance.

There are essentially two types of loading, lumped and continuous.

The effect of position of the load impedance on antenna current distribution is shown in figure 3.8, this is analysed in more detail in the next section.

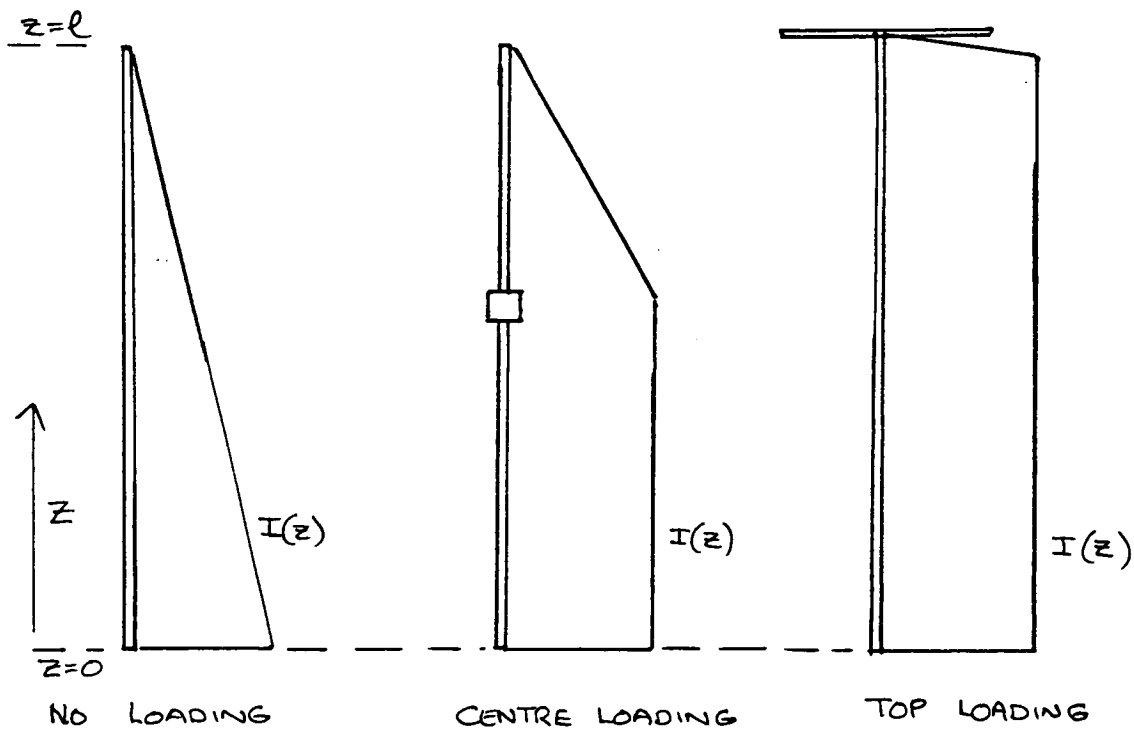

Figure 3.8: The effect of loading on current distribution

Base loading is essentially another form of the impedance matching previously discussed in that it has no effect on the current distribution within the antenna. An autotransformer (usually a tapped coil) is inserted in the base of the antenna. The problems of the tuning unit (high voltage, low efficiency) are those of base loading.

Top loading consists of adding capacitance to the top of the antenna, usually in the form of a capacitive 'hat'. In practical terms this applies to antennas fixed in frequency and location, although there are instances of its use in mobile communications in the amateur handbooks.

The term centre loading is used here to cover all other lumped loading positions and consists of placing an inductor at or near the centre of the antenna.

The alternative to lumped loading is to form the antenna from a helical coil. The radiator is wound on to a dielectric former using either copper wire or tape. As the inductance per unit length depends on coil pitch it is essentially constant with variation of wire diameter or tape width, however the capacitance per unit length is proportional to the surface area. In order to obtain reactive resonance for electrically short antennas this capacitance must be minimised. The radiation resistance of an electrically short helically wound antenna is nearly the same as for the equivalent monopole (KRAUS [3]) however the surface losses are substantially increased due to the increased wire length and decreased diameter. For example a popular 1.5m (five feet) helical whip contains approximately 8m of 0.6mm diameter copper wire and has an ac resistance of 2.0Ω at 3.5 MHz which results in an antenna loss resistance of 1.0Ω, the radiation resistance is approximately 0.12Ω where a sinusoidal current distribution is assumed. The maximum efficiency before matching is therefore 11%. The antenna is then matched to 50Ω by the use of a base mounted auto-transformer which introduces more copper losses.

In order to tune to a number of frequencies helical whip antennas are tapped at fixed points and the user has to run a shorting lead from one tap point to another. While such a system is very low cost it is also inflexible and cumbersome (although remote control of switching using relays is available).

3.5 THE CENTRE LOADED MONOPOLE

The centre loaded monopole and its image is modelled as shown in figure 3.9 using the equivalent dipole with three voltage generators. While the example shown is centre loaded the theory applies equally to any loading position within the antenna. The centre generator, representing the feed, is twice the feed voltage. The other two generators represent the loading coil and its image, the impedance of the loading coil is obtained from the compensation thereom of network theory as

$$V_g = -I(\frac{\ell}{2})Z_L. \tag{3.43}$$

If the current in the symmetric dipole is

$$I_1(z) = \frac{V_T}{Z_1} f_1(\ell_1, z) \tag{3.44}$$

and the currents $I_2(z)$ and $I_3(z)$

$$I_i(z) = \frac{V_g}{Z_i} f_i(\ell_i, z) \tag{3.45}$$

where $f_j(\ell_j, 0) = 1$, j=1-3, and Z_i is the monopole impedance, then the value of V_g and hence Z_L can be determined.

The asymmetrical dipole is modelled as shown in figure 3.10 by the sum of two monopoles of unequal length. This is acceptable because the field at any point on the antenna is mainly due to the currents which are close to the field point. Hence provided the model is not too asymmetric and that continuity of current obtains at the junction of the two monopoles the model is valid.

With $I_a(0) = I_b(0)$ for monopole 1

$$\begin{aligned} I_a(0) &= \frac{V_a}{Z(\frac{\ell}{2})} = I_b(0) = \frac{V_b}{Z(\frac{3\ell}{2})} = \frac{V_g}{Z_T} \\ V_a &= V_g \frac{Z(\frac{\ell}{2})}{Z_T} \end{aligned}$$

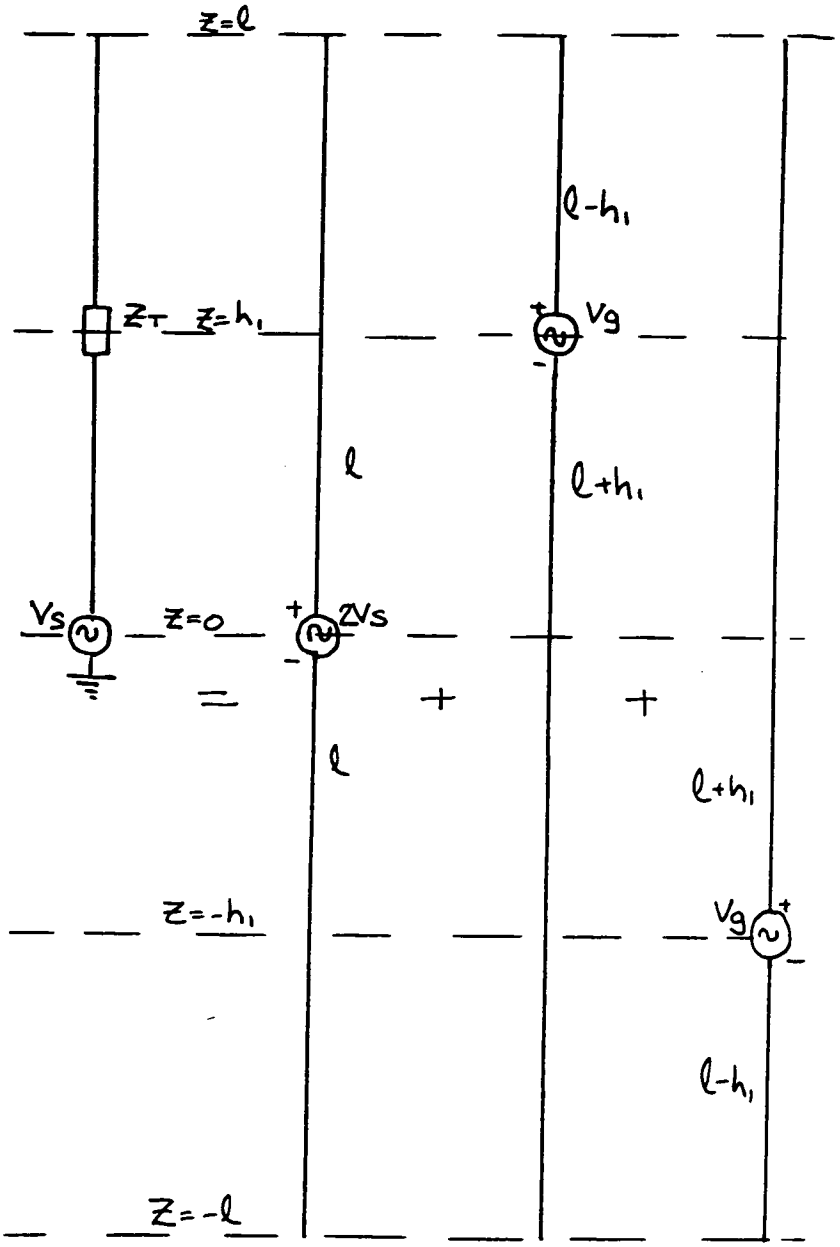

Figure 3.9: The model of the centre loaded monopole

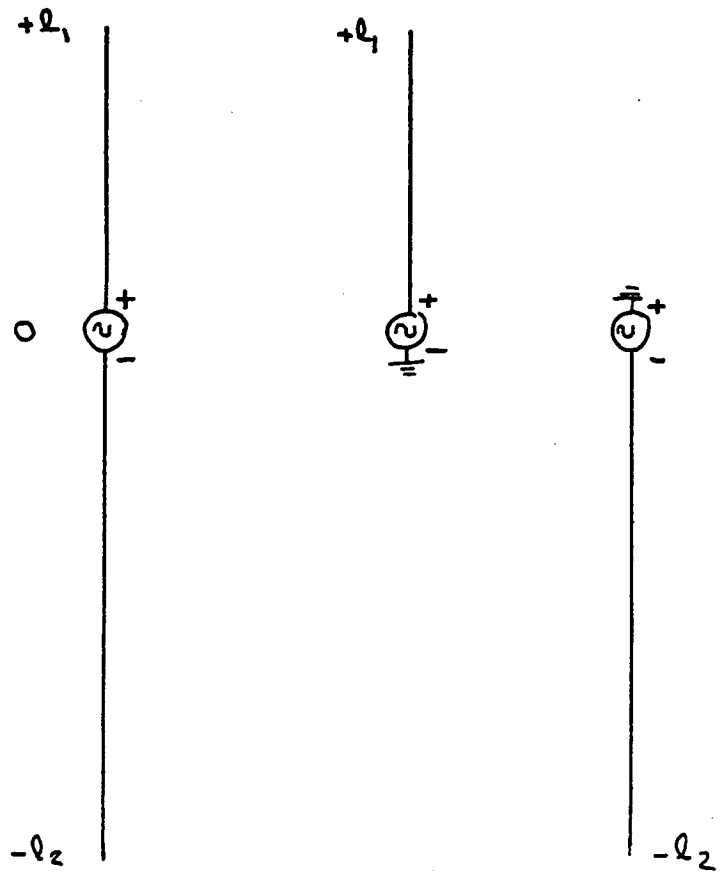

Figure 3.10: The asymmetric dipole

$$
\begin{aligned}
V_b &= V_g \frac{Z(\frac{3\ell}{2})}{Z_T} \\
Z_T &= Z(\frac{\ell}{2}) + Z(\frac{3\ell}{2}) \\
I_2(z') &= \frac{V_g f(\frac{\ell}{2}, z')}{Z(\frac{\ell}{2}) + Z(\frac{3\ell}{2})} \quad z' >= 0 \\
I_3(z') &= \frac{V_g f(\frac{3\ell}{2}, z')}{Z(\frac{\ell}{2}) + Z(\frac{3\ell}{2})} \quad z' <= 0.
\end{aligned} \tag{3.46}
$$

When 3.46 is referenced to z instead of z' the current distribution is

$$
\begin{aligned}
I_2(z) &= \frac{V_g f(\frac{\ell}{2}, z - \frac{\ell}{2})}{Z(\frac{\ell}{2}) + Z(\frac{3\ell}{2})} \quad \ell \geq z \geq \frac{\ell}{2} \\
&= \frac{V_g f(\frac{3\ell}{2}, \frac{\ell}{2} - z)}{Z(\frac{\ell}{2}) + Z(\frac{3\ell}{2})} \quad \frac{\ell}{2} \geq z \geq -\ell.
\end{aligned} \tag{3.47}
$$

Similarly for the second asymmetric dipole of figure 3.9

$$
\begin{aligned}
I_3(z) &= \frac{V_g f(\frac{3\ell}{2}, z + \frac{\ell}{2})}{Z(\frac{\ell}{2}) + Z(\frac{3\ell}{2})} \quad \ell \geq z \geq -\frac{\ell}{2} \\
&= \frac{V_g f(\frac{\ell}{2}, \frac{\ell}{2} + z)}{Z(\frac{\ell}{2}) + Z(\frac{3\ell}{2})} \quad -\frac{\ell}{2} \geq z \geq -\ell.
\end{aligned} \tag{3.48}
$$

The current distribution in the symmetric dipole is

$$
I_1(z) = \frac{V_T}{2Z(\ell)} f(\ell, z). \tag{3.49}
$$

The current $I(\frac{\ell}{2})$ is thus obtained as

$$
\frac{V_g}{Z(\frac{\ell}{2}) + Z(\frac{3\ell}{2})} + \frac{V_g f(\frac{3\ell}{2}, \ell)}{Z(\frac{\ell}{2}) + Z(\frac{3\ell}{2})} + \frac{V_T}{2Z(\ell)} f(\ell, \frac{\ell}{2}). \tag{3.50}
$$

By substituting 3.50 in 3.43 and rearranging

$$V_g = V_T \frac{Z_L}{Z(\ell)} \frac{f(\ell, \frac{\ell}{2})(Z(\frac{\ell}{2}) + Z(\frac{3\ell}{2}))}{Z(\frac{\ell}{2}) + Z(\frac{3\ell}{2}) + Z_L(1 + f(\frac{3\ell}{2}, \ell))}. \tag{3.51}$$

The current at z=0 is

$$\frac{V_g f(\frac{3\ell}{2}, \frac{\ell}{2})}{Z(\frac{\ell}{2}) + Z(\frac{\ell}{2})} + \frac{V_T}{2Z(\ell)} + \frac{V_g f(\frac{3\ell}{2}, \frac{\ell}{2})}{Z(\frac{\ell}{2}) + Z(\frac{3\ell}{2})}. \tag{3.52}$$

3.52 can be rearranged with 3.51 substituted for V_g to give the terminal admittance

$$Y_T = \frac{1}{2Z(\ell)} - \frac{1}{Z(\ell)} \left\{ \frac{Z_L f(\ell, \frac{\ell}{2}) f(\frac{3\ell}{2}, \frac{\ell}{2})}{Z(\frac{\ell}{2}) + Z(\frac{3\ell}{2}) + Z_L(1 + f(\frac{3\ell}{2}, \ell))} \right\}. \tag{3.53}$$

For a normalised admittance of 0.5 (100 Ω)

$$z_L = \frac{z(\frac{3\ell}{2}) + z(\frac{\ell}{2})}{\frac{f(\ell, \frac{\ell}{2}) f(\frac{3\ell}{2}, \frac{\ell}{2})}{(\frac{1}{2} - z(\ell))} - 1 - f(\frac{3\ell}{2}, \ell)} \tag{3.54}$$

where $z = \frac{Z}{50}$.

The change in input admittance with loading impedance is

$$\Delta Y_T = \frac{dY_T}{dZ_L} \Delta Z_L = \left\{ -\frac{Y_0}{Z_L} + \frac{Y_0(1 + f(\frac{3\ell}{2}, \ell))}{Z(\frac{\ell}{2}) + Z(\frac{3\ell}{2}) + Z_L(1 + f(\frac{3\ell}{2}, \ell))} \right\} \Delta Z_L \tag{3.55}$$

where $Y_0 = \{Y_T - \frac{1}{2Z(\ell)}\}$.

A FORTRAN program has been written to evaluate the impedances required for resonance of the loaded monopole. This is in two parts: the first evaluates the various f_i and Z_i and the second the impedances and other interpreted

information. These programs are in the appendices. The equations used to determine f_i and Z_i are those presented by HARRISON [8] which are higher order solutions to the dipole equations.

Figure 3.11 shows the variation of loading impedance with frequency for the 2.7m monopole with a diameter of 32mm, together with the theoretical efficiency of the antenna. The coil reactance varies from $\approx 4k\Omega$ at 2 MHz to $\approx$ 250 Ω at 18 MHz, an inductance range of 144:1. The required Q has a range of 8:1. The graph showing bandwidth represents the total change in loading impedance between the two points VSWR = 3:1. At the low frequencies where f(ℓ,h) and Z(ℓ) are effectively constant for a small change in frequency this represents the actual bandwidth, at higher frequencies the approximation breaks down but, for reasons outlined previously, this is unimportant.

Figures 3.12 to 3.14 show the effects of loading coil position on the various parameters for positions between 0.2ℓ and 0.8ℓ for frequencies of 2, 6 and 10 MHz. As would be expected the higher the loading point the greater the value of inductance required and the higher the efficiency. Bandwidth reduces with the height of loading point in a linear manner.

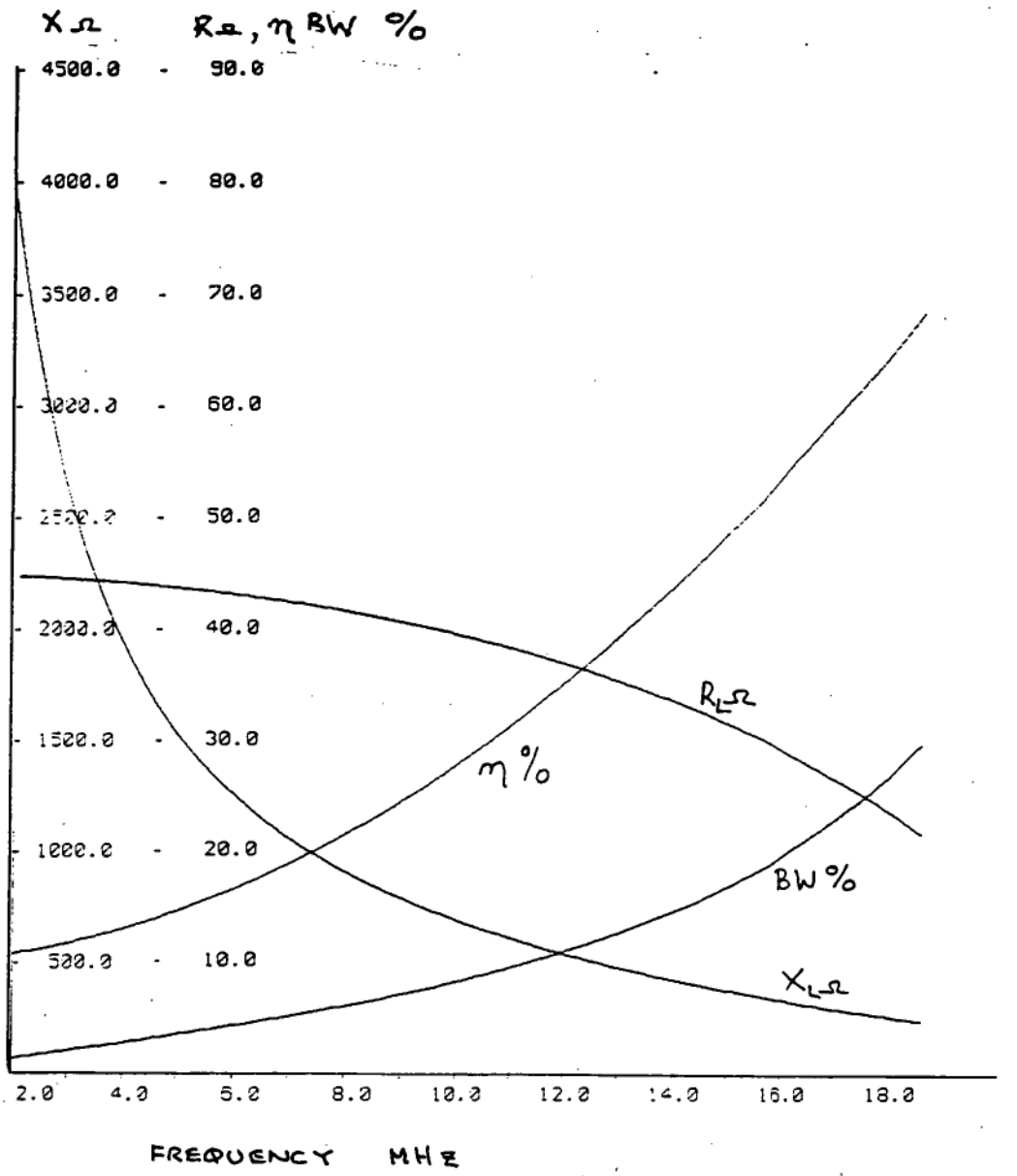

Figure 3.11: Computed values of R, X, BW, and η for the centre loaded antenna using equation 3.54

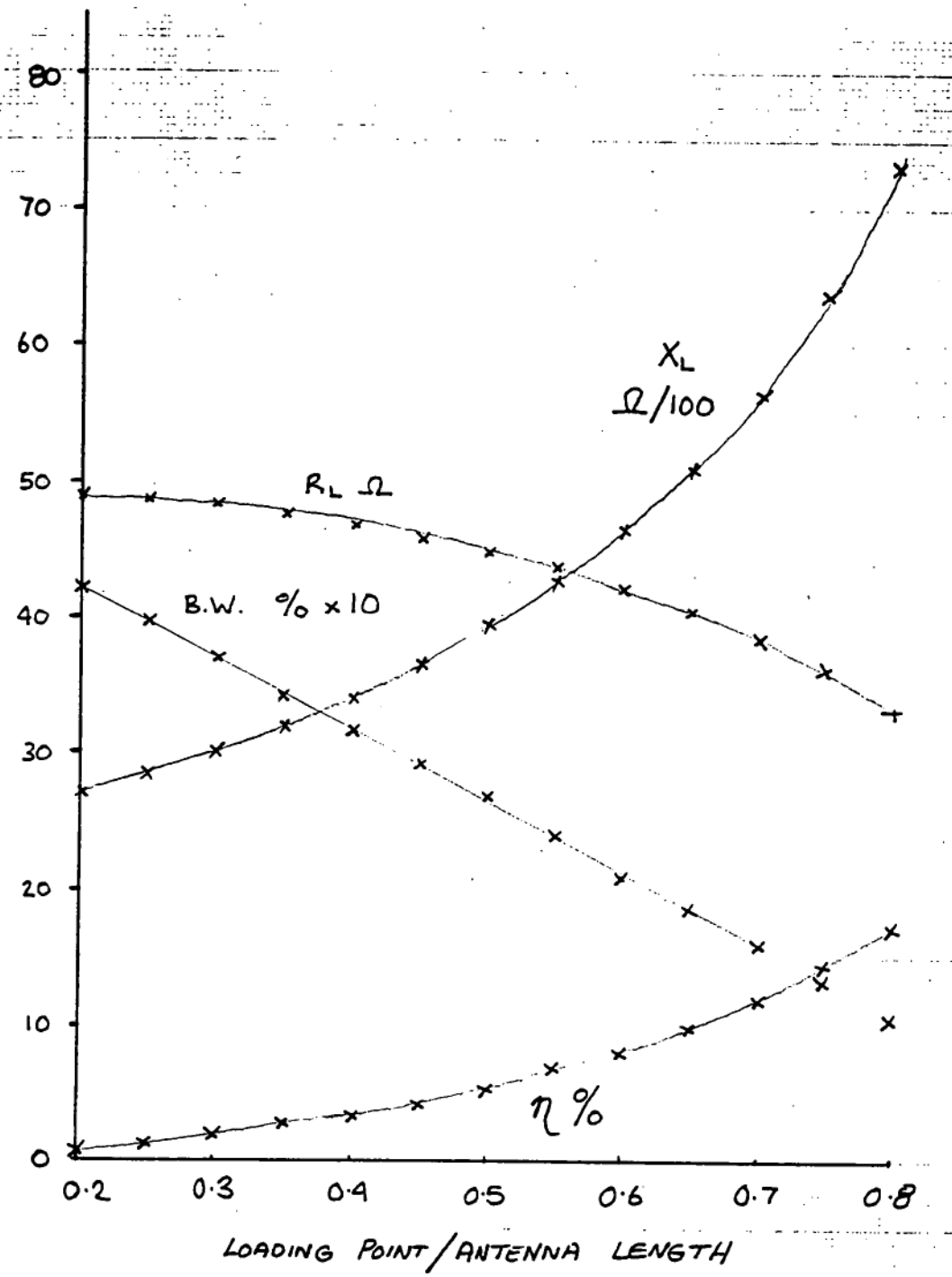

Figure 3.12: The variation of load parameters with load position at 2.0 MHz using equation 3.54

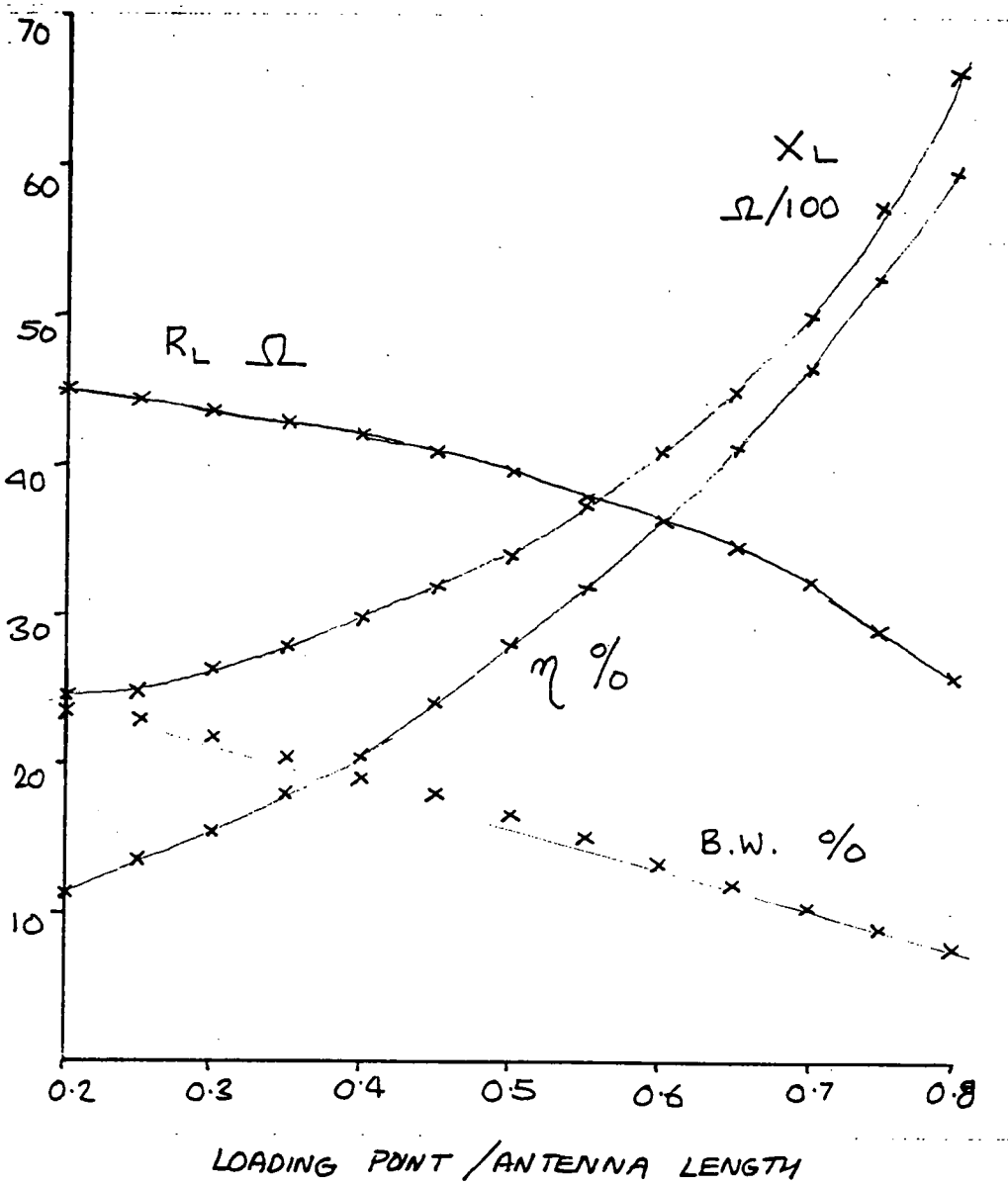

Figure 3.13: The variation of load parameters with load position at 6.0 MHz using equation 3.54

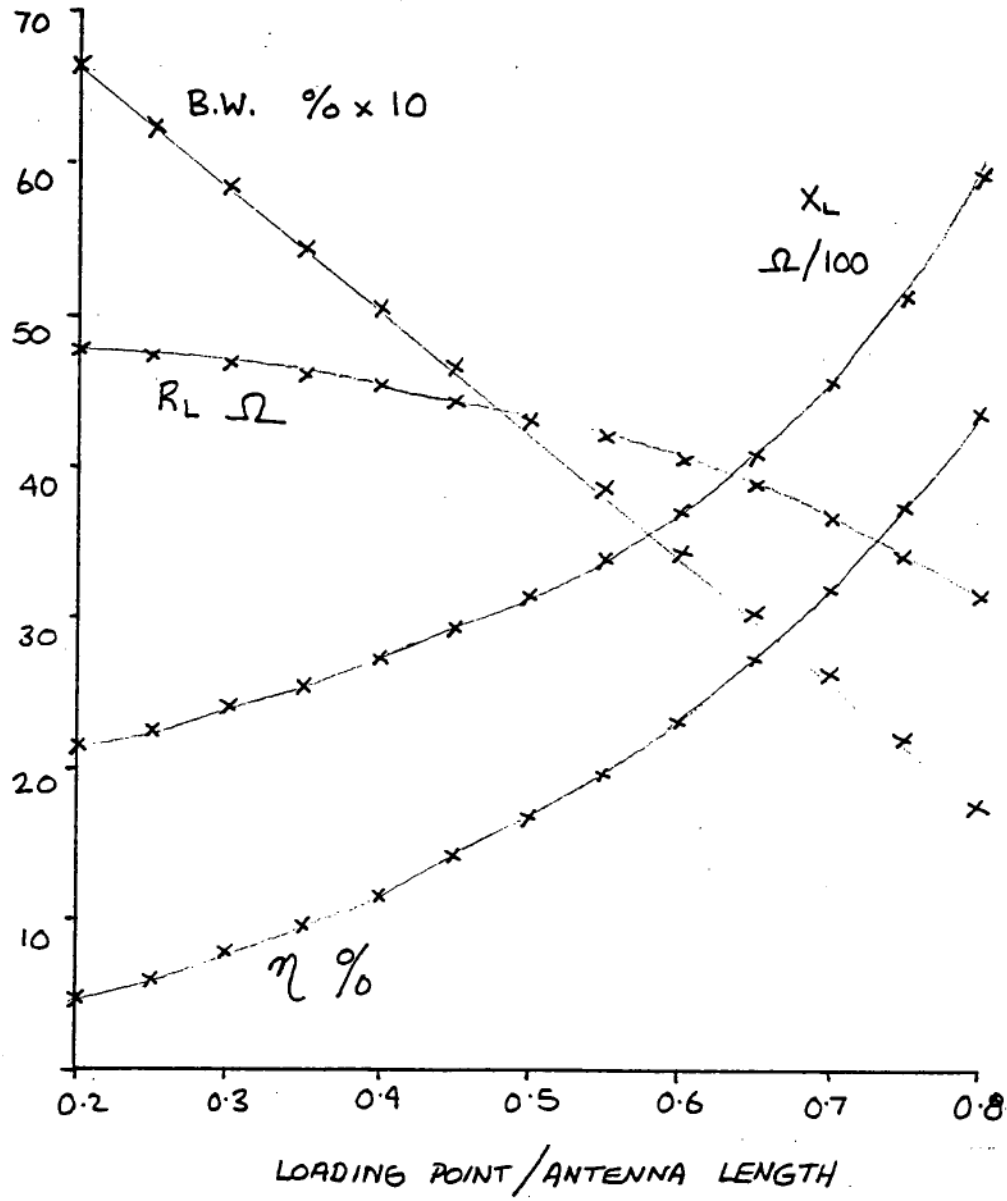

Figure 3.14: The variation of load parameters with load position at 10.0 MHz using equation 3.54

Chapter 4

COMPUTATIONAL ELECTROMAGNETICS

4.1 INTRODUCTION

Computational Electromagnetics (CEM) provides a set of tools for the analysis of complex electromagnetic problems, many of which have no analytical solution, over the entire electromagnetic spectrum. Consequently there are a number of techniques and the selection of the most suitable technique depends largely on the physical dimensions of the problem in terms of wavelength.

The typical approach to a problem is to define a transfer function, using the physical principles and their mathematical interpretation, which establishes a one to one relationship between an input (forcing function) and an output (response). This transfer function, called the field propagator, is converted into a computer model using various numerical approximations to the mathematical processes involved (i.e. integration, differentiation).

For any model to be of use it must be both accurate and economical. Accuracy requires comparison with known results, either experimental or computational, in order to determine errors and an understanding of the techniques involved to avoid instabilities in the computational process. An economical model must suit the manpower and computational facilities available.

One method widely used in CEM and particularly in HF problems is the Method of Moments (MOM [10]). MOM uses the theory of linear operators to describe the field propagator as a matrix operating on an input vector (basis function) to produce the output vector. If the input vector represents current and the output represents voltage then the matrix represents the impedance relationship between the two.

4.2 A MOMENT METHOD SOLUTION

The starting point for the moment method solution are equations

$$\begin{aligned} \nabla \times \underline{H} &= \underline{J} + j\omega\epsilon\underline{E} \\ \underline{H} &= \frac{1}{\mu}\nabla \times \underline{A}. \end{aligned} \tag{4.1}$$

Replacing ω by ck and c by $\frac{1}{\mu\epsilon}$ and using equation for $\underline{A}$ equation becomes

$$\underline{E} = \frac{-j}{4\pi k\eta_0}\int_{V'} \underline{F} dV' \tag{4.2}$$

where

$$\underline{F}(\underline{r}, \underline{r}') = \nabla \times \nabla \times \left\{ \frac{\underline{J}(\underline{r}')exp(jk|\underline{r} - \underline{r}'|}{|\underline{r} - \underline{r}'|} \right\}. \tag{4.3}$$

If the current is flowing in a wire in the $\hat{\underline{x}}_j$ direction then $\underline{F}$ becomes

$$\underline{F}(\underline{r}, \underline{r}') = \nabla \times \nabla \times \left\{ \frac{I_j exp(-jkr)}{r} \hat{\underline{z}}_j \right\} \tag{4.4}$$

where $r = \sqrt{z^2 + {\rho_0}^2 + a^2}$ and $\rho = \sqrt{{\rho_0}^2 + a^2}$ with z, ρ_0 the cylindrical coordinates of point $\underline{r}'$ with the origin at $\underline{r}$.

The curl of a vector $\underline{G}$ in cylindrical coordinates is

$$\nabla \times \underline{G} = \hat{\rho}\left\{ \frac{1}{\rho}\frac{\partial G_z}{\partial \theta} - \frac{\partial G_\theta}{\partial z} \right\} + \hat{\theta}\left\{ \frac{\partial G_\rho}{\partial z} - \frac{\partial G_z}{\partial \rho} \right\} + \hat{z}\left\{ \frac{1}{\rho}\frac{\partial}{\partial \rho}[\rho G_\rho] - \frac{1}{\rho}\frac{\partial G_\rho}{\partial \theta} \right\} \tag{4.5}$$

as the curl is a function of $\underline{r}$ 4.3 becomes

$$\begin{aligned} & I_j \nabla \times \left\{ -\frac{\partial}{\partial \rho} \left[\frac{exp(-jkr)}{r} \right] \hat{\theta} \right\} \\ & = I_j \nabla \times \left\{ (1+jkr) \frac{exp(-jkr)}{r^3} \hat{\theta} \right\} \end{aligned} \tag{4.6}$$

and so the radial component of $\underline{F}$ in 4.4 is

$$\begin{aligned} & I_j \left(-\frac{\partial}{\partial z} \left\{ (1+jkr) \frac{exp(-jkr)}{r^3} \right\} \right) \\ & = I_j \rho z (3 + 3jkr - k^2 r^2) \frac{exp(-jkr)}{r^5} \\ & I_j \left\{ \frac{1}{\rho} \frac{\partial}{\partial \rho} \left[\rho (1+jkr) \frac{exp(-jkr)}{r^3} \right] \right\} \\ = I_j & \left\{ (1+jkr)(2r^2 - 3\rho^2) + k^2 \rho^2 r^2 \right\} \frac{exp(-jkr)}{r^5}. \end{aligned} \tag{4.7}$$

Equations 4.7 are components of the field at $\underline{r}$ referred to the cylindrical coordinate system with origin $\underline{r}'$ and reference vector $\hat{z}_j$ the distance between the two points being $z_{ij}\hat{z}_j$ and $\rho_{ij}\hat{\underline{\rho}}_{ij}$. Hence the value of $\underline{F}$ in the $\hat{z}_i$ direction is

$$F(i,j) = F_{z_j}(i,j)(\hat{\underline{z}}_i \cdot \hat{\underline{z}}_j) + F_{\rho_{ij}}(i,j)(\hat{\underline{z}}_i \cdot \hat{\underline{\rho}}_{ij}). \tag{4.8}$$

By integrating 4.8 over the length of element j the electric field at the centre of element i due to element j is obtained as

$$E(i,j) = \frac{-j}{4\pi k \eta_0} \int_{-\frac{d\ell}{2}}^{\frac{d\ell}{2}} F(i,j) dz_j. \tag{4.9}$$

If I_j is set at 1.0 then the right hand side of 4.9 is therefore the mutual impedance between the two elements i, j at element i.

The above solution is extended to a wire body consisting of n elements by the matrix representation

$$E[i] = \sum_{j=1}^{n} Z[i,j]I[j]. \tag{4.10}$$

By taking the inverse of matrix $Z[i,j]$ the current vector $I[i]$ can be obtained from

$$I[i] = \sum_{j=1}^{n} Y[i,j]E[j] \tag{4.11}$$

where $E[j]$ is the feed voltage vector. The above equation can be applied to a monopole loaded at some point by using the triple generator fed model discussed in chapter 3 so that

$$I[l] = Y[l,l]E[l] + Y[l,k]E[k] + Y[l,m]E[m]$$

with

$$E[k] = E[m] = -Y[k,l]E[l]Z_L. \tag{4.12}$$

A program has been written to evaluate the mutual admittance matrix of a wire body from the mutual impedance matrix. The convergence of the solution for a 1 metre dipole with a diameter of 20.0mm is shown in table 4.1 compared with solutions obtained by other methods.

4.3 COMMERCIAL PACKAGES

MININEC is a suite of BASIC programs based on the Method of Moments which is available in the public domain, however the version used in this project is a commercial package available from ARTECH HOUSE [11] The package also contains a compiled suite of the programs.

MININEC is based on thin wire models of bodies. Each wire is made up of a number of segments with current pulses to be determined on each segment due to a number of voltage sources. There is provision for lumped parameter loading of wire segments making it a useful package to analyse the loaded monopole.

no of segments	Zin
3	3.35-j606
5	2.63-j781
7	2.33-j893
9	2.14-j971
13	1.97-j1086
17	1.86-j1153
21	1.82-j1165
25	1.78-j1169
3 [4]	1.10-j1358
hallens	1.85-j1244

Table 4.1: Impedance of 1m dipole from various techniques

ELNEC is a similar package which is based on MININEC but features improved user interface plus a number of minor improvements.

Each program package allow the user to analyse problems either in free space or above a ground plane and provide facilities for graphical representation of calculated data such as current distribution, radiation pattern etc.

Table 4.2 shows the results for a number of antenna problems. The 'calculated' column was obtained during the calculation of the load impedances for the loaded monopole. The monopole impedances are obtained from a 28 segment model of a monopole above an ideal ground plane. The same model was used to determine the load impedances at segment 14 for resonance of the loaded monopole shown in table 4.3. The dipole impedances in table 4.4 were obtained using a 33 segment model. A comparison between the two sets shows a 1-2% difference between the equivalent monopole impedances for a 70% difference in segment length (33 at 0.164m and 28 at 0.096m). The CEM values are within 5% of the calculated values.

A comparison between the CEM values of load impedance and those obtained in chapter 3 some little difference between reactances but no change in load resistance for both ELNEC and MININEC. The load impedances were not actually calculated using either program package, that facility is not available, but estimated impedance values were placed in the segmented

		MININEC	ELNEC	calculated
1.35m	2 MHz	0.027-j3435	0.025-j3430	0.030-j3659
	6 MHz	0.229-j1135	0.229-j1133	0.275-j1229
	10 MHz	0.647-j669	0.647-j668	0.756-j719
2.7m	2 MHz	0.109-j2102	0.109-j2097	0.122-j2183
	6 MHz	1.00-j675	1.00-j674	1.09-j713
	10 MHz	2.96-j374	2.95-j373	3.19-j392
4.05m	2 MHZ	0.25-j1538	0.26-j1539	0.28-j1578
	6 MHz	2.4-j470	2.4-j470	2.52-j491
	10 MHz	7.5-j227	7.5-j227	7.8-j236

Table 4.2: CEM results for monopole above ground plane

		MININEC	ELNEC	calculated
2.7m	2 MHz	37+j4035	35.5+j4025	44.77+j3923
	6 MHz	37+j1300	37+j1300	43.1+j1253
	10 MHz	37+j717	37+j715	39.5+j685

Table 4.3: CEM results for loaded monopole above ground plane

model until near resonance was reached (49.5 to 50.5 Ω with reactance $<$ 2 Ω). The load impedances are added to the calculated self impedance of the relevant segment before the matrix is inverted to obtain the admittance matrix whereas the calculated impedances are obtained from superposition. The method of superposition is an accurate method for this type of problem and so there is a need for more investigation into the use of the two program packages under these circumstances.

		MININEC	ELNEC
1.35m	2 MHz	0.053-j6957	0.053-j6980
	6 MHz	0.473-j2298	0.476-j2306
	10 MHz	1.33-j1354	1.34-j1358
2.7m	2 MHz	0.22-j4235	0.22-j4235
	6 MHz	2.05-j1360	2.05-j1363
	10 MHz	6.0-j753	6.0-j754
4.05m	2 MHZ	0.51-j3103	0.51-j3109
	6 MHz	4.86-j948	4.87-j950
	10 MHz	15.12-j458	15.13-j459

Table 4.4: CEM results for dipole in free space

Chapter 5

THE MOONRAKER 'AT' SERIES ANTENNA

5.1 INTRODUCTION

The 'AT' series centre loaded monopole antenna has been manufactured by MOONRAKER AUSTRALIA for several years and to date several thousand have been sold. Early problems associated with the antenna design have been structural, due to vibration, and environmental.

The antenna is manufactured in two main versions: one 2.7m high with anti-vibration mount for mobile use and the other 5.1m high for base station and marine use. The vast majority of sales have been of the mobile type antenna which is the antenna used in the experimental work. The mobile version is currently available in two frequency ranges 2-13.5 MHz and 3.5-18 MHz (low and high bands), where the antenna can be tuned to a VSWR of better than 1.5 over the frequency range. Recent developments have resulted in a version which covers the range 2-30 MHz using the same technology.

5.2 THE PRODUCTION ANTENNA

The antenna is shown in figure 5.1. It is tuned by mechanically varying the value of the loading coil impedance. The approximate values of loading coil impedance are shown in figure 3.11 for the centre loaded antenna. The

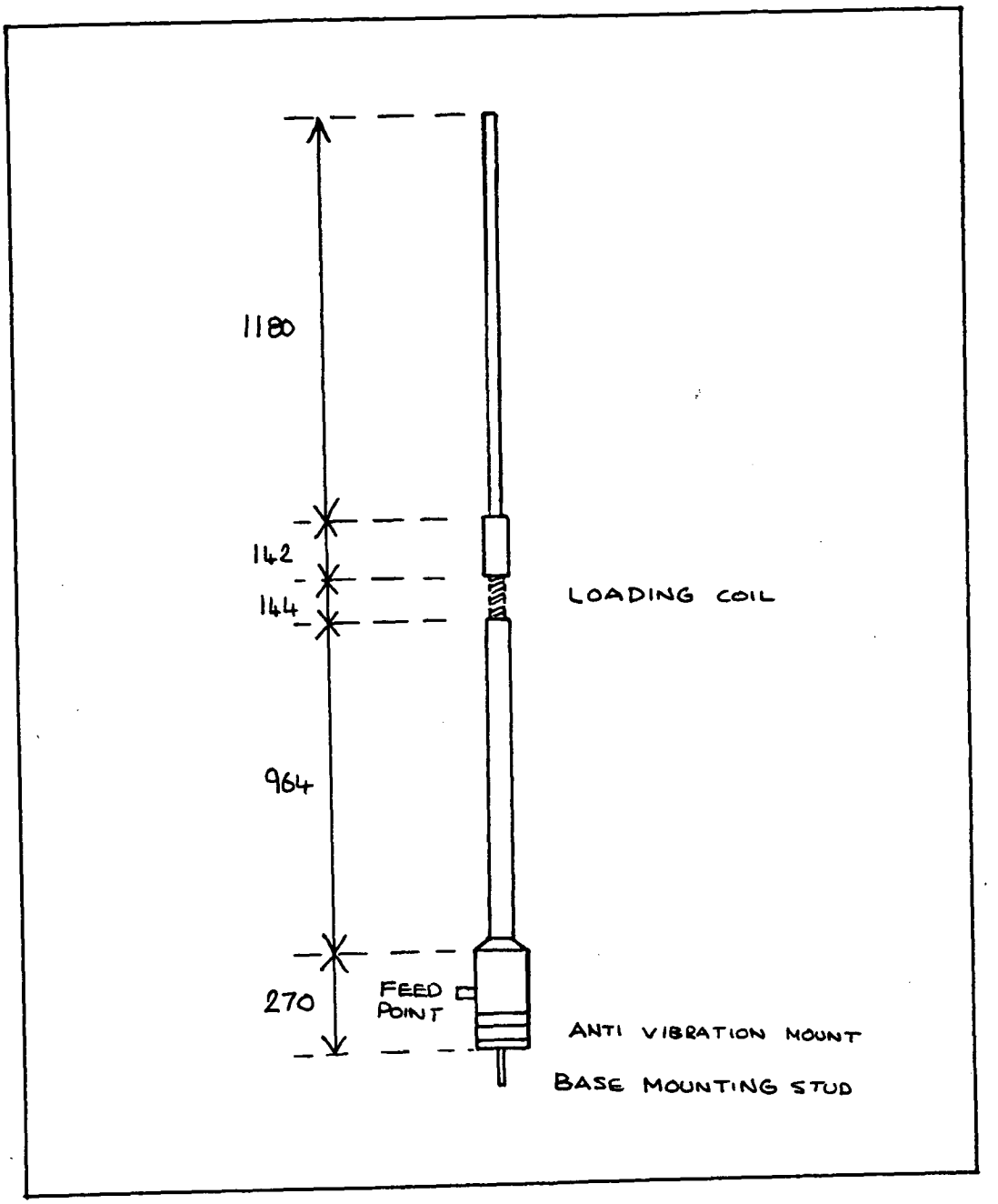

Figure 5.1: The 2.7m MOONRAKER 'AT' series antenna

offset feed point h_2 and difference in load impedance point make these values indicative only, these effects will be investigated later in this chapter. The variable loading coil (figure 5.2) consists of a fixed winding with variable core properties. The properties (μ_r , Q) are varied by driving the core assembly into or out of the coil. Magnetic coupling between the coil and core is through a fibreglass coil former resulting in a gap between coil and core of $\approx$ 1mm, which is the limit imposed by the structural requirements, the coil assembly is strengthened by a fibreglass shroud which transmits the bending force due to the top section of the antenna providing stress relief to the coil former.

The position of the core is varied by means of a stepping motor which drives a lead screw with a pitch of 7.0mm. The stepping motor rotates at 200 steps per revolution providing a lineal resolution of 35μm.

The main difference between the two frequency ranges is in the number and pitch of turns in the coil and the components used for the core. Typically the low band antenna has 71 turns wound at 22 t.p.i. (turns per inch) and the high band antenna 41 turns wound at 13 t.p.i. . Before production the components are tested and the number of turns for a particular combination is determined in order for the antenna to meet specifications. The test antenna used in this work differs from the production antenna in that it has a removeable coil former in order to facilitate speedy changing of the core components and the coil has 75 turns wound at 22 t.p.i. in order to increase travel at the low frequency end. Electrical continuity is by a tight slide fit between the removeable section of the antenna and the fixed base.

The magnetic core, which is D.C. insulated from the antenna radiators, consists of three magnetically different components, which are held together by a nylon former. The components are

(i)The ferrite core :

The ferrite core is a polycrystalline soft ferrite material which is manufactured by blending $\approx$50%(mol) of iron oxide with (divalent) nickel zinc oxide together with small quantities of magnesium,managanese, copper or cobalt (The exact details are not available from the manufacturer), the mixture is extruded and fired to produce a ceramic ferrite rod. The rod is then cut

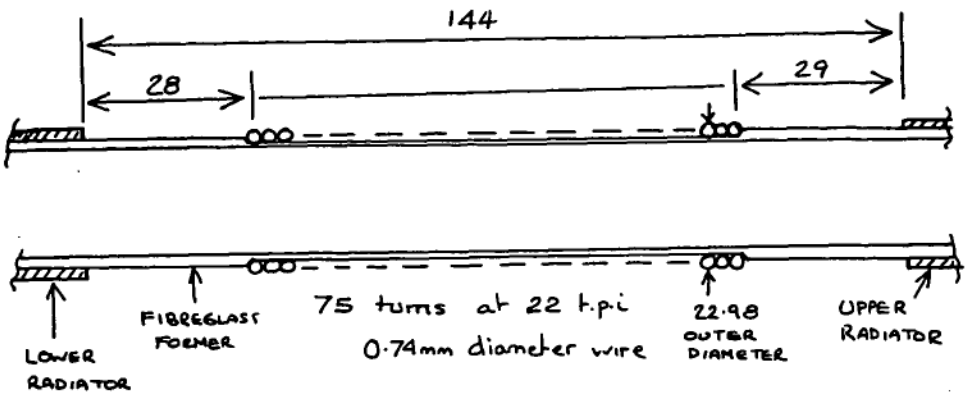

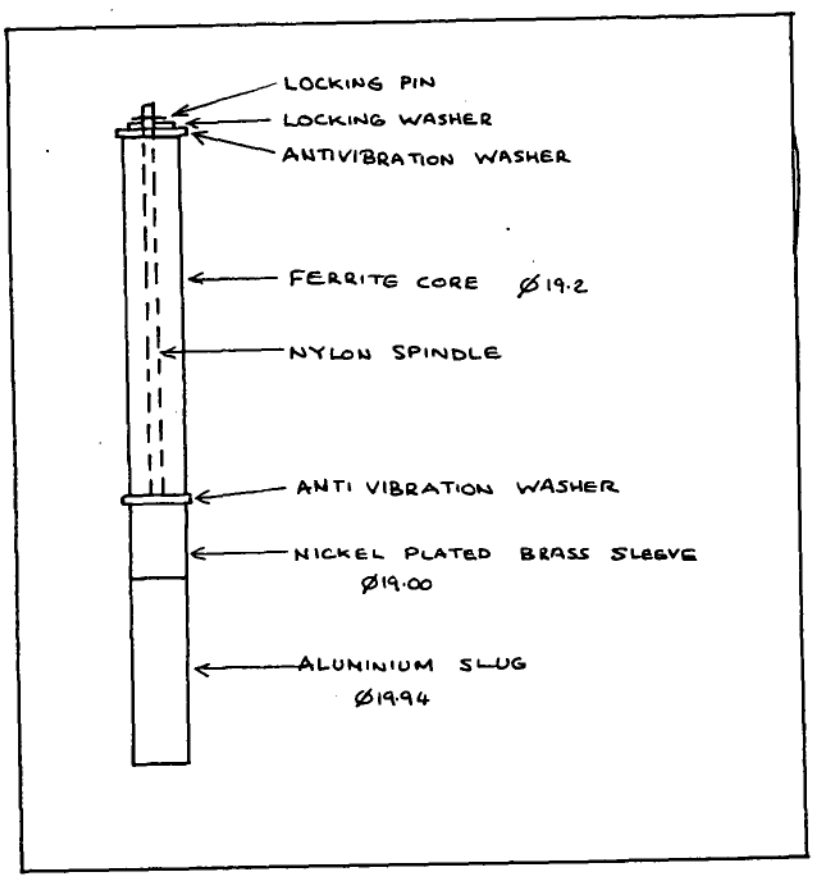

Figure 5.2: Details of the loading coil

initial permeability	μ_i	125	
maximum permeability	μ_m	450	
saturation flux density	B_s^*	0.235	T
residual flux density	B_r	0.120	T
Curie Temperature	T_c	350	^oC
resistivity	ρ	10^{10}	Ω-m
frequency range		0.2-10	MHz
Temperature Coefficient	$\frac{\delta\mu_i}{\delta T}$	0.15	$\%/^oC$
loss factor	$(\mu_i Q)^{-1}$	32×10^{-6} @ 2.5MHz	
coercive force	H_c	128	A/m
thermal conductivity		$\approx$4.0	W/(m K)
specific heat		.750	J/(kg K)
density		4700	kg m^{-3}

(* measured at 796 A/m (10 Oersteds))

Table 5.1: Typical properties of the material

the required length. Because the rods are extruded a small percentage are outside the specification for parallel sides, an important requirement for the core when driven into a coil former.

The properties of the material are shown in figure 5.3 and summarised in table 5.1.

The initial permeability varies between $\approx$120 and $\approx$160 over the frequency range 1MHz to 20MHz and the losses ($\frac{\tan\delta}{\mu_i}$) between 3.0 $\times 10^{-5}$ to 3.0 $\times 10^{-4}$ over the same frequency range. The effect of temperature on initial permeability is an increase of $\approx$ 10% over the temperature range 20 to 40 degrees celsius but is small above that until 200 degrees. The losses in the loading coil are dissipated in the ferrite core at low frequency and so the operating temperature will be higher than ambient and will depend on the duration of the transmission.

The initial permeability (μ_i) shown in the manufacturers data (figure 5.3) is obtained by measuring the inductance of a toroid which forms a closed magnetic circuit, this value cannot be used for a rod. In a magnetic circuit the

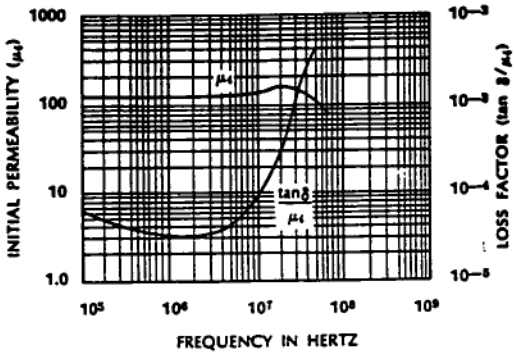

FIGURE 1:
Initial Permeability and Loss Factor vs Frequency. Measured on a .375 inch OD toroid using a Boonton Electronics Model 63-H Inductance Bridge and a Boonton Radio Type 260A Q Meter.

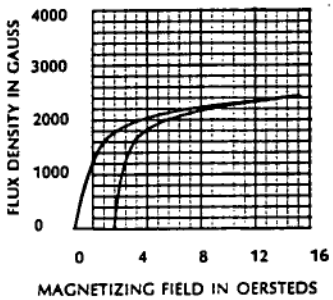

FIGURE 2:
Hysteresis loop for a 1 inch OD toroid in 61 material measured on a DC Hysteresigraph.

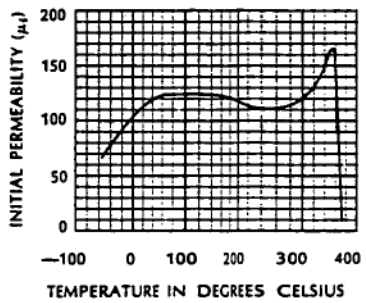

FIGURE 3:
Initial Permeability vs Temperature including the Curie point. Measured on a 1 inch OD toroid using a Boonton Electronics Model 63-H Inductance Bridge at 100 KHz.

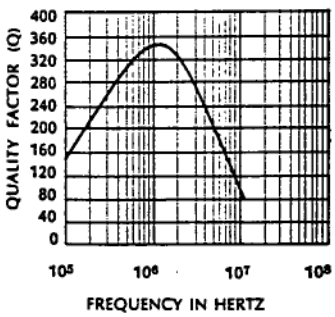

FIGURE 4:
Quality Factor vs Frequency for a .375 inch OD toroid in 61 material. Test equipment included a Boonton Electronics Model 63-H Inductance Bridge and a Boonton Radio Type 260A Q Meter.

FIGURE 5:
μ_i Q Product (Initial Permeability x Quality Factor) vs Frequency. Test equipment included a Boonton Electronics Model 63-H Inductance Bridge and a Boonton Radio Type 260A Q Meter.

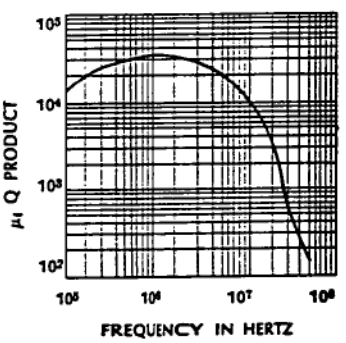

Figure 5.3: Ferrite characteristics from the FAIR-TITE product guide, FAIR-RITE PRODUCT CORP. Wallkill N.Y. USA

introduction of the large air gap represented by the rod substantially changes the closed magnetic circuit characteristics. This change is represented by the shape factor of the ferrite rod (figure 5.4). In addition the rod is hollow and so the actual permeability will be less than the rod permeability.

For production purposes the ferrite cores are tested using a MARCONI Circuit Magnification Meter using a fixed coil and a series capacitance of 40pF which is preset using a reference coil of $10\mu H$ ($\pm 5\%$) the capacitor being tuned for resonance at 7.958 MHz (see 5.5). The current through the coil is a few milliamps, which is considerably less than the current under normal operating conditions (1A rms at 50W). The core is placed in the coil and the frequency varied until a maximum is measured, the coil Q and resonant frequency are recorded. The distribution of these values for a typical production batch of ferrites is shown in table 5.2.

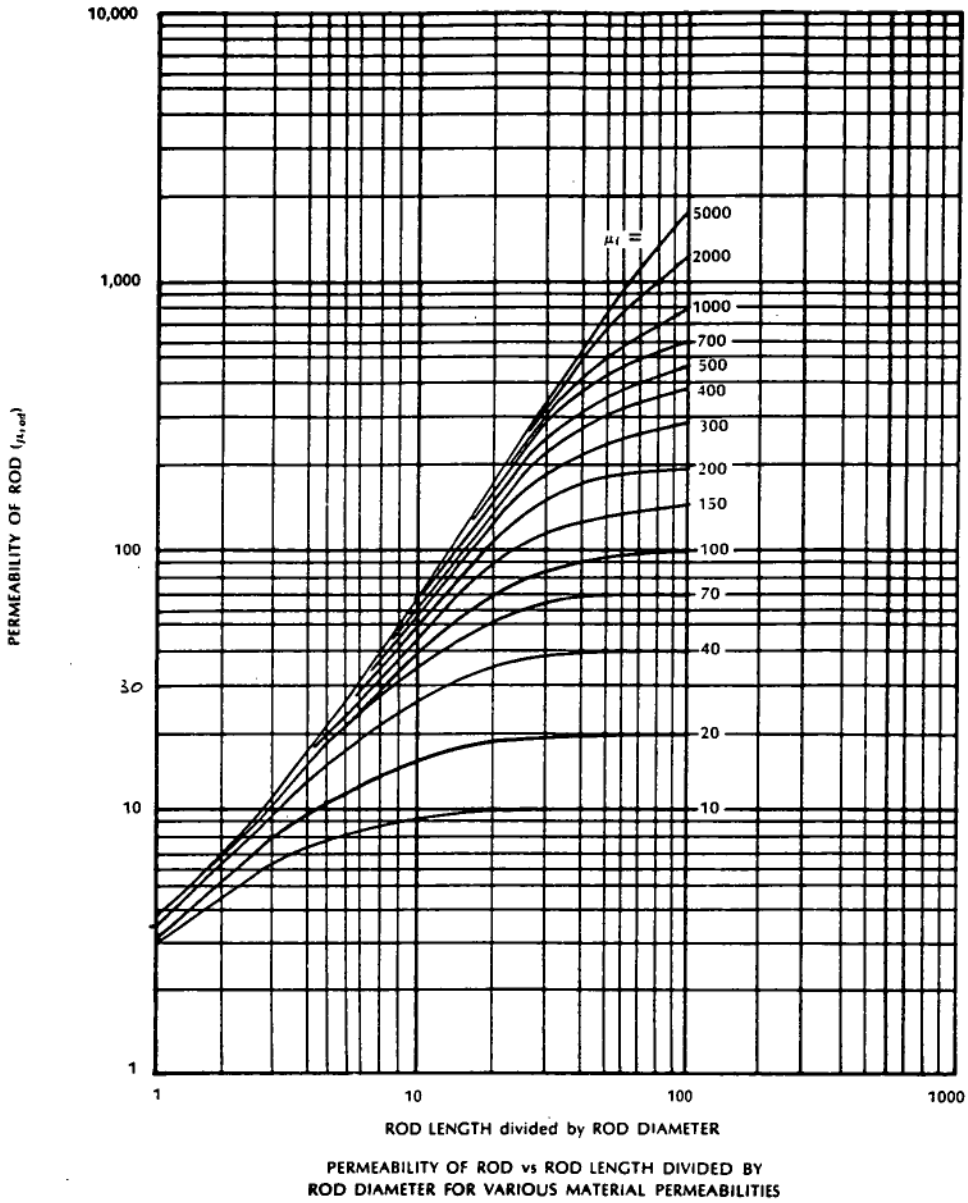

Figure 5.4: Permeabilty of ferrite rods

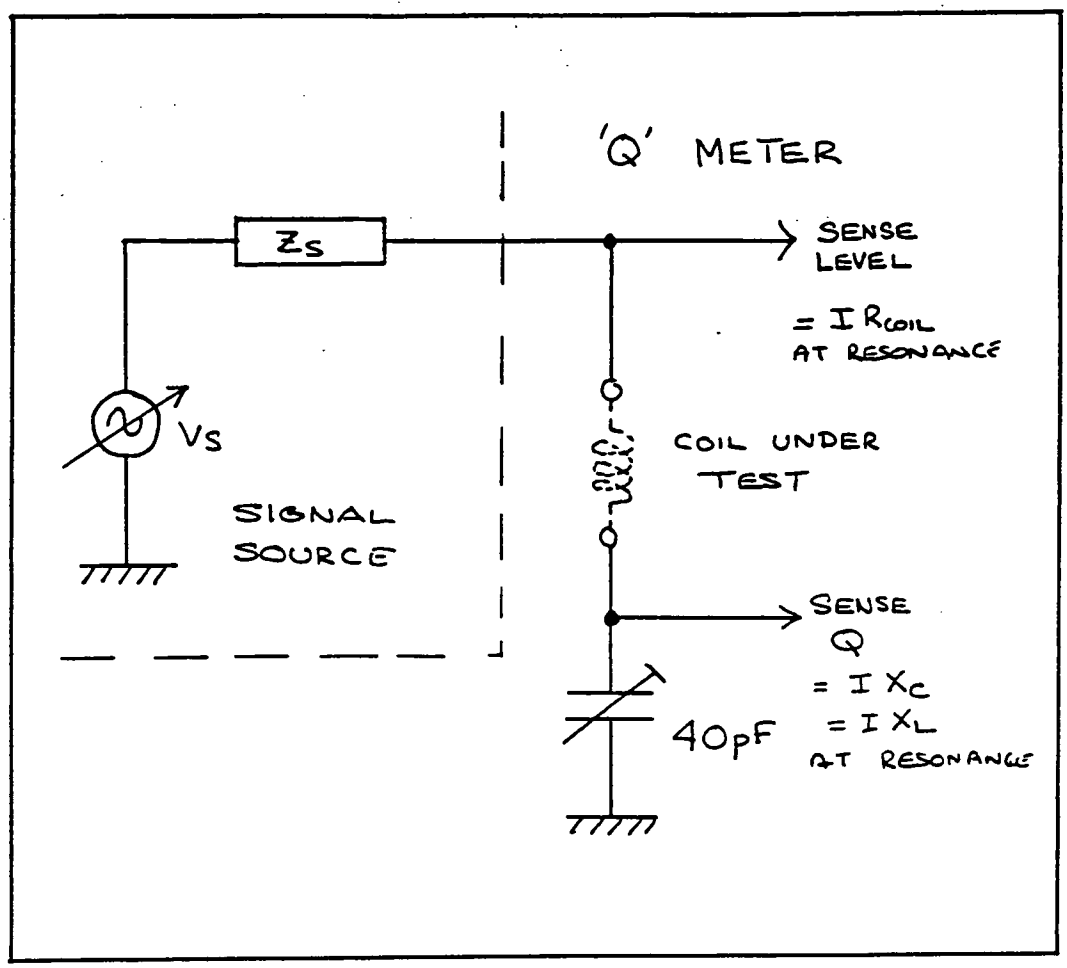

Figure 5.5: Measurement of rod permeability and Q

ferrite	freq	Q	ferrite	freq	Q
1	2851	100	31	2865	90
2	2825	90	32	2875	100
3	2825	90	33	2874	95
4	2825	90	34	2876	97
5	2817	90	35	2854	84
6	2807	95	36	2851	90
7	2809	95	37	2860	90
8	2830	90	38	2867	92
9	2823	97	39	2887	95
10	2825	97	40	2862	87
11	2805	95	41	2879	85
12	2825	95	42	2810	97
13	2836	87	43	2809	95
14	2809	95	44	2828	92
15	2827	97	45	2821	95
16	2868	90	46	2807	90
17	2871	88	47	2821	95
18	2866	90	48	2814	95
19	2853	87	49	2798	95
20	2883	100	50	2820	92
21	2870	96	51	2813	90
22	2876	100	52	2809	90
23	2839	100	53	2811	92
24	2892	95	54	2824	90
25	2848	100	55	2802	90
26	2877	97	56	2860	95
27	2867	97	57	2856	95
28	2850	97	58	2862	90
29	2850	93	59	2846	97
30	2876	97	60	2859	93

Table 5.2: Ferrite Q and resonant frequency for a batch of 60 ferrite cores

(ii)The nickel sleeve :

The nickel plated brass sleeve provides a lossy short circuit. The number of turns short circuited in the coil is fixed when the drive is above a certain point hence the effective losses are fixed with position but vary with frequency. Below this point losses vary with position. The losses also vary with the depth of the nickel plating and so different losses can be produced by varying plating depth.

Pure wrought nickel (alloy 200) has a maximum permeability of 1000 and a resistivity (ρ) of $9.6 \times 10^{-8} \Omega m$. The presence of impurities can cause variations in ρ of -20% in this value.

From equation 3.8 the skin depth of nickel is thus $\frac{4.93}{\sqrt{f}} \mu m$ where f is in MHz thus a coating of $\approx$0.02 mm is greater than five skin depths for 2 MHz and above. Measured depth of nickel plating on 0.81mm diameter wire used to hold the sleeves during plating is 0.03mm (0.880mm $\pm$ 0.005mm after plating, 0.815mm $\pm$ 0.005 before plating from a set of 20 measurements) therefore the electrical depth of plating will only vary with the permeability of the nickel.

The brass is prepared by cleaning with an appropriate acid and therefore its surface conductivity is unaffected. The nickel plating is by a commercial plating company which produces among other items automotive bumper bars.

For production purposes the nickel sleeves are tested using the same equipment as the ferrite rods but at a fixed frequency (6.900 MHz). The nickel sleeve is placed on an aluminium test sleeve and slowly inserted into the test coil, the maximum value of Q is recorded. Nickel sleeves with Q values at the extremities of the useful range are used as references and are tested with each batch in order to compensate for variations in test conditions. Measurements do vary depending on the direction in which the nickel sleeve is placed on the aluminium sleeve, the Q can vary by as much as 10%. The Q also permanently changes if the sleeve is heated (i.e. by being subjected to large RF powers). The reason for this is that the crystalline structure of the

nickel plating is subject to severe stress in order to achieve the high standard of finish required for ornamental plated products. The crystal orientations (111, 110 and 101) have considerably different values of permeability. When heated the stress is relieved and permeability changes. Under normal operating conditions for the antenna the nickel sleeve does not dissipate high powers and is thermally connected to the aluminium shorting sleeve so it is not expected that the temperature will be sufficient to permanently change the characteristics of the nickel sleeve.

(iii)The aluminium shorting slug

This provides effective shorting of the lower section of the coil and is manufactured from standard aluminium tubing.

The efficiency of the centre loaded antenna at low frequencies is low ($< 10\%$) and so the effects of power dissipation within the ferrite core are important in determining the stability of the antenna.

Figure 5.4 shows that a rod with an initial permeability of 125 and a length-diameter ratio of 6.6 has a rod permeabilty of ≈ 25 and a variation of $\pm$ 2 in rod permeability for a variation of $\pm$ 25 in initial permeability. The change in initial permeability due to a temperature rise from 20 to 40 degrees celsius is $\approx +20$. An approximation to the loading reactance at 2.0 MHz is $3.5k\Omega$ so a change in temperature of +20 degrees will increase the reactance to $\approx 3.75\ k\Omega$ which is more than enough to detune the antenna. Analysis of the thermal conductivity of the ferrite core for a uniform power dissipation throughout results in a temperature difference between the centre and the outer layer of 0.16 degrees per watt. For a power dissipation of 100W in the ferrite the time taken for a temperature rise of 16 degrees is 20 seconds . This simple analysis ignores several aspects of thermal analysis but reveals that there is a potential problem in the use of the ferrite material in situations where long term power dissipation is required such as data transmission using FSK.

The measurements on the ferrite rods and nickel sleeves obtained before this

project do not permit accurate prediction of antenna performance, partly because the lack of repeatability of measurements due to unsuitable setup procedure .

The lack of a reliable model of the antenna makes product development a time consuming task and so the first objective is to produce a viable model which is economical for commercial research and is hopefully useful in a more theoretical environment.

Of interest are the effects of μ_{rod} , Q_{rod}, and Q_{ni} on the antenna input impedance and prediction of the frequency response of an antenna given the core parameters in order to reduce the rejection rate of components and hence the manufacturing costs.

5.3 A MODEL OF THE ANTENNA

The model of the loaded antenna developed in chapter 3 requires modification in order to apply more accurately to the 'AT' series antenna. The various differences are: the offset feed, the lower loading point (which also changes as the shorting sleeve rises in the coil) and the change in antenna radius (the top whip section) and the finite load dimensions (compared with the point load used in the model).

Harrisons model is adapted to the 'AT' series antenna by replacing the symmetric dipole in figure 3.9 with two asymmetric dipoles representing the offset feed in the antenna; this is shown in figure 5.6.

Each single term involving the symmetric dipole is therefore relaced by the sum of the two equivalent terms in the asymmetric dipoles. The resulting equation for terminal admittance is

$$\begin{aligned} Y_{IN} &= Y0 - \frac{Z_L * F1 * F2}{Z1 * Z2} \\ Y0 &= \frac{(1 + f(l + h_2, 2h_2))}{Z(l - h_2) + Z(l + h_2)} \\ F1 &= (f(l + h_1, h_1 + h_2) + f(l + h_1, h_1 - h_2)) \end{aligned}$$

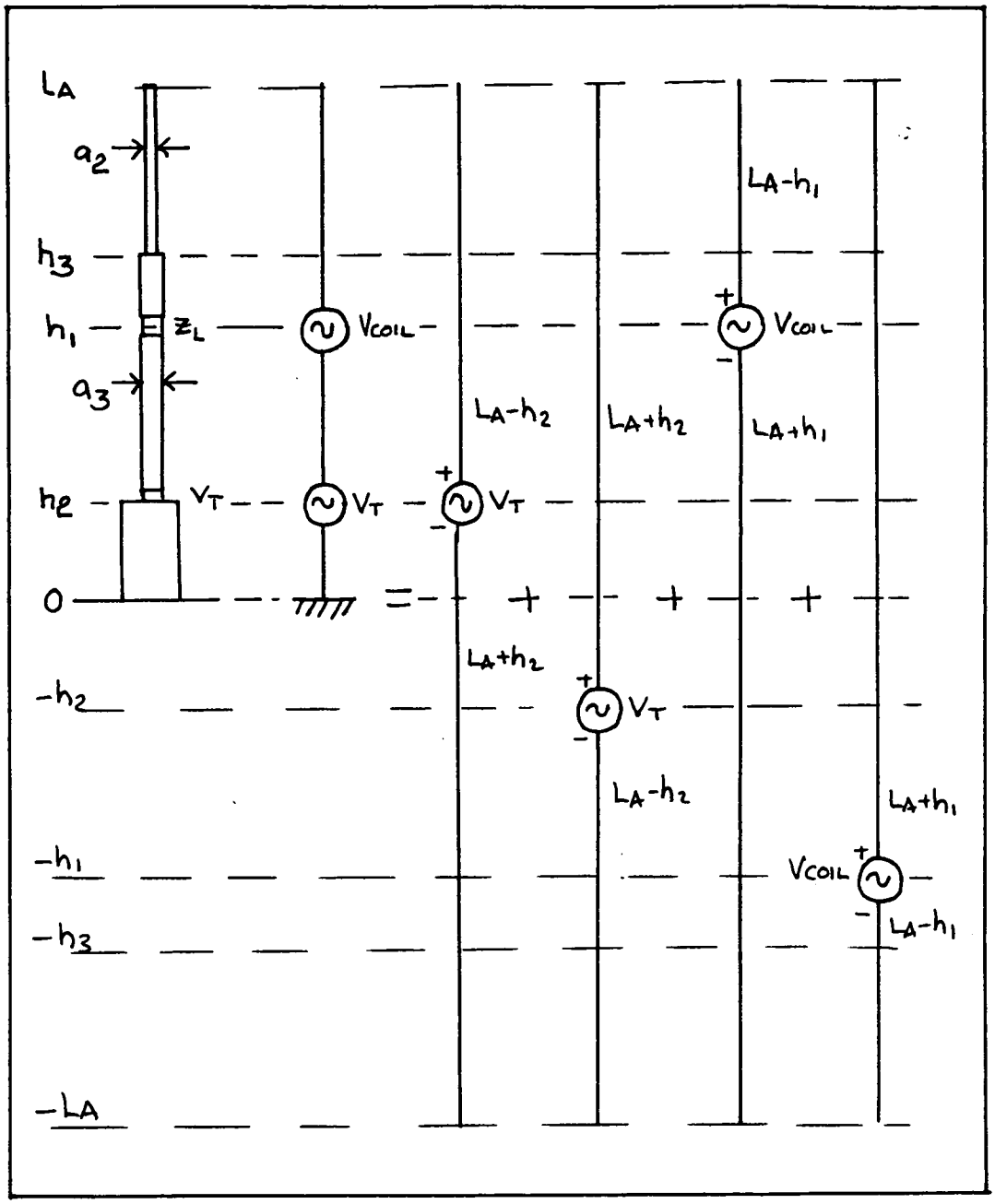

Figure 5.6: The model of the 'AT' series antenna

$$
\begin{aligned}
F2 &= (f(l-h_2, h_1-h_2) + f(l+h_2, h_1+h_2)) \\
Z1 &= Z(l-h_2) + Z(l+h_2) \\
Z2 &= Z(l-h_1) + Z(l+h_1) + Z_L(1 + f(l+h1, 2h_1). \qquad (5.1)
\end{aligned}
$$

The model has been further refined by the use of a second radius for the top section, thus incorporating the whip sections used in 'AT' type antennas.

Impedance values and other characteristics are shown in figure 5.7.

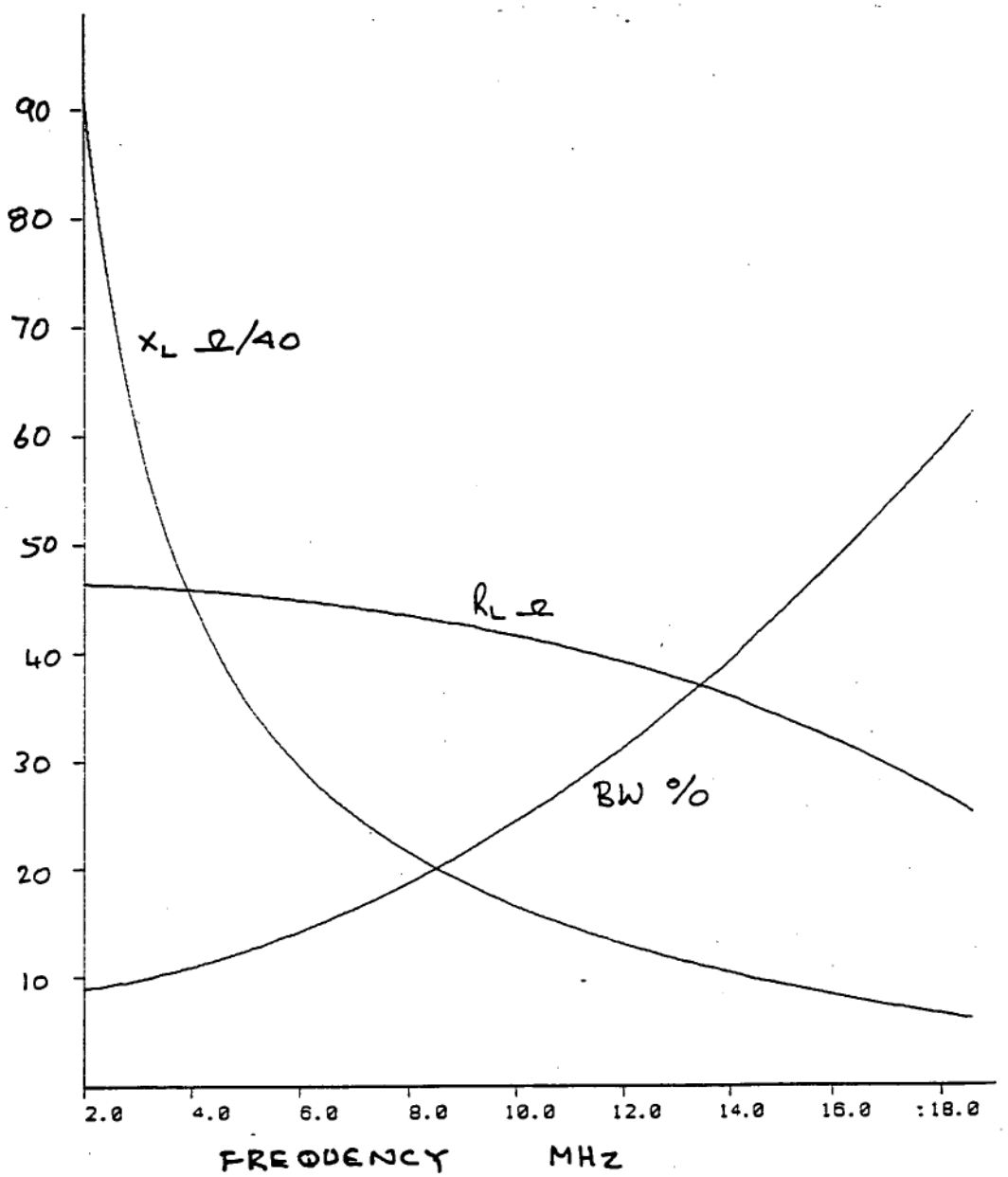

Figure 5.7: Computed values for the MOONRAKER 'AT' series antenna from equation 5.1

Chapter 6

EXPERIMENTAL WORK

6.1 EXPERIMENTAL SYSTEM

A block diagram of the experimental system is shown in figure 6.1 where the device under test (DUT) is either an antenna or a calibration load.

The host computer transfers one of the test programs to the control computer and receives the raw data which is then stored on disk without processing, initially visual inspection of the raw data has been used to provide data integrity.

Power to the test system is from a lead acid battery and hence there is a stable power supply with little inherent noise, tests were performed outside with no mains power and so there is little 50Hz noise pickup by the RF cables. The power requirement for the system is 1A for the test system, $\approx$1.5A for the stepping motor drive (intermittent) and up to 15A for the transceiver, depending on power level. The battery used is 75Ah.

All testing is based on a Z80 microcomputer PCB designed by the staff of the Physics Department of the University of Tasmania. The interface between the PCB and the antenna was designed and built by the author who also wrote and tested all contolling software. The interface performs the functions necessary to drive the stepping motor and also test the voltage levels on the antenna control cable to determine whether open or short circuits exist

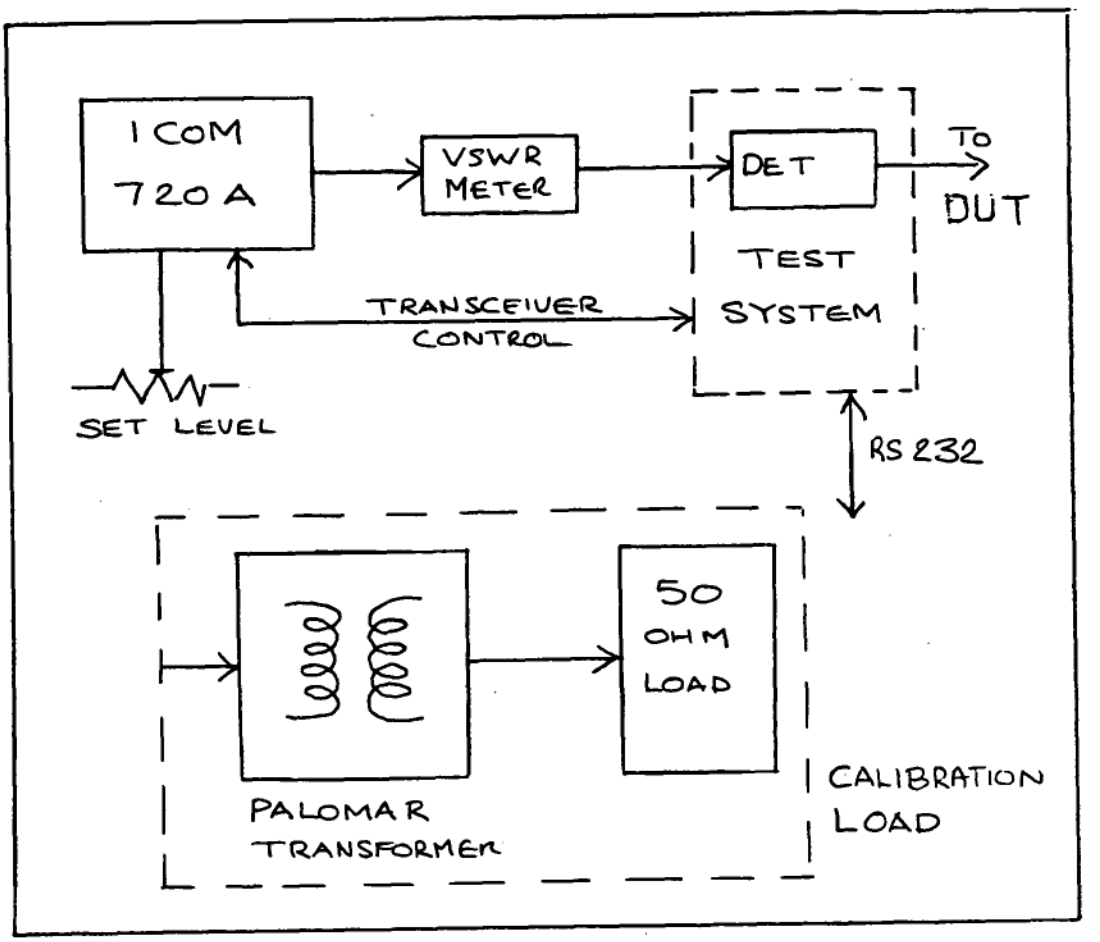

Figure 6.1: Experimental system

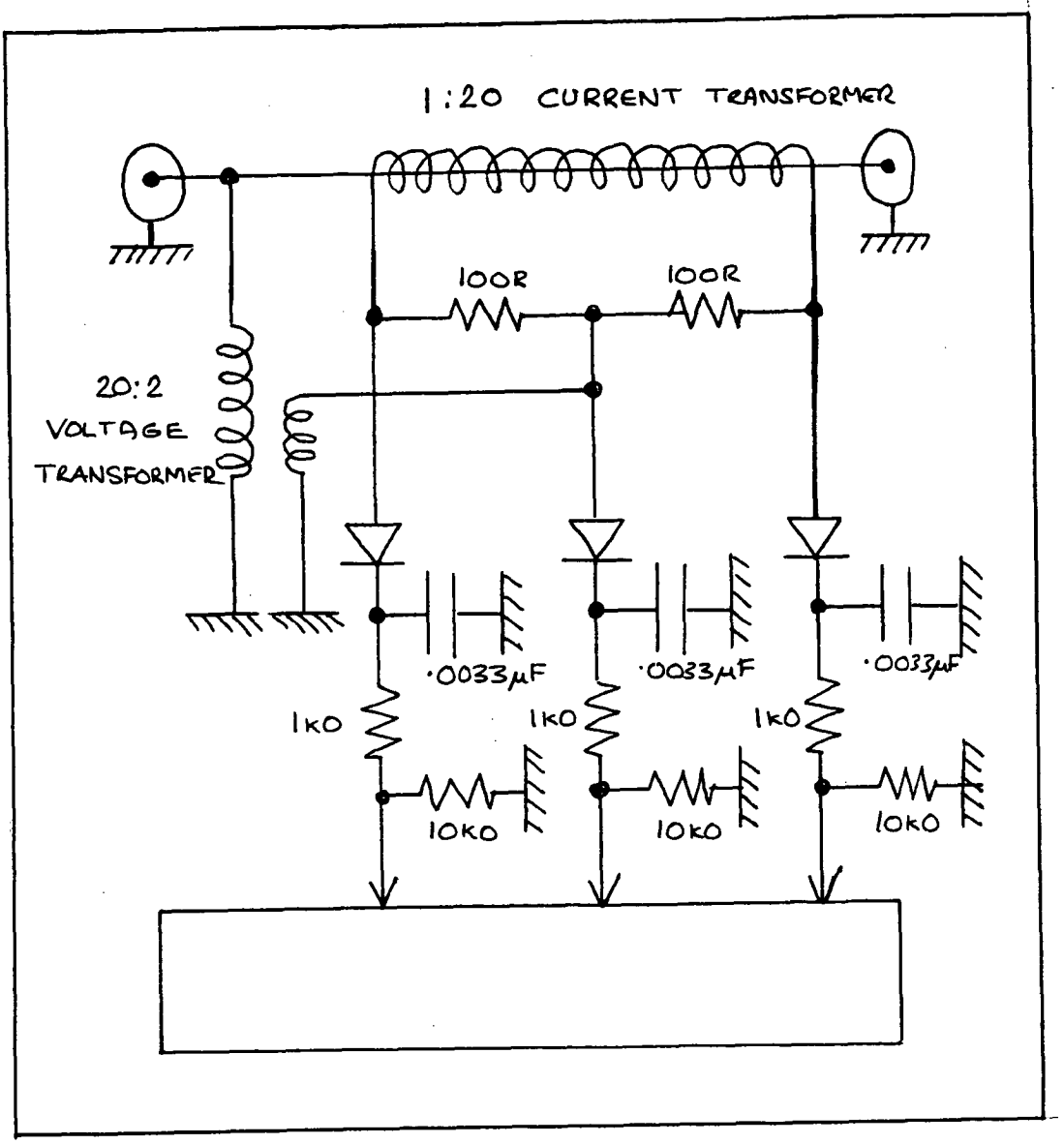

Figure 6.2: VSWR bridge

cuits exist prior to testing. The entire system is mounted in a rugged metal box to withstand the rigours of handling in a manufacturing environment. Data transfer between host and control computer is via an RS-232 link at 2400 baud. Faster baud rates are unnecessary as the test time is limited by the stepping motor drive time (200 pulses per second) across the maximum travel of the drive screw (approximately 16 seconds). Attached to the control computer is a simple user I/O consisting of a LED indicator and a pushbutton to allow local control of tests.

The requirement is for a self contained test system which can be used as a production test system and perform the rigorous tests required for research and development. The test system also needs to be able to withstand the rigours of handling by factory staff.

The heart of the test system is the detector bridge (figure 6.2) which measures V_1, V_2 and V_4 where

$$\begin{aligned} V_4 &= \frac{V}{10} \\ V_1 = \frac{V_f}{10} &= |V_4 + V_I| \\ V_2 = \frac{V_r}{10} &= |V_4 - V_I| \\ V_I &= \frac{50I}{10}. \end{aligned} \tag{6.1}$$

V and I are the rf voltage and current. The order 1, 2 and 4 refer to the sequence that the voltages are measured by the system. These will now be referred to as V_f, V_r and V (the forward voltage,reflected voltage and the terminal voltage), the factor of 1/10 will henceforth be implied as most calculations involving these results involve ratios, those requiring the factor will explicitly state this.

The linearity of the test system is shown in the appendices which contains a number of X-Y plots of V_f versus V_r and V versus I before the system was permanently wired as shown in figure 6.2. Details of the load impedances are contained in the following section on unit calibration. Analysis of the slopes of the plots reveal a reasonable accuracy for work at the power levels

The voltages are measured by an *Analogue Devices* AD574 12 bit ADC via an analogue multiplexer, the AD574 has a conversion time of $25\mu s$. In all experiments the voltages are measured together with a +5V reference as V_3. All voltage measurements are taken from a set of 16 measurements with the average obtained by summing all 16 12 bit numbers and masking the four least significant bits by a right shift. The deviation is measured by summing the absolute value of each table entry minus the average and masking the four LSB's, these processes are outlined below.

$$V_{ave} = \left\{ \sum_{i=0}^{i=15} v[i] \right\} div 16 \tag{6.2}$$

$$\delta V_{ave} = \left\{ \sum_{i=0}^{i=15} |v_{ave} - V[i]| \right\} div 16 \tag{6.3}$$

All experiments were performed using an ICOM 720A transceiver as the signal source, the transceiver has the facility for remote control of frequency, transmission mode and other options,together with a remote press-to-talk (PTT) line which turns transmission on and off.

The RF signal used is keyed CW mode (RTTY) at the frequencies shown in the results. These frequencies were specifically allocated by the DOTC to MOONRAKER for experimental purposes.

In all experiments a *DAIWA* VSWR meter was placed in circuit between the test set and the signal source, this was merely as an indication that tests were proceding as required and was not used for experimental results.

Tests fall into two categories: Calibration and Antenna tests.

6.2 CALIBRATION

The load impedance was varied by means of a *Palomar* transformer giving load impedances of [50, 32, 22, 16, 12.5 and 8 Ω] and [50, 78, 114, 156, 200 and 312 Ω] when connected in the reverse and forward directions respectively.

and 312 Ω] when connected in the reverse and forward directions respectively. The forward and reverse 50Ω measurements give a good indication of the insertion loss of the transformer at the various frequencies.

The transformer, which is rated at 200W PEP, consists of a ferrite toroid with a switch selected turns ratio, when tested on a return loss bridge at 0dBm with a calibrated load the transformer return loss was greater then 30dB up to 30MHz with a rapid deterioration to 40MHz, however this does not show the effects of core saturation.

The load placed on the transformer was a 50Ω power meter which has a VSWR of better than 1.05:1 over the frequency range used. The pad is included to reduce the effect of transformer switching on the transceiver, the approximate VSWR of the input to the pad for an open or short circuit load is 3:1 which does not affect the transceiver load detection circuitry.

The test was performed under control of the host computer with manual control of the transmitted power level. When a measurement set was made the local I/O was used to indicate that a change of power was required. Because of the pad a power range of 6 to 20W was available, without the pad 8 to 70W.

Although referred to as calibration this test does not use a calibrated load and is effectively the best calibration test available. Analysis is based on the assumption that the transformer presents a resistive load to the test set. Any variation from this should result in data anomalies which will be apparent on analysis.

6.3 ANTENNA TESTS

A number of tests were performed on components and a set of eight ferrite cores and five nickel sleeves were then used to provide data. The test data for these samples is in tables 6.1 and 6.2.

Data sets consist of all measurements between two reference VSWR points. The start of a data set is when the VSWR was $< 5{:}1$, and the end is when

ferrite no	resonant frequency kHz	Q
1	2.872	260
2	2.886	255
3	2.894	265
4	2.883	277
5	2.886	240
6	2.863	254
7	2.869	258
8	2.875	274

Table 6.1: Ferrite cores used in antenna testing

nickel no	Q
1	61
2	88
3	80
4	94
5	86

Table 6.2: Nickel sleeves used in antenna testing

VSWR > 7:1. In each test the core was driven to the lower end of its travel by 3200 steps at 200 steps per second, this causes 'hammering' when the drive is at the end of its travel so that the position is undetermined when the drive stops, to overcome this the motor was stepped for 32 steps at 10 steps per second which ensured that the core always started in the same position.

Prior to the design of this system all production tests were performed using a variable speed stepping motor drive under manual control, frequencies were set by front panel control of the transceiver. The advent of remote control facilities has three benefits :

Firstly testing is essentially a matter of connecting the antenna to the test set involving the plugging in of the stepping motor drive connections and the screwing on of the UHF plug. This allows the testing to be performed by unskilled staff releasing Technical staff for more useful duties.

Secondly all testing produces a complete range of data which can be used in the long term to build a more complete picture of the production antennas and allow a more complete set of data for quality control.

Thirdly the data available from prototype testing is more complete than that obtained using previous methods. This allows a far more thorough analysis of the effects of changing antenna components.

The effects of Saturation Induction were investigated by replacing the antenna with a power meter and setting the transmitted power to various levels up to 80W. The antenna was then replaced and tuned at that power level,using an automatic tuner. Power was then reduced to the minimum level and the frequency varied until the best VSWR was obtained. The reason for this approach is that the power level remains low when the load is untuned and rapidly increases when the load is within the tuned range of the transceiver, it was found that the only way this could be properly tested using the experimental setup was to reduce the stepping rate to such an extent that temperature effects dominated.

6.4 EXPERIMENTAL DATA ANALYSIS

The Data is in sets of four 12 bit numbers where 0FFF hex is +10volts (the actual value is only relevant when it is necessary to obtain power values). Calibration tests also included the deviation.

The D.C. voltage obtained from each detector is assumed to be $\sqrt{2}V_{meas}$ or the peak voltage, this is also implied in all calculations and only used where necessary.

The calibration results were analysed as representing the value of a resistance close to the required value line voltage measurement indicates whether the value is above or below 50 Ω.

The measured values were analysed by calculating a series solution to the measurement set and then plotting the VSWR between the two points VSWR = 3.0:1. Figure 6.3 illustrates this process for a single data set. These are available for the eight ferrite cores and the five nickel sleeves.

From this data the minimum is assumed to be the resonant point and the variation is assumed to be purely reactive. The effects of cable length have not been taken into account as the VSWR is constant for any length, however this should be considered if the voltage is to be used.

6.5 EXPERIMENTAL RESULTS

The graphs of calculated VSWR's vs core position are shown in figures 6.4,6.5 and 6.6 for the ferrite cores and figures 6.7 and 6.8 from the nickel sleeves. Nickel sleeve no 1 is used in the ferrite core tests and ferrite core no 1 in the nickel sleeve tests. The format of each graph is the same with the horizontal scale in divisions of 10 steps with step numbers indicated every 50 steps to the right of the step. The vertical scale is in VSWR units of 0.5 with each test core vertically offset by (test core number -1), VSWR is only shown for VSWR $\leq$ 3.0.

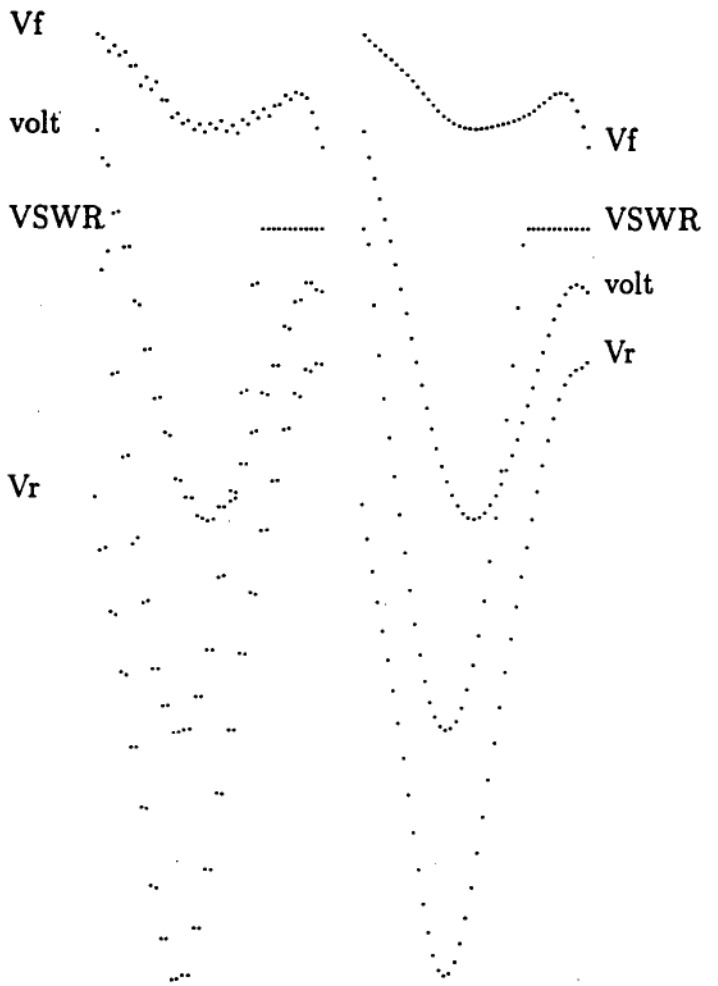

Figure 6.3: Graph of data set before and after smoothing

Figure 6.9 shows the position of the various core components at the test frequencies and at the extremities of core travel.

The effect of the power level on resonance at 2.065 MHz is shown in figure 6.10 for nominal power levels 12 to 80 watts.

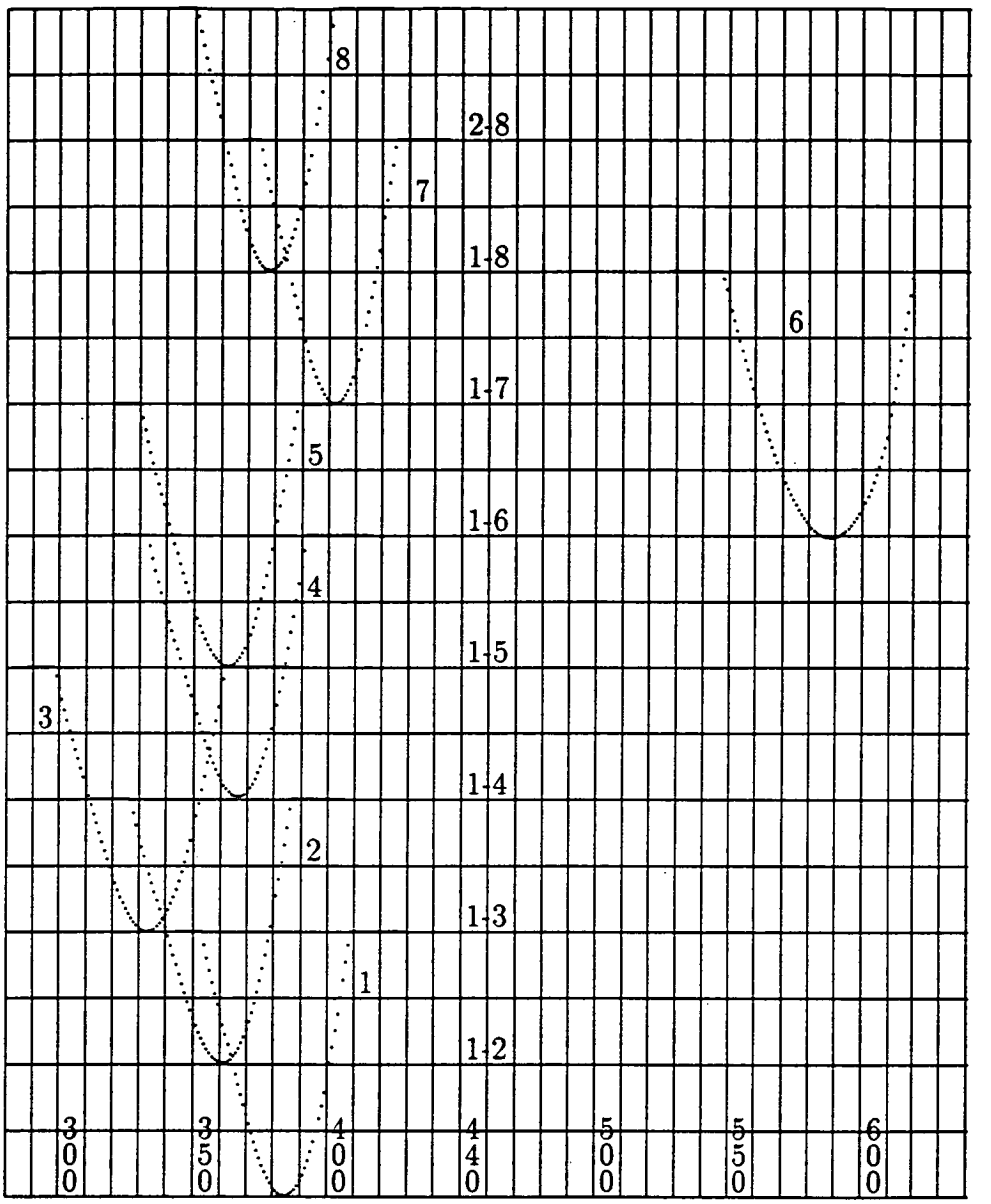

Figure 6.4: VSWR vs core position for ferrite cores at 2.065 MHz

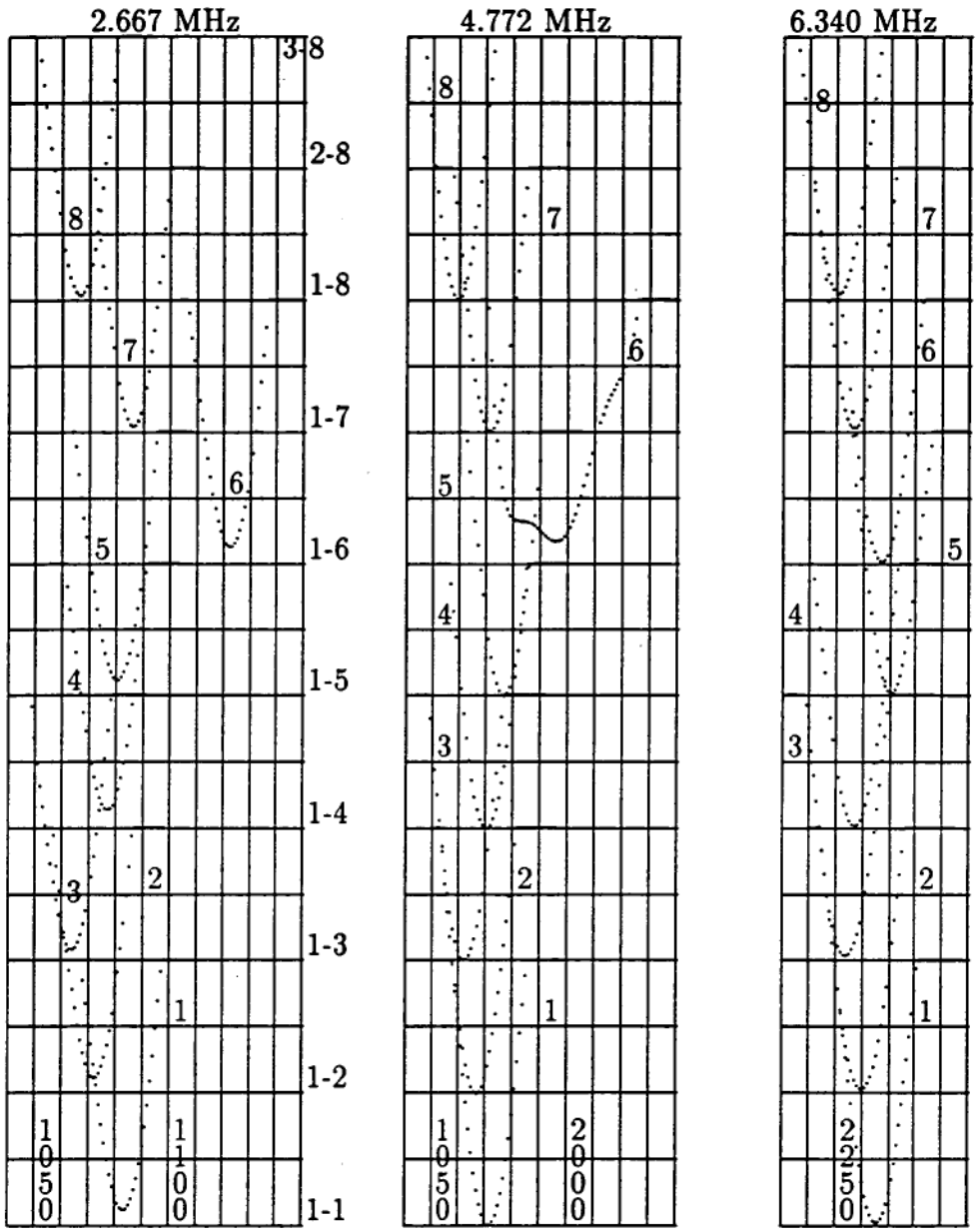

Figure 6.5: VSWR vs core position for ferrite cores at 2.667 to 6.340 MHz

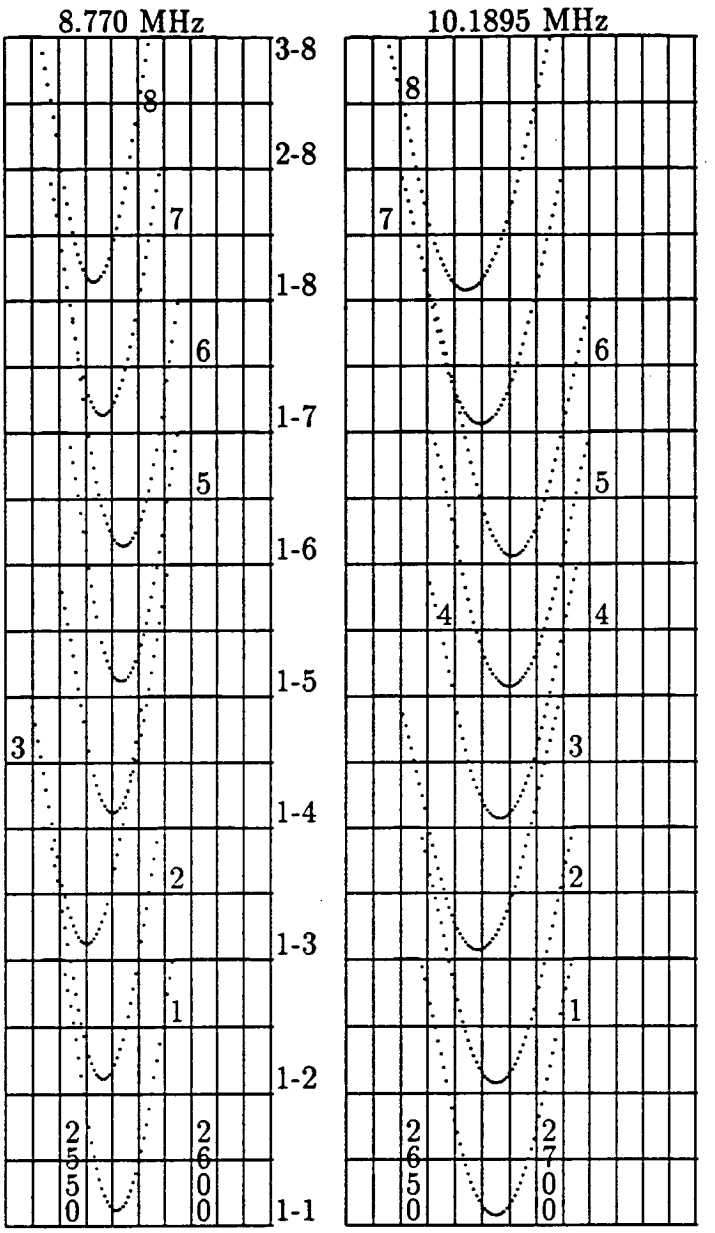

Figure 6.6: VSWR vs core position for ferrite cores at 8.770 and 10.1895 MHz

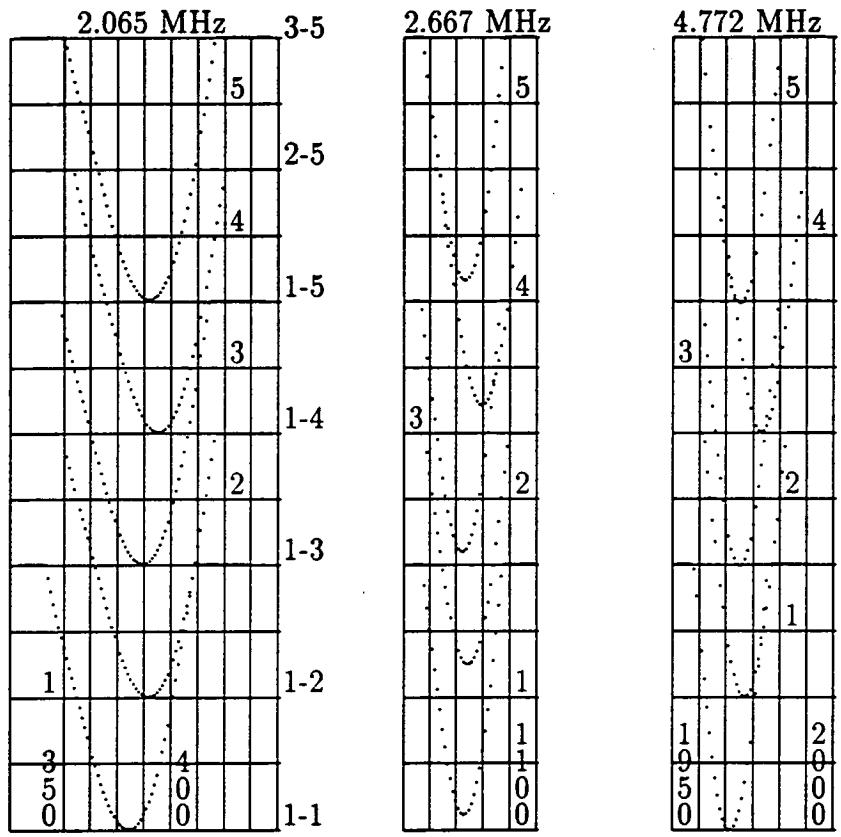

Figure 6.7: VSWR vs core position for nickel sleeves at 2.065 to 4.772 MHz

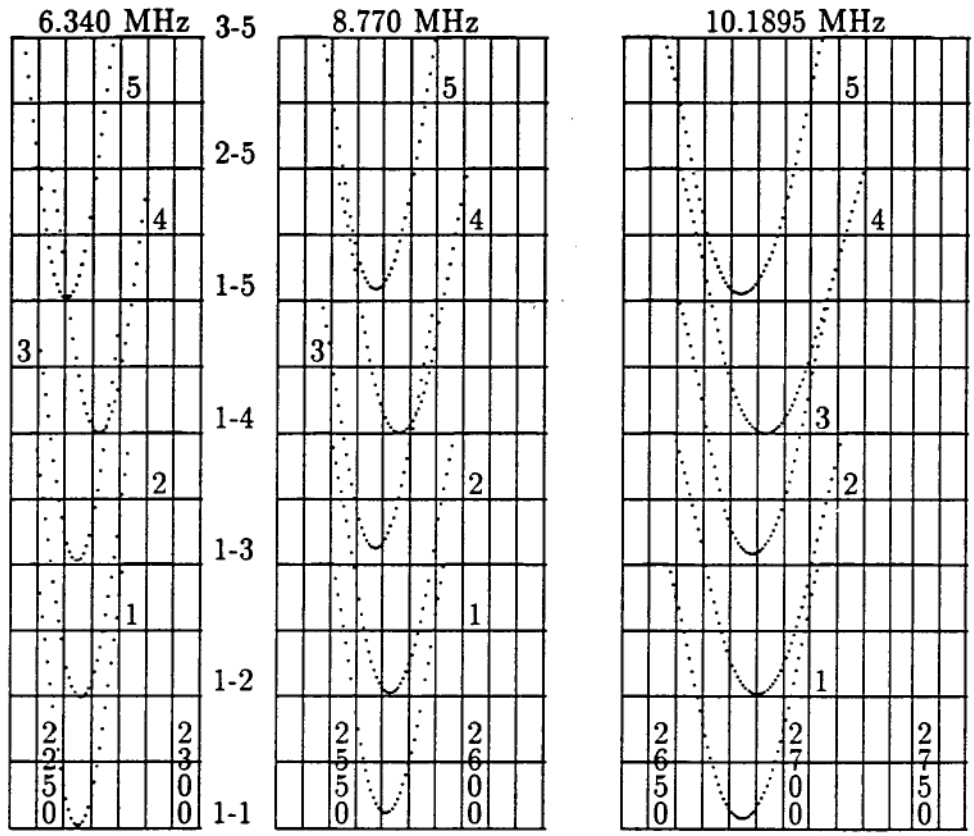

Figure 6.8: VSWR vs core position for nickel sleeves at 6.340 to 10.1895 MHz

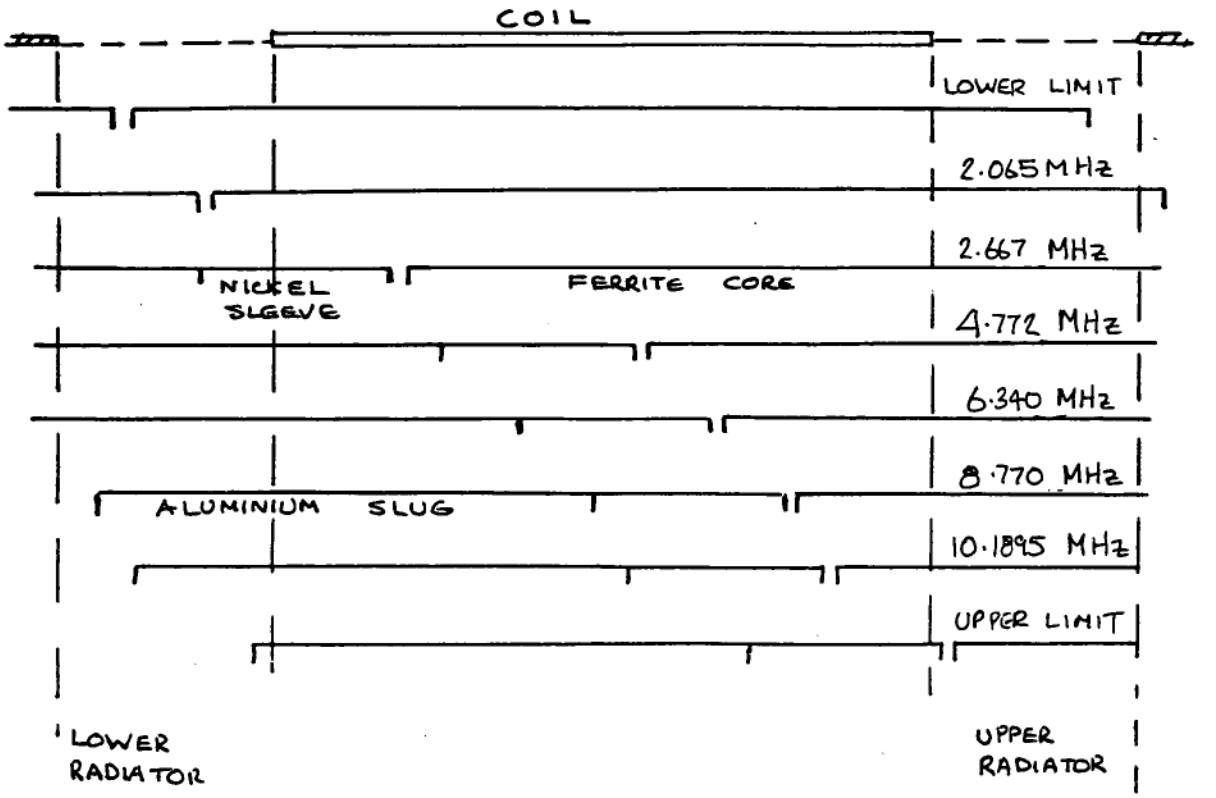

Figure 6.9: Median Position of Core for Measured Frequencies

Chapter 7

ANALYSIS OF RESULTS

7.1 FERRITE AND NICKEL TESTS

Wheeler's equation for the inductance of a single layer coil of length ℓ, radius r, and number of turns N, which is wound on a noninductive core is:

$$L = 0.03937 \frac{(Nr)^2}{9r + 10\ell} \ \mu H \tag{7.1}$$

where ℓ and r are measured in mm. 7.1 is accurate to within 1%. When applied to the test coils for the ferrite cores and nickel sleeves the calculated and measured values are:

test coil	N	r mm	ℓ mm
ferrite	32	11.8	73.0
nickel	49	11.7	57.0

test coil	calculated (7.1)	measured
ferrite	6.71	6.46
nickel	19.16	17.59.

The reference coil used to preset the 40 pF capacitor was a MARCONI 10 μH test coil in a shielded can with a stated tolerance of $\pm 5\%$, hence the measured values are within $\pm 5\%$ of the actual values (ignoring frequency error which is less than 1kHz). Consequently the measured value of the ferrite test coil

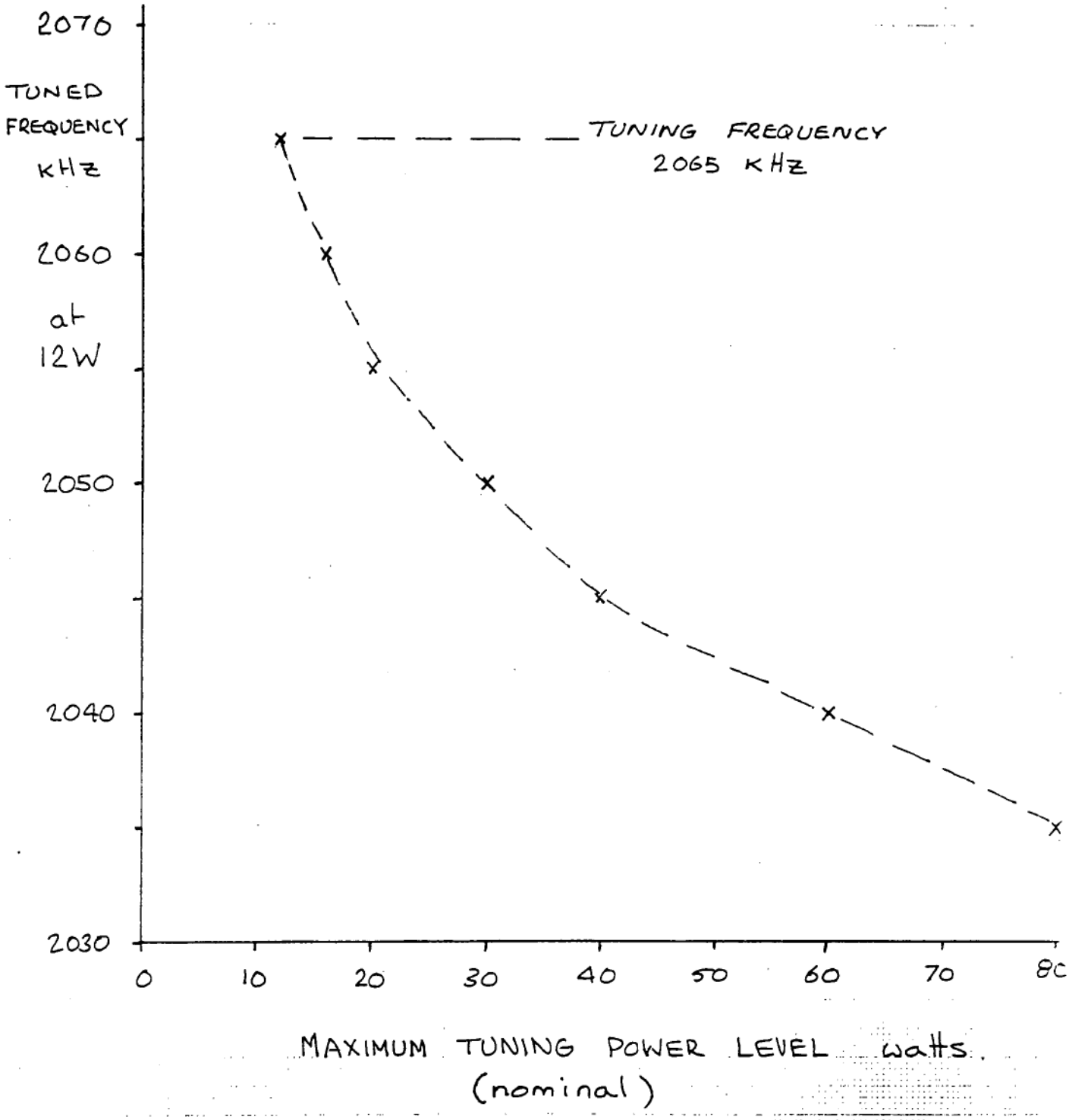

Figure 6.10: Effects of RF power level on resonance ot antenna

is close to that predicted but that of the nickel test coil is 9% too low. There are two potential sources of error, firstly the extra inductance of the coil due to the coil wiring and secondly, as the coil is measured above a conducting surface there is an image coil which is negatively coupled to the coil under test which reduces the effective inductance.

The measured quality factors of the test coils were 268 and 278 respectively resulting in a copper loss of 1.5 Ω at 9.9 MHz for the ferrite test coil and 2.4 Ω at 6.0 MHz for the nickel test coil. Corrected values of copper losses are therefore $0.477\sqrt{f}$ Ω and 2.56 Ω respectively.

The corrected parameters for the ferrite cores are:

ferrite no	resonant frequency	Q_{meas}	μ_{meas}	Q_{corr}
1	2.872	260	11.88	307
2	2.886	255	11.77	300
3	2.894	265	11.70	314
4	2.883	277	11.79	330
5	2.886	240	11.77	279
6	2.863	254	11.96	298
7	2.869	258	11.91	304
8	2.875	274	11.86	326

and for the nickel sleeves the corrected values of quality factor are

nickel sleeve	Q_{meas}	Q_{corr}	R_{loss} Ω
1	61	84	6.86
2	88	144	4.00
3	80	124	4.65
4	94	160	3.60
5	86	140	4.12.

The measured values of permeability of the ferrite rods are below that expected from table 5.1 in conjunction with figure 5.3 (low 20's). The reason for this is that the ferrite rod is hollow with nominal outer and inner diameters of 0.75 and 0.15 inches (± 0.03 inches). If a uniform flux density is assumed within the core then the effective permeability is

$$\mu_{eff} = \frac{OD^2 \mu_{rod}}{(OD^2 - ID^2) + \mu_{rod} ID^2} \tag{7.2}$$

and so the rod permeability is

$$\mu_{rod} = \frac{\mu_{eff}(OD^2 - ID^2)}{OD^2 - \mu_{eff} ID^2}. \tag{7.3}$$

The corrected permeabilities are:

ferrite no	μ_{eff}	μ_{rod}
1	11.88	21.73
2	11.77	21.35
3	11.70	21.11
4	11.79	21.42
5	11.77	21.35
6	11.96	22.01
7	11.91	21.84
8	11.86	21.66

which are within the range expected.

The corrected values of quality factor of the ferrite cores are within the range quoted in the manufacturers data (figure 5.3).

The interpretation of the nickel sleeve data assumes that the variable is the permeability of the nickel plating. Nickel Alloy has a maximum permeability of 1000 (unstressed). however the three crystal orientations have permeabilities of 500 to 1500. The quality factor is measured by inserting the sleeve into the test coil thus shorting out a number of the turns. The inductor short circuited by the sleeve has some residual inductance and the higher this value of residual inductance the higher the length of short circuit and a larger area is presented to the coil. The surface resistance is proportional to $\sqrt{\mu}$ for a fixed frequency and if the residual inductance depends on μ then the high values of permeability will have a low quality factor.

frequency MHz	coil resistance	coil reactance
2.065	45.6	3614
2.667	45.0	2787
4.772	44.7	1525
6.340	43.8	1120
8.770	42.0	768
10.1895	41.0	634.

Table 7.1: Coil Impedance at Test Frequencies

7.2 ANTENNA IMPEDANCE

Calculated values of loading coil impedance obtained in chapter 5 are summarised in table 7.1 for the test frequencies.

The inductance of the antenna coil by equation 7.1 (N = 75, ℓ = 86.6mm, r = 11.12mm) is 28.35 μH. Hence calculated reactance at 2.065 MHz for the ferrite cores (with μ_{eff} ranging from 11.70 to 11.96) is 4303 to 4400 $k\Omega$, which is 20% greater than that shown in the table. The effective permeability required to give that impedance is 9.83.

There are several possible explations:

Incorrect calculations- the calculated reactances for the centre loaded monopole are in close agreement with those obtained using ELNEC and so it is assumed that the reactances are correct (even though the resistances do not agree).

Reduction in permeability due to length change- the length/diameter ratio is important in determining the rod permeability. For example the rod permeability reduces by 30% for a 15% change in length between L/D = 7 and L/D =6 (the L/D ratio of the ferrite rod is 6.7).

Reduction in permeability due to saturation of the core- the permeability of a ferrite core also depends on the field intensity and will reduce as saturation is approached.

Distribution of load impedance- the load impedance varies over the range of loading points (h = 0.45ℓ to 0.49ℓ) as shown in figures 3.12 to 3.14, thus the actual load impedance will be somewhat larger than those calculated. However this difference is only a few per cent, insufficient to account for the change in permeabilty.

As the ferrite cores were selected as typical of a batch, it is useful to consider the production antenna.

The inductance of the loading coil (71 turns at 22 t.p.i.) is 26.68 μ_{rod} μH (or 312.2 to 319.1 μH using the corrected rod permeabilities). The minimum frequency of operation is around 1.95 MHz at which the reactance ranges from 3825 to 3910 Ω. The calculated load reactance at 2 MHz is 3732 Ω and at 2.065 MHz, 3614 Ω. Thus it is evident that the model agrees with observation. This also reveals that saturation is not a factor in the permeability of the core at low power levels (antenna tests are performed at 8 to 12 W).

At the low frequencies the losses are substantially within the ferrite core. The quality factor is thus 82 at 2 MHz which is 25 to 30 % of the measured quality factor. Copper losses, while present, have little effect on Q. Thus it must be assumed that core losses are non linear with power density: the measured Q is the voltage across a 40 pF capacitor, 10 volts rms corresponding to a Q of 500. Hence i_{coil} is 5Qf μA. An estimate of i_{coil} during testing is the feed current or 400 mA at 8W. For a typical Q of 300 at 2.87 MHz the test current is 1% of the operating current.

7.3 ANTENNA TESTS

Before considering the numerical results it is useful to examine the effects of power level on permeability (figure 6.10). This test is indicative only as the power meter was uncalibrated. An estimate of the reduction in permeability between power levels of 12 to 80 watts is 1.7%. This poses a problem for the user- modern HF transceivers do not have power level controls, when the load VSWR is less than a preset level (usually 1.8:1) the transmitted power rises to the maximum level permitted for that channel. At low frequencies if the antenna tuning power level is too high for the 'AT' series antenna then

the antenna will be untuned once power is reapplied and the internal power limiting will prevent the power level rising to the 'tuned' level. As most voice communications use SSB for maximum efficiency the average power level is low, hence the antenna should be tuned at a more appropriate level than the maximum carrier level. This test was repeated at 2.667 MHz with slight variation in tuned frequency but insufficient to affect the power limiting circuitry. The reason for this is that a 1% change in reactance at 2.065 MHz in a tuned antenna (VSWR = 1:1) gives a VSWR of 2:1 whereas at 2.667 MHz the resulting VSWR is 1.7:1.

The xy plots of the response of the detector bridge (in the appendices) were selected as typical over the frequency range. The forward and reverse connected transformer shows that the insertion loss is small and the calculated resistances for the various loads show that the system is linear over the power range with a variation of a few per cent in calculated resistances.

The antenna test data reveals 'pairs' of measurements which is clearly shown in figure 6.3. Initially this was thought to be a stepping motor or drive problem but on investigation the stepping motor was driving the core along the full length of its travel with the correct number of steps (3200). The same results ensued with a number of production antennas. As this does not affect the electrical tests it has been ignored (it does affect lineal resolution which changes from 35 μm to 70 μm).

Figure 6.9 shows that at 2.065 MHz the ferrite core extends through the coil, however the inductance has been reduced to 278.5 μH, corresponding to a reduction in effective permeability of 20%. This demonstrates that the dominating factor in determining the effective permeability is the length/diameter ratio.

The resonant positions of the ferrite cores at 2.065 MHz (figure 6.4) are in accordance with their relative permeabilities. The remaining graphs show that the relative resonant postions are not maintained over the frequency range. This indicates that the frequency dependence of material permeability is not straightforward and hence cannot be predicted from the single measurement of μ_{rod}. The reduced spread of resonant points is indicative of the dominance of the length/diameter ratio in determining permeability.

The number of steps between the transition points VSWR = 3.0:1 for 2.065 MHz reveal no connection with the measured quality factor (Q). This is not unexpected as Q is measured at low power density where the effects of saturation are non existent. Consequently the measured Q does not provide any useful information.

The nickel sleeve graphs (figures 6.7 and 6.8) show the impact of the nickel sleeve on resonant point starts at 2.065 MHz even though it is 10mm from the coil. The reason for this variation is that the field on the sleeve is almost zero and consequently the field is modified at the end face of the ferrite core which reduces its effective permeability.

The relative positions of resonant points are maintained across the frequency range but there is little to distinguish the individual sleeves.

Wheeler's equation can be used to determine the inductance of the coil components of figure 6.9. If the three lengths ℓ_1, ℓ_2 and ℓ_3 correspond to the lengths of the coil with aluminium, nickel and ferrite cores respectively then

$$L = L_1 + L_2 + L_3 + 2k_{12}\sqrt{L_1 L_2} + 2k_{13}\sqrt{L_1 L_3} + 2k_{23}\sqrt{L_2 L_3} \qquad (7.4)$$

where $L_i = \mathrm{L}(\ell_i)$, and is some multiple of the value obtained from equation 7.1 for the air cored inductor, this multiple being the effective relative permeability of the core material.

The various coupling coefficients are determined from the air cored inductors $\mathrm{L}(\ell_1 + \ell_2 + \ell_3)$, $\mathrm{L}(\ell_1 + \ell_2)$ and $\mathrm{L}(\ell_2 + \ell_3)$ and the constituent components which are tabulated for the mean tuned positions of the antenna core in table 7.2.

For a first order solution the inductors L_1 and L_2 are assumed to be short circuited and so the effective permeabilities are:

frequency	2.667	4.772	6.340	8.770	10.1895
ℓ_1	-	22	32.5	42.0	47
ℓ_2	14	25.4	25.4	25.4	25.4
ℓ_3	73	39.6	29.1	19.6	14.6
ℓ_{12}	-	47.4	57.9	67.4	72.4
ℓ_{23}	87	65	54.5	45	40
L_1	-	5.46	8.97	12.25	14.00
L_2	2.94	6.58	6.58	6.58	6.58
L_3	23.2	11.42	7.82	4.68	3.12
L_{12}	-	14.14	17.84	21.21	23.00
L_{23}	28.2	20.36	16.64	13.30	11.55
k_{12}	-	0.175	0.149	0.133	0.126
k_{13}	-	0.018	0.018	0.017	0.018
k_{23}	0.125	0.136	0.156	0.184	0.204

Table 7.2: Components of inductance of tuned antenna

frequency	X_L	L_{calc}	L_3	μ_{eff}
2.667	2787	166.3	23.2	7.17
4.772	1525	50.86	11.42	4.45
6.340	1120	28.12	7.82	3.60
8.770	768	13.94	4.68	2.98
10.1895	634	9.90	3.12	3.17

The effective permeabilities are an upper bound to the actual permeabilities and illustrate the effect of the length/diameter ratio. It is apparent that the first order model is incorrect because of the increase in effective permeability at 10.1895 MHz.

The shorting sleeves are not perfect short circuits, this is obvious when considering the maximum operating frequency (13.2 MHz) of the low band antenna, which has a load reactance of 434.5 Ω (5.24 μH). A short circuited inductor can be represented by an image inductor of the same magnitude but with a negative coupling coefficient with $L' = L_o + L_i + 2k_{io}\sqrt{L_o L_i}$ where L_i is the image of L_o. Hence L' =$2L_o$(1-k) = αL_o.

An estimate of α from the maximum operating frequency is the ratio of the

actual inductance to the air cored inductor 5.24/26.68 = 0.196. However this does not account for the nature of the short circuit. It is a reasonable assumption that the coupling coefficients between the aluminium cored inductor and image and the nickel cored inductor and image are equal (they are both the same height above the core), however the permeability of the nickel is >> 1 and so it is to be expected that the inductance of the nickel cored inductor is greater than that of the aluminium cored inductor. One approximation is to use the equivalent rod permeability of ≈ 3 (L/D = 1). The coil inductance is thus

$$L_T = \alpha L_1 + 3\alpha L_2 + 2k_{12}\sqrt{3L_1L_2} \tag{7.5}$$

for the low band coil.

	length mm	N	L
ℓ_T	82	71	26.65
ℓ_1	60	52	18.78
ℓ_2	22	19	5.49

hence $k_{12} = 0.117$ and $\alpha = 0.133$. This can be substituted into the equations for inductance to give

$$\begin{aligned} L &= 0.133L_1 + 0.4L_2 + \mu_{eff}L_3 \\ &+ 0.461k_{12}\sqrt{L_1L_2} + 0.73k_{13}\sqrt{l_1L_3\mu_{eff}} + 1.264k_{23}\sqrt{l_2L_3\mu_{eff}} \\ &= L_1' + L_2' + L_3' \end{aligned} \tag{7.6}$$

where L_i' is the effective inductance of inductor i including mutual inductance terms. The calculated inductors are then solved for μ_{eff} as

frequency	μ_{eff}	L_1'	L_2'	L_3'	L_T
2.667	6.97	-	2.90	163.40	166.3
4.772	3.84	1.07	4.33	45.40	50.81
6.340	2.72	1.55	4.26	22.53	28.33
8.770	1.58	1.96	3.72	7.55	13.23
10.1895	1.13	2.19	3.53	4.19	9.91

If the quality factor of the ferrite core is considered constant over the frequency range then the losses are $\frac{\omega L_3'}{80}$ which is used to determine the losses in the remainder of the circuit.

frequency	R_{loss}	ferrite loss	remainder	nickel loss (est)
2.667	45.0	34.2	10.8	10.8
4.772	44.7	17.0	27.7	26.2
6.340	43.8	11.2	32.6	30.2
8.770	42.0	5.2	36.8	35.5
10.1895	41.0	3.4	37.6	38.3

where the estimated nickel losses are based on the losses at 2.667 MHz adjusted for length and frequency. There are several sources of error in this result.

Firstly there is no allowance for copper loss in the coil which decreases the Q of the inductor. Thus the actual Q of the ferrite core will be higher than that measured. Secondly the quality factor reduces with frequency which increases ferrite losses and thirdly the effects of loading coil position increases the value of inductance

This model therefore provides an approximation to the loading coil if the effective permeabilities of the ferrite core and nickel sleeve are known, however as end effects and length/diameter ratio affect the permeability of the ferrite core it is difficult to predict the performance of a particular combination.

7.4 CONCLUSION

The model developed by the use of superposition is a useful one; there is confirmation in the results obtained from the numerical packages. However there is a discrepancy between the two methods over the resistance of the loading coil which needs to be resolved. Harrison's model uses known antenna current distributions and impedances and so, if the principles involved are correct, is accurate for a point load. The change in load with position has been investigated and the change in resistance for a distributed load is small. The numerical packages are approximations which converge on the correct

solution as the number of segments are increased and so it is reasonable to assume that they are not as accurate as the superposition method.

The experimental work shows that there is strong agreement between the calculated load reactance and calculated coil inductance at the minimum frequency of operation. The model of the loading coil provides a means of analysing the antenna operation but requires a more detailed understanding of the effects of frequency and power level together with the effects of the length/diameter ratio and end effects due to the nickel sleeve on the permeability of the ferrite core.

A test system has been developed which allows in depth testing of the 'AT' series antenna. This provides the manufacturer with a low cost method of rapidly testing production using unskilled staff, whilst building a data base for subsequent analysis of material characteristics. When combined with the data obtained from initial testing of antenna core components this will provide a method of making design decisions which will speed up the manufacturing process.

Appendix A

REFERENCES

1 R.W.P. KING The Linear Antenna - Eighty Years of Progress

PROC IEEE 55 January 1967

2 R.W.P. KING The Theory of Linear Antennas

Harvard University Press 1956

3 J.D.KRAUS Antennas (second edition)

McGRAW-HILL 1988

4 C.A.BALANIS Antenna Theory - Analysis and Design

John Wiley and Son 1982

5 MITTRA (Ed) Computer Techniques for Electromagnetics

Pergamon 1973

6 JASIK and JOHNSON (Eds) Antenna Engineering Handbook
(second edition)

McGRAW-HILL 1961

7 M.M.WIENER Monopole Element at the center (sic) of a circular ground plane whose radius is small or comparable to a wavelength

IEEE TRANS A&P AP-35 no 5 may 1988

8 C.W.HARRISON Monopole with Inductive Loading

IEEE TRANS A&P JULY 1963

9 E.K.MILLER A selective survey of computational electromagnetics

IEEE TRANS A&P vol 36 september 1988

10 R.F.HARRINGTON Field Computation by the Moment Method

MacMillan 1968

11 J.W.ROCKWAY et al. The MININEC Sytem - Microcomputer Analysis of Wire Antennas

Artech House 1988

12 R.LEWALLEN ELNEC Software Package
(Privately published)

Appendix B

LOADED MONOPOLE PROGRAMS

The impedance of the monopole of half length ℓ is:

$$Z(\ell) = J30\frac{\psi_{dr}}{T(\ell)(1 - cos(\beta\ell) - sin(\beta\ell))} \tag{B.1}$$

The current at some point z is

$$F(\ell, z) = -J\frac{Z(\ell)}{30\psi_{dr}}((sin(\beta|z|) - sin(\beta\ell)) + T(\ell)(cos(\beta z) - cos(\beta\ell))) \tag{B.2}$$

where $F(\ell, 0) = 1.0$ and

$$\begin{aligned}
T(\ell) &= \frac{(\psi_{du} + E_a(\ell,\ell))sin(\beta\ell) - J\psi_{di} - S_a(\ell,\ell)}{C_a(\ell,\ell) - cos(\beta\ell)(E_a(\ell,\ell) + \psi_{du})} \qquad \text{(B.3)}\\
E_a(\ell, z) &= \int_{-\ell}^{+\ell} \frac{e^{-j\beta R_h}}{R_h} dz'\\
C_a(\ell, z) &= \int_{-\ell}^{+\ell} cos(\beta z')\frac{e^{-j\beta R_h}}{R_h} dz'\\
S_a(\ell, z) &= \int_{-ell}^{+\ell} sin(\beta|z'|)\frac{e^{-j\beta R_h}}{R_h} dz'\\
\psi_{du} &= \int_{-\ell}^{+\ell} \frac{(cos(\beta z) - cos(\beta\ell))}{1 - cos(\beta\ell)} \left[\frac{e^{-j\beta R}}{R} - \frac{e^{-j\beta R_h}}{R_h}\right] dz'
\end{aligned}$$

$$
\begin{aligned}
\psi_{di} &= -\int_{-\ell}^{+\ell} \frac{sin(\beta(\ell - |z|))}{1 - cos(\beta\ell)} \left[\frac{sin(\beta R)}{R} - \frac{sin(\beta R_h)}{R_h}\right] dz' \\
\psi_{dr} &= \int_{-\ell}^{+\ell} \frac{sin(\beta(\ell - |z'|))}{sin(\beta\ell)} \left[\frac{cos(\beta R)}{R} - \frac{cos(\beta R_h)}{R_h}\right] dz' \\
R_h &= \sqrt{(\ell - z')^2 + a^2} \\
R &= \sqrt{z'^2 + a^2}.
\end{aligned}
$$

these are used in the following programs. The first determines the various $F(\ell_i, \ell_j)$ and $Z(\ell_i)$ for the antenna and the second uses these values to determine the load impeadance for a 50Ω match, the efficiency and the bandwidth. Program *centre loaded* is the template used for varying length, frequency, loading point etc.

```
      program centre_loaded

c
c     based on HARRISON: MONOPOLE WITH INDUCTIVE LOADING
c
c     IEEE TRANS A&P JULY 1963
c
c     adapted to suit antenna fed at point above ground
c     as in AT series antenna
c
c     LA antenna length
c     H1 loading point
c     H2 height of feed point above ground plane
c     H3 height above ground plane of radius transition
c     a1 radius of lower section
c     a2 radius of upper section
c     P1-3 heights obtained from LA & H1-3 for sub-antennas
c     Z1-4 the four sub-antenna impedances
c     F1-6 current distribution functions
c     PSIdr see Harrison
```

```
c     Th ditto
c
      double precision LA,H2,H1,beta,freq,pi,a1,a2,P1,P2,P3,H3,
     - bet,a,hval
      complex*16 PSIdr1,Th1,PSIdr2,Th2,PSIdr3,Th3,PSIdr4,Th4,
     - Z3,Z1,Z2,Z4,
     - F1,F2,F3,F4,F5,F6,FIJ,Zin,J,one
      common beta,J,zero

10    format(f10.5)
      zero=dcmplx(0,0)
      one=dcmplx(1.,0)
      J=dcmplx(0,1)
      a1=.016
      a2=.003
      pi=3.141593
      LA=2.7
      H2=0.0
      H3=LA-1.2
      H1=1.26
      bet=2*pi/300.0
      open(unit=1,file='landm1.dat',status='new',ERR=14)
      goto 24
14    open(unit=1,file='landm1.dat',status='old',ERR=26)
24    freq=2.000

25    beta=bet*freq
           write(*,*)freq
           n_seg=150
           P1=LA-H1
           P2=0.0
           P3=H3-H1
145        call  getvalues(P1,a1,P2,a2,P3,Th1,PSIdr1,n_seg)
           P2=H1-H2
           P3=H3-H2
           call  getvalues(P1,a1,P2,a2,P3,Th2,PSIdr2,n_seg)
           P2=H1+H2
```

```
            P3=H3+H2
            call  getvalues(P1,a1,P2,a2,P3,Th3,PSIdr3,n_seg)
            P2=2*H1
            P3=H3+H1
            call  getvalues(P1,a1,P2,a2,P3,Th4,PSIdr4,n_seg)

            Z1  = Zin(LA-H1,PSIdr1,Th1)
            Z2  = Zin(LA-H2,PSIdr2,Th2)
            Z3  = Zin(LA+H2,PSIdr3,Th3)
            Z4  = Zin(LA+H1,PSIdr4,Th4)

            F1 = FIJ(Z3,PSIdr3,LA+H2,2*H2,Th3)
            F2 = FIJ(Z2,PSIdr2,LA-H2,H1-H2,Th2)
            F3 = FIJ(Z3,PSIdr3,LA+H2,H1+H2,Th3)
            F4 = FIJ(Z4,PSIdr4,LA+H1,H1+H2,Th4)
            F5 = FIJ(Z4,PSIdr4,LA+H1,H1-H2,Th4)
            F6 = FIJ(Z4,PSIdr4,LA+H1,2*H1,Th4)

            write(1,15)freq,LA,H1,H2,H3,a1,a2,
     -             Z1,Z2,Z3,Z4,F1,F2,F3,F4,F5,F6
15             format(7(f8.4,1x),20(E15.5E3,1x),/)
            freq=freq+0.5
           if(freq.lt.30.1)goto 25
26     close(unit=1)
       end

       subroutine getvalues(L1,ra,L2,rb,L3,Th,PSIdr,n_seg)
c
c antenna of length L1+L2 with radius a1 up to L3
c calculates Th and PSIdr as per harrison
c variable names use nomenclature as per harrison
c
       complex*16          J,T1,T2,Th,PSIdr,EA,CA,SA,PSIdu,PSIdi,expnr,expnrl

       double precision    L,r,zpr,asqr,delta,rh,cosbtar,sinbtar,cosbtrh,
     -                     a,sinbtrh,betah,betaz,cosbth,sinbth,sinbhz,beta,
     -                     L1,L2,ra,rb,absz,aasqr,absqr,L3
```

```
      common              beta,J,zero

15    format(f10.5)
      L=L1+L2
      aasqr=ra**2
      absqr=rb**2
      delta=L/n_seg
      EA=zero
      CA=zero
      SA=zero
      PSIdr=zero
      PSIdu=zero
      PSIdi=zero
      betah=beta*L
      cosbth=cos(betah)
      sinbth=sin(betah)

      do 100 i=0,2*n_seg-1
                zpr=(float(i-n_seg)+0.5)*delta
                absz=dsqrt(zpr**2)
                asqr=absqr
                if (absz.lt.L3) asqr=aasqr
                r=dsqrt(zpr**2+asqr)
                rh=dsqrt((L-zpr)**2+asqr)
                cosbtar=cos(beta*r)
                sinbtar=sin(beta*r)
                cosbtrh=cos(beta*rh)
                sinbtrh=sin(beta*rh)
                expnr=dcmplx(cosbtar,-sinbtar)*delta/r
                expnrh=dcmplx(cosbtrh,-sinbtrh)*delta/rh
                betaz=beta*zpr
                sinbhz=sin(beta*(L-abs(zpr)))
                EA=EA+expnrh
                SA=SA+sin(beta*abs(zpr))*expnrh
                CA=CA+cos(betaz)*expnrh
                PSIdi=PSIdi-sinbhz*(sinbtar/r - sinbtrh/rh)*delta/
```

```
     -                  (1-cosbth)
                 PSIdu=PSIdu+(cos(betaz)-cosbth)*(expnr-expnrh)/
     -                  (1-cosbth)
                 PSIdr=PSIdr+sinbhz*(cosbtar/r-cosbtrh/rh)*delta/
     -                   sinbth
100   continue

      Th=((PSIdu+EA)*sinbth-J*PSIdi-SA)/(CA-cosbth*(EA+PSIdu))
      return
      end

      complex*16   function Zin(L,PSIdr,Th)
      complex*16 J,PSIdr,Th
      double precision L,beta,betah
      common beta,J

                 betah=beta*L
                 Zin=J*30*PSIdr/(Th*(1.-cos(betah))-sin(betah))
                 return
      end

      complex*16 function FIJ(Z,PSIdr,LI,LJ,Th)
      complex*16 Z,PSIdr,Th,J,psi
      double precision LI,LJ,beta,betah,betaz
      common beta,J

       betah=beta*LI
       betaz=beta*LJ
       abbetaz=abs(betaz)
       psi=30.0*PSIdr
c
       FIJ=-J*Z*((sin(abbetaz)-sin(betah))+Th*(cos(betaz)-cos(betah)))/
     -               psi
       return
      end

ccccccccccccccccccccccccccccccccccccccccccccccccccccccccccccccccccccccccccccc
```

```
ccccccccccccccccccccccccccccccccccccccccccccccccccccccccccccccccccccccccc

      program centre_loaded_impedance

c
c     based on HARRISON: MONOPOLE WITH INDUCTIVE LOADING
c
c     IEEE TRANS A&P JULY 1963
c
c analyse results from c_loaded.for
c
      double precision freq,LA,H1,H2,H3,a1,a2
      complex*16 Z1,Z2,Z3,Z4,F1,F2,F3,F4,F5,F6,J,one,zero,
     -     load,deltay,y0,ld,vcoil,icoil,
     -     x0,A0,A,B,D,E
      character*16 filename
      real eff,res,highest,lowest,calcrho,vswr
      common one

      zero=dcmplx(0,0)
      one=dcmplx(1.,0)
      J=dcmplx(0,1)
      open(unit=2,file='cllmimp.dat',status='new',ERR=5)
      goto 8
5     open(unit=2,file='cllmimp.dat',status='old',ERR=35)
8     filename='landm1.dat'
10    open(unit=1,file=filename,status='old',ERR=30)
12      read(1,15,end=26)freq,LA,H1,H2,H3,a1,a2,
     -       Z1,Z2,Z3,Z4,F1,F2,F3,F4,F5,F6
15    format(7(f8.4,1x),20(E15.5E3,1x),/)
      write(*,*)freq
      y0=-(one+F1)/(Z2+Z3)+1/50.0
      A0=(Z2+Z3)*y0/((F2+F3)*(F4+F5))
      load=-A0*(Z1+Z4)/(one+A0*(one+F6))
      deltay = y0/load - y0*(one+F6)/(Z1+Z4+load*(one+F6))
      icoil=(F2+F3)/(Z2+Z3)*(Z1+Z4)/(Z1+Z4+load*(one+F6)))
      vcoil=load*icoil
```

```
      res=0.5*cdabs(load+dconjg(load))
      x0=load-one*res
      A=(one+F1)/(Z2+Z3)
      B=-(F$+F%)*(F2+F3)/(Z2+Z3)
      D=Z1+Z4
      E=one+F6
      vswr=3.0
      lowest=calcrho(A,B,D,E,load,0.5,1.0,vswr)
      highest=calcrho(A,B,D,E,load,1.0,2.0,vswr)
      eff=(1.0-50*res*cdabs(icoil)**2)*100.0
      write(2,20)freq,LA,H1,H2,H3,a1,a2,
     -  load,deltay,icoil,vcoil,eff
20 format(7(f8.4,1x),/,4(2(E15.5E2,1x),/),f7.3,/)
      write(2,22)vswr,lowest,highest
      goto 12
22     format(1x,f4.2,1x,f7.5,1x,f7.5)
26    close(unit=1)
30    close(unit=2)
35    end

      real function calcrho(A,B,D,E,z,mmin,mmax,vswr)

      complex*16 zlpr,yterm,one,A,B,D,E,z

      real rho,min,max,mmin,mmax,centre,rhomax,rhomin,error,vswr

      common one

      min=mmin
      max=mmax
      rho=(vswr-1.0)/(vswr+1.0)
50    rhomax=1.001*rho
      rhomin=0.999*rho

100   centre=0.5*(min+max)
      error=(max-centre)/max
      if(error.lt.0.0)error=-error
```

```
      if(error.lt. 0.0001)goto 200
      zlpr=centre*z
      yterm=50*(A+(B*zlpr)/(D+E*zlpr))
      rho=cdabs((yterm-one)/(yterm+one))
190   if(rho.gt.rhomax)goto 220
      if(rho.lt.rhomin)goto 210
200      calcrho=centre
205      return
210   if(max.gt.1.0)goto 225
215      max=centre
         goto 100
220   if(max.gt.1.0)goto 215
225      min=centre
         goto 100
      end
```

Appendix C

CALIBRATION DATA

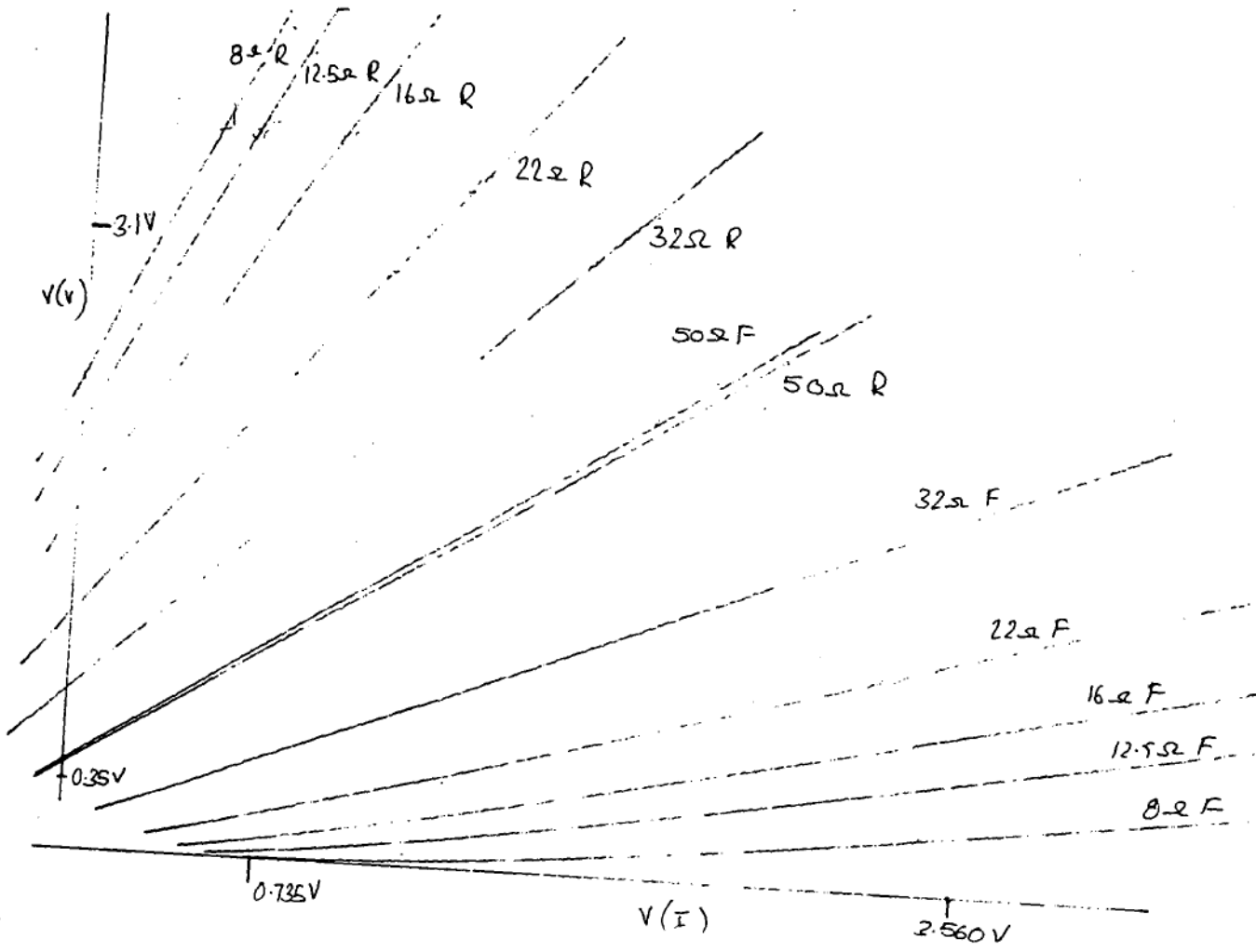

Figure C.1: Voltage vs Current for Transformer at 7 MHz

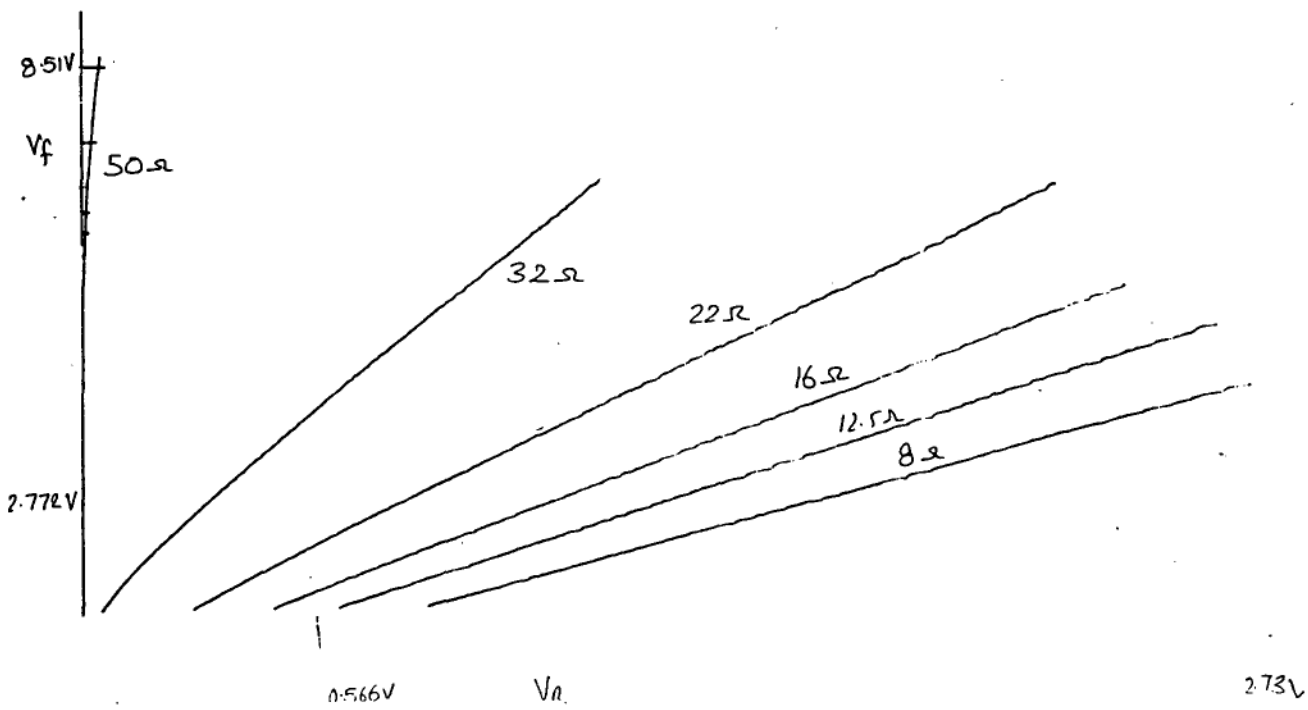

Figure C.2: Forward vs Reflected Voltage for Transformer at 7 MHz

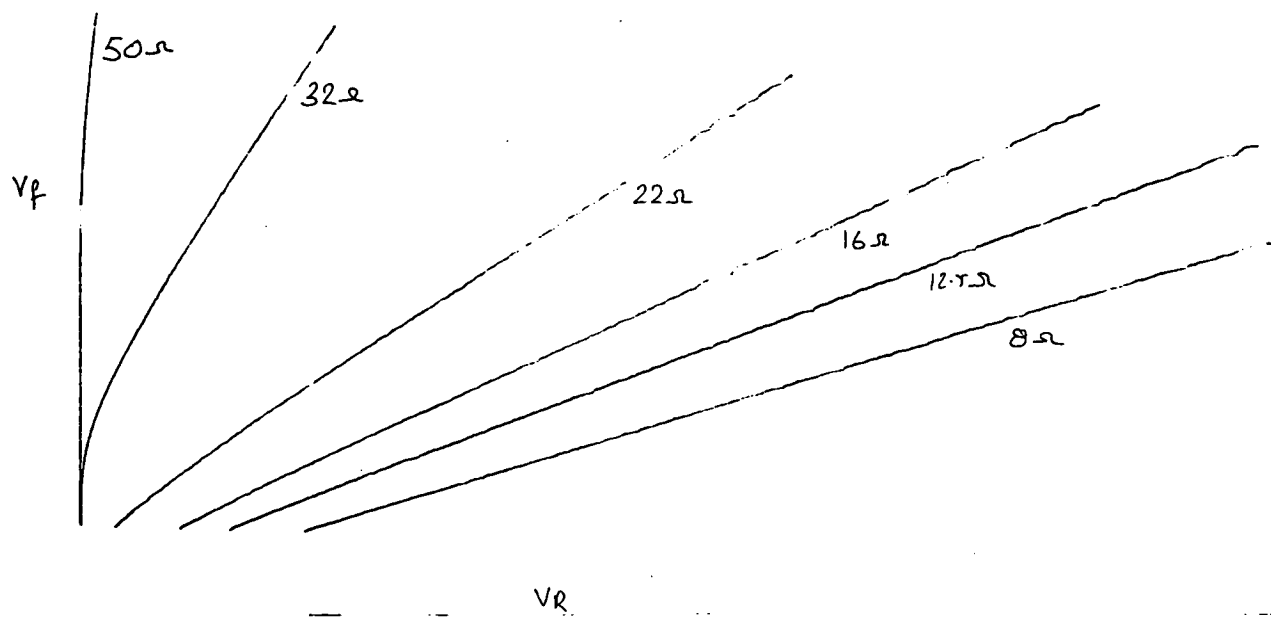

Figure C.3: Forward vs Reflected Voltage for reversed Transformer at 7 MHz

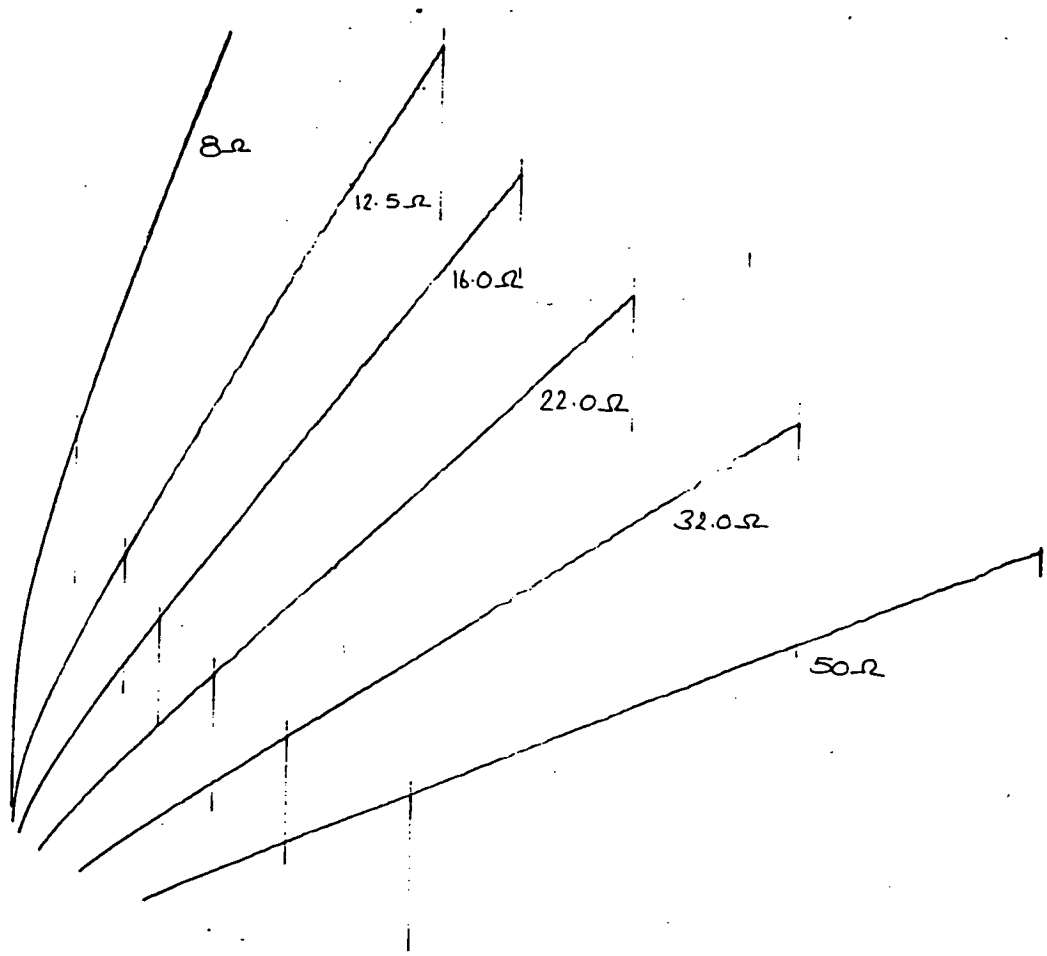

Figure C.4: Voltage vs Current for Transformer at 2 MHz

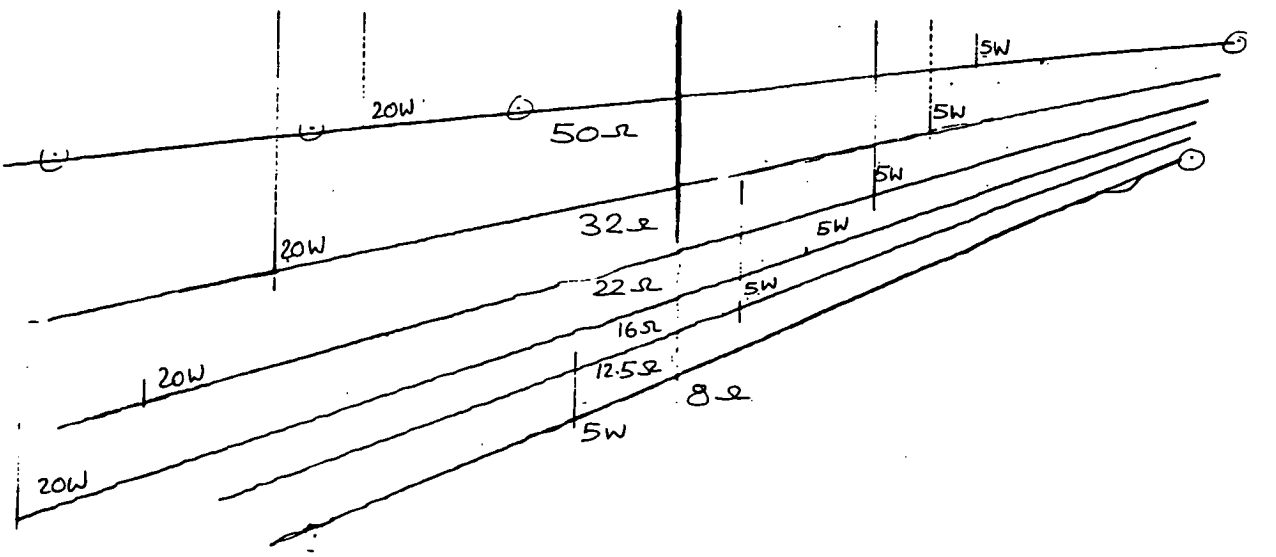

Figure C.5: Voltage vs Current for reversed Transformer at 2 MHz

frequency is 2.0650 MHz

50.00	1308	0	656	0.0000	50.000
50.00	1827	0	966	0.0000	50.000
50.00	2266	0	1232	0.0000	50.000
50.00	2708	0	1477	0.0000	50.000
50.00	3297	14	1844	0.0042	50.426
32.00	1337	140	870	0.1047	61.696
32.00	1849	253	1239	0.1368	65.852
32.00	2314	350	1577	0.1513	67.821
32.00	2753	444	1892	0.1613	69.229
22.00	1368	388	1050	0.2836	89.592
22.00	1962	611	1524	0.3114	95.226
22.00	2458	798	1948	0.3247	98.072
22.00	2901	966	2295	0.3330	99.922
16.00	1393	573	1184	0.4113	119.878
16.00	2095	920	1797	0.4391	128.298
16.00	2627	1177	2257	0.4480	131.172
16.00	3126	1432	2712	0.4581	134.534
12.50	1516	800	1393	0.5277	161.732
12.50	2249	1226	2079	0.5451	169.844
12.50	2814	1543	2613	0.5483	171.400
12.50	3349	1861	3105	0.5557	175.067
8.00	1781	1195	1782	0.6710	253.925
8.00	2650	1807	2656	0.6819	264.353
8.00	3306	2266	3315	0.6854	267.885
8.00	3892	2690	3911	0.6912	273.794

reverse trans

50.00	1278	0	638	0.0000	50.000
50.00	1785	0	923	0.0000	50.000
50.00	2231	0	1197	0.0000	50.000
50.00	2664	0	1450	0.0000	50.000
32.00	1240	121	429	0.0976	41.109
32.00	1830	248	708	0.1355	38.065
32.00	2297	345	919	0.1502	36.942
32.00	2718	442	1118	0.1626	36.013
22.00	1326	372	338	0.2805	28.092
22.00	1941	605	570	0.3117	26.237
22.00	2438	780	752	0.3199	25.761
22.00	2899	958	924	0.3305	25.162
16.00	1387	581	253	0.4189	20.478
16.00	2093	919	463	0.4391	19.489
16.00	2627	1184	630	0.4507	18.932
16.00	3099	1414	778	0.4563	18.668
12.50	1507	787	208	0.5222	15.693
12.50	2276	1233	403	0.5417	14.862
12.50	2840	1552	549	0.5465	14.663
12.50	3368	1859	689	0.5520	14.435
8.00	1786	1194	183	0.6685	9.933
8.00	2678	1813	363	0.6770	9.630
8.00	3313	2245	498	0.6776	9.608

frequency is 2.6670 MHz

50.00	1275	0	637	0.0000	50.000
50.00	1799	0	941	0.0000	50.000
50.00	2234	0	1202	0.0000	50.000
50.00	2671	0	1470	0.0000	50.000
32.00	1312	136	854	0.1037	61.565
32.00	1824	244	1220	0.1338	65.443
32.00	2303	346	1559	0.1502	67.680
32.00	2721	441	1873	0.1621	69.342
22.00	1332	377	1019	0.2830	89.476
22.00	1941	596	1505	0.3071	94.312
22.00	2430	777	1908	0.3198	97.005
22.00	2876	954	2279	0.3317	99.636
16.00	1366	572	1162	0.4187	122.040
16.00	2085	921	1798	0.4417	129.124
16.00	2603	1172	2249	0.4502	131.901
16.00	3095	1424	2700	0.4601	135.218
12.50	1503	786	1376	0.5230	159.623
12.50	2257	1228	2080	0.5441	169.339
12.50	2801	1553	2604	0.5544	174.439
12.50	3342	1859	3098	0.5563	175.354
8.00	1746	1166	1740	0.6678	251.034
8.00	2647	1812	2653	0.6845	267.006
8.00	3284	2262	3310	0.6888	271.331
8.00	3876	2687	3904	0.6932	275.988

reverse trans

50.00	1262	0	618	0.0000	50.000
50.00	1765	0	923	0.0000	50.000
50.00	2222	0	1183	0.0000	50.000
50.00	2646	0	1424	0.0000	50.000
32.00	1217	120	420	0.0986	41.025
32.00	1831	248	704	0.1354	38.071
32.00	2282	348	915	0.1525	36.768
32.00	2729	445	1125	0.1631	35.980
22.00	1278	356	320	0.2786	28.213
22.00	1949	603	569	0.3094	26.371
22.00	2445	785	751	0.3211	25.697
22.00	2899	961	929	0.3315	25.104
16.00	1399	582	254	0.4160	20.621
16.00	2069	917	463	0.4432	19.290
16.00	2619	1176	629	0.4490	19.012
16.00	3107	1416	780	0.4557	18.693
12.50	1524	790	215	0.5184	15.860
12.50	2253	1219	400	0.5411	14.891
12.50	2830	1546	548	0.5463	14.671
12.50	3350	1850	688	0.5522	14.423
8.00	1776	1189	185	0.6695	9.899
8.00	2650	1795	360	0.6774	9.618
8.00	3240	2201	485	0.6793	9.548

frequency is 4.7720 MHz

50.00	1267	0	628	0.0000	50.000
50.00	1764	0	916	0.0000	50.000
50.00	2223	0	1186	0.0000	50.000
50.00	2663	0	1440	0.0000	50.000
32.00	1308	122	844	0.0933	60.287
32.00	1797	217	1190	0.1208	63.734
32.00	2244	308	1513	0.1373	65.909
32.00	2694	402	1833	0.1492	67.539
22.00	1352	372	1022	0.2751	87.959
22.00	1936	583	1494	0.3011	93.089
22.00	2387	752	1862	0.3150	95.994
22.00	2858	925	2240	0.3237	97.853
16.00	1364	558	1141	0.4091	119.231
16.00	2060	900	1757	0.4369	127.586
16.00	2569	1144	2200	0.4453	130.281
16.00	3075	1392	2643	0.4527	132.709
12.50	1533	797	1386	0.5199	158.288
12.50	2198	1180	2005	0.5369	165.914
12.50	2790	1524	2551	0.5462	170.379
12.50	3287	1816	3017	0.5525	173.453
8.00	1761	1176	1747	0.6678	251.026
8.00	2605	1775	2608	0.6814	263.855
8.00	3265	2238	3254	0.6855	267.916
8.00	3848	2657	3840	0.6905	273.090

reverse trans

50.00	1264	0	624	0.0000	50.000
50.00	1760	0	910	0.0000	50.000
50.00	2218	0	1180	0.0000	50.000
50.00	2652	0	1434	0.0000	50.000
32.00	1218	124	443	0.1018	40.760
32.00	1806	251	721	0.1390	37.798
32.00	2266	350	942	0.1545	36.621
32.00	2721	452	1157	0.1661	35.755
22.00	1299	374	371	0.2879	27.645
22.00	1955	621	633	0.3176	25.893
22.00	2434	803	827	0.3299	25.193
22.00	2872	972	1006	0.3384	24.714
16.00	1411	597	313	0.4231	20.269
16.00	2094	942	544	0.4499	18.972
16.00	2590	1184	713	0.4571	18.627
16.00	3079	1428	882	0.4638	18.316
12.50	1521	803	283	0.5279	15.448
12.50	2289	1252	510	0.5470	14.643
12.50	2829	1563	675	0.5525	14.413
8.00	1799	1206	323	0.6704	9.867
8.00	2525	1715	524	0.6792	9.552

frequency is 6.3400 MHz

50.00	1222	0	600	0.0000	50.000
50.00	1751	0	895	0.0000	50.000
50.00	2234	0	1176	0.0000	50.000
50.00	2671	0	1434	0.0000	50.000
32.00	1252	110	801	0.0879	59.632
32.00	1814	222	1208	0.1224	63.945
32.00	2287	318	1530	0.1390	66.150
32.00	2733	410	1852	0.1500	67.650
22.00	1253	339	949	0.2706	87.090
22.00	1922	582	1482	0.3028	93.433
22.00	2417	766	1886	0.3169	96.396
22.00	2896	946	2270	0.3267	98.513
16.00	1417	584	1181	0.4121	120.108
16.00	2076	907	1766	0.4369	127.588
16.00	2614	1168	2238	0.4468	130.775
16.00	3085	1403	2650	0.4548	133.413
12.50	1465	761	1321	0.5195	158.097
12.50	2226	1199	2030	0.5386	166.748
12.50	2802	1533	2555	0.5471	170.804
12.50	3330	1843	3050	0.5535	173.941
8.00	1807	1206	1780	0.6674	250.666
8.00	2619	1782	2598	0.6804	262.903

reverse trans

50.00	1215	0	602	0.0000	50.000
50.00	1758	0	910	0.0000	50.000
50.00	2199	0	1167	0.0000	50.000
50.00	2652	0	1430	0.0000	50.000
32.00	1213	125	450	0.1031	40.658
32.00	1799	251	731	0.1395	37.756
32.00	2284	355	963	0.1554	36.548
32.00	2710	450	1165	0.1661	35.759
22.00	1237	355	366	0.2870	27.701
22.00	1931	621	650	0.3216	25.666
22.00	2406	802	843	0.3333	25.000
22.00	2888	990	1043	0.3428	24.471
16.00	1295	549	288	0.4239	20.228
16.00	2085	946	559	0.4537	18.789
16.00	2643	1223	751	0.4627	18.365
16.00	3103	1458	915	0.4699	18.033
12.50	1505	803	293	0.5336	15.208
12.50	2281	1258	527	0.5515	14.453
12.50	2819	1577	694	0.5594	14.126
12.50	3330	1882	856	0.5652	13.891
8.00	1779	1206	352	0.6779	9.598
8.00	2683	1855	615	0.6914	9.123
8.00	3320	2307	808	0.6949	9.001

frequency is 8.7700 MHz

50.00	1302	0	629	0.0000	50.000
50.00	1718	0	867	0.0000	50.000
50.00	2174	0	1131	0.0000	50.000
50.00	2612	0	1376	0.0000	50.000
32.00	1326	116	848	0.0875	59.587
32.00	1774	200	1161	0.1127	62.706
32.00	2233	286	1484	0.1281	64.689
32.00	2684	380	1799	0.1416	66.493
22.00	1334	361	1003	0.2706	87.102
22.00	1890	561	1446	0.2968	92.212
22.00	2398	748	1855	0.3119	95.333
22.00	2859	917	2225	0.3207	97.219
16.00	1333	536	1104	0.4021	117.252
16.00	2021	868	1694	0.4295	125.282
16.00	2547	1122	2155	0.4405	128.737
16.00	3065	1373	2602	0.4480	131.147
12.50	1505	773	1341	0.5136	155.601
12.50	2241	1198	2020	0.5346	164.861
12.50	2814	1527	2542	0.5426	168.648
12.50	3353	1840	3036	0.5488	171.613
8.00	1779	1176	1737	0.6610	245.025
8.00	2634	1775	2589	0.6739	256.636
8.00	3277	2224	3212	0.6787	261.206
8.00	3712	2542	3645	0.6848	267.265

reverse trans

50.00	1290	0	637	0.0000	50.000
50.00	1738	0	897	0.0000	50.000
50.00	2198	0	1162	0.0000	50.000
50.00	2621	0	1407	0.0000	50.000
32.00	1296	152	521	0.1173	39.503
32.00	1778	255	759	0.1434	37.457
32.00	2263	371	1000	0.1639	35.915
32.00	2694	469	1215	0.1741	35.172
22.00	1296	392	451	0.3025	26.777
22.00	1889	628	718	0.3325	25.050
22.00	2411	834	952	0.3459	24.299
22.00	2859	1011	1155	0.3536	23.876
16.00	1342	590	375	0.4396	19.462
16.00	2054	954	649	0.4645	18.285
16.00	2586	1229	859	0.4753	17.785
16.00	3054	1469	1040	0.4810	17.522
12.50	1479	808	373	0.5463	14.670
12.50	2200	1243	628	0.5650	13.898
12.50	2782	1591	836	0.5719	13.618
12.50	3282	1900	1018	0.5789	13.335
8.00	1763	1223	498	0.6937	9.042
8.00	2614	1847	815	0.7066	8.597
8.00	3267	2314	1060	0.7083	8.538
8.00	3622	2579	1201	0.7120	8.410

frequency is 10.1985 MHz

50.00	1226	0	587	0.0000	50.000
50.00	1776	0	893	0.0000	50.000
50.00	2220	0	1144	0.0000	50.000
50.00	2638	0	1376	0.0000	50.000
32.00	1241	94	784	0.0757	58.195
32.00	1765	191	1148	0.1082	62.135
32.00	2278	286	1508	0.1255	64.357
32.00	2716	377	1815	0.1388	66.118
22.00	1235	319	919	0.2583	84.825
22.00	1920	568	1460	0.2958	92.012
22.00	2425	756	1871	0.3118	95.297
22.00	2871	917	2222	0.3194	96.929
16.00	1310	526	1081	0.4015	117.092
16.00	2075	896	1742	0.4318	125.997
16.00	2593	1143	2185	0.4408	128.828
16.00	3101	1391	2626	0.4486	131.345
12.50	1501	766	1329	0.5103	154.218
12.50	2258	1201	2022	0.5319	163.623
12.50	2818	1529	2531	0.5426	168.619
8.00	1235	797	1193	0.6453	231.963
8.00	2037	1355	1980	0.6652	248.680
8.00	2461	1649	2400	0.6701	253.079

reverse trans

50.00	1225	0	597	0.0000	50.000
50.00	1807	0	931	0.0000	50.000
50.00	2199	0	1156	0.0000	50.000
50.00	2656	0	1420	0.0000	50.000
32.00	1238	139	511	0.1123	39.906
32.00	1784	255	787	0.1429	37.494
32.00	2251	369	1028	0.1639	35.916
32.00	2703	473	1259	0.1750	35.107
22.00	1255	382	470	0.3044	26.665
22.00	1926	649	788	0.3370	24.796
22.00	2388	838	1012	0.3509	24.024
22.00	2858	1023	1239	0.3579	23.641
16.00	1241	543	376	0.4376	19.563
16.00	2050	965	711	0.4707	17.993
16.00	2622	1265	953	0.4825	17.456
16.00	3069	1500	1140	0.4888	17.170
12.50	1234	668	333	0.5413	14.879
12.50	2057	1170	651	0.5688	13.743
12.50	2828	1642	953	0.5806	13.266
12.50	3351	1972	1159	0.5885	12.953
8.00	1248	863	377	0.6915	9.119
8.00	2127	1507	742	0.7085	8.531
8.00	3085	2209	1142	0.7160	8.274
8.00	3521	2538	1331	0.7208	8.112

Appendix D

THERMAL EFFECTS ON FERRITE CORES

A solid cylinder of radius r_o , length ℓ , thermal conductivity K and specific heat C which is subject to a uniform power dissipation P_o has a power density of

$$\frac{P_o}{\pi r_o^2 \ell} \text{ W}/m^3$$

A cylindrical section of radius r has a net power flow at equilibrium of

$$P_o(\frac{r}{r_o})^2$$

and a temperature gradient of

$$\delta T(r) = -\frac{P(r)}{KA(r)}$$

where A(r) is the surface area of the cylindrical section.

Hence

$$T(r) = \int_0^r \delta T(s) = \frac{-P_o r^2}{4\pi K r_o^2 \ell} + T(0)$$

at r=r_o $T(r_o) = T_A = \frac{-P_o}{4\pi K \ell} + T(0)$

consequently the rise in temperature at the centre is

$\frac{P_o}{4\pi K \ell}$

from the data for the ferrite cores (table 5.1), K = 4.0 W/(m K). The radius is 9.5 mm and the length 126 mm hence ΔT is 0.158 degrees per watt. For a power flow of 100 W this is $\approx$ 16 degrees above the local ambient.

The specific heat is 750 J kg K and density 4700 kg m^3 hence the energy for a temperature rise of 1 degree is 126 J.

Ignoring the thermal time constant the time required for a temperature rise of 16 degrees is 20 seconds.